The Dissertation Committee for Shannon Elise Weigum Certifies that this is the approved version of the following dissertation:

DEVELOPMENT OF A CELL-BASED LAB-ON-A-CHIP SENSOR FOR DETECTION OF ORAL CANCER BIOMARKERS

Committee:

John T. McDevitt, Supervisor

David Hoffman

Lara Mahal

Rebecca Richards-Kortum

Jason Shear

DEVELOPMENT OF A CELL-BASED LAB-ON-A-CHIP SENSOR FOR DETECTION OF ORAL CANCER BIOMARKERS

by

Shannon Elise Weigum, B.A., M.S.

Dissertation

Presented to the Faculty of the Graduate School of

The University of Texas at Austin

in Partial Fulfillment

of the Requirements

for the Degree of

Doctor of Philosophy

The University of Texas at Austin

August 2008

Dedication

To Kyle for giving me wings

Acknowledgements

There are a number of individuals whom I would like to thank for their help and support throughout this amazing journey. First and foremost, I would like to extend my deepest gratitude, respect, and admiration for my advisor Dr. John T. McDevitt. John has provided endless support and encouragement for me in every endeavor, successful or not, and always seemed to strike that perfect balance between support and independence which has truly helped me to grow as a scientist. For this, I am forever indebted to him. I would also like to express my sincerest appreciation to each of my committee members, Drs. Lara Mahal, Rebecca Richards-Kortum, David Hoffman, and Jason Shear, for their invaluable participation and insight which has helped to shape this dissertation.

Furthermore, my sincere thanks are extended to Dr. Rebecca Richards-Kortum and Dr. Elizabeth Hsu for their assistance and guidance in the initial stages of this project to identify suitable oral cancer biomarkers. To our clinical collaborators at the University of Texas Health Science Center in San Antonio, Drs. Spencer Redding, Chih-Ko Yeh, Alan Lin, and Fred Villereal for their efforts in identifying and collecting patient samples, along with Dr. Stan McGuff for his expertise in oral pathology. Special thanks to Dr. Nadarajah Vigneswaran and his research team at the University of Texas Health Science Center at Houston and Dr. Michelle Williams at M.D. Anderson Cancer Center who

came through with additional samples at a critical time in the course of the pilot study which strengthened the value of the study results.

To the entire McDevitt Group, past and present, with particular thanks to Dr. Pierre Floriano for his invaluable assistance writing Imag J macros, as well as for his humor and inherent French sarcasm which could always make me smile. To Dr. Nicolaos Christodoulides for opening the door for me in John's laboratory and whose friendship and guidance has extended far beyond my time here at UT, for which I will always be grateful. To Dr. Mehnaaz Ali and Michael Griffin for all of their advice, encouragement, and friendship over the years which has truly helped to make graduate school an enjoyable experience. To Shelley Acosta for her diverse technical assistance and agreeable wit. To my fellow graduate students, Jesse Jokerst, Alexis Lennart, Amanda Pollard, Archana Raamanathan, Sara Goodwin, and Lauren Lytwak for creating a work environment filled with friends as well as colleagues.

I must also thank Drs. Joseph R. Koke and Dana Garcia at Texas State University who helped me to build confidence in myself and my research, without which this would not have been possible. I am eternally grateful for their continued guidance and support in all aspects of my career.

My deepest thanks to my darling husband, Kyle, who has more patience and love for me than I often deserve. I appreciate your faith in me, which always encourages me to do more than I ever believed I could. Your support and friendship is the best gift you could have ever given me. I would also like to thank all my friends and family for their genuine love, support and understanding over the years.

DEVELOPMENT OF A CELL-BASED LAB-ON-A-CHIP SENSOR FOR DETECTION OF ORAL CANCER BIOMARKERS

Publication No._____

Shannon Elise Weigum, Ph.D.

The University of Texas at Austin, 2008

Supervisor: John T. McDevitt

Oral cancer is the sixth most common cancer worldwide and has been marked by high morbidity and poor survival rates that have changed little over the past few decades. Beyond prevention, early detection is the most crucial determinant for successful treatment and survival of cancer. Yet current methodologies for cancer diagnosis based upon pathological examination alone are insufficient for detecting early tumor progression and molecular transformation. Development of new diagnostic tools incorporating tumor biomarkers could enhance early detection by providing molecular-level insight into the biochemical and cellular changes associated with oral carcinogenesis.

The work presented in this doctoral dissertation aims to address this clinical need through the development of new automated cellular analysis methods, incorporating lab-on-a-chip sensor techniques, for examination of molecular and morphological biomarkers associated with oral carcinogenesis. Using the epidermal growth factor receptor (EGFR)

as a proof-of-principle biomarker, the sensor system demonstrated capacity to support rapid biomarker analysis in less than one-tenth the time of traditional methods and effectively characterized EGFR biomarker over-expression in oral tumor-derived cell lines. Successful extension from *in vitro* tumor cell lines to clinically relevant exfoliative brush cytology was demonstrated, providing a non-invasive method for sampling abnormal oral epithelium. Incorporation of exfoliative cytology further helped to define the important assay and imaging parameters necessary for dual molecular and morphological analysis in adherent epithelium. Next, this new sensor assay and method was applied in a small pilot study in order to secure an initial understanding of the diagnostic utility of such biosensor systems in clinical settings. Four cellular features were identified as useful indicators of cancerous or pre-cancerous conditions including, the nuclear area and diameter, nuclear-to-cytoplasm ratio, and EGFR biomarker expression. Further examination using linear regression and ROC curve analysis identified the morphological features as the best predictors of disease while a combination of all features may be ideal for classification of OSCC and pre-malignancy with high sensitivity and specificity. Further testing in a larger sample size is necessary to validate this regression model and the LOC sensor technique, but shows strong promise as a new diagnostic tool for early detection of oral cancer.

Table of Contents

List of Tables

List of Figures

Chapter 1: Oral Cancer Pathology, Detection, and the use of Adjunctive Diagnostic Techniques

1.1 OVERVIEW

The following dissertation details the development of a cellular sensor for detection of biomarkers associated with oral cancer and pre-cancerous lesions using a membrane-based lab-on-a-chip (LOC) platform. This general LOC approach has been developed over the past decade and serves as a miniaturized diagnostic platform suitable for whole cell immunoassays as described previously for $CD3^+/CD4^+$ immune monitoring in HIV patients.[1] The LOC sensor system utilizes a size-selective membrane that functions as a microsieve to capture and screen cells from bodily fluids, such as whole blood and saliva, or biopsy suspensions. Once captured, a series of immunofluorescent reagents are passed over the sensor membrane revealing the number and phenotype of cells present via automated imaging and microscopy.

In the following section, the motivation for this research is provided emphasizing the U.S. and global significance of oral cancer. In addition, a brief synopsis of oral cancer biology and clinical pathology is discussed. Particular attention is paid to the detection of pre-malignant lesions and the value of histological diagnosis for prediction of malignant development in order to provide perspective on existing procedures and the need for new diagnostic techniques targeting early tumorigenesis. Various adjunctive devices to aid diagnosis are summarized followed by a description of the LOC approach for characterization of oral cancer and pre-cancerous risk using molecular and morphological biomarkers. A short description of the chapter contents to follow in the dissertation is outlined at the end of this section.

1.2 MOTIVATION

Oral cancer accounts for 3-5 % of all cancers in the United States with an estimated 34,000 new cases and nearly 8,000 deaths in 2007 alone.[2] Worldwide the problem is more pronounced afflicting over 300,000 people per year, particularly in western Europe and developing countries where high incidence rates reflect the prevalence of specific risk factors such as tobacco and alcohol use.[3] The long-term prognosis for patients with oral cancer is poor, with 5-year and 10-year survival rates at 60% and 48%, respectively.[2] These survival rates are among the lowest for all major cancers and have increased only moderately in the past few decades, despite significant advancements in surgical procedures and treatment for oral cancer.[2, 4]

Beyond prevention, early detection is the most crucial determinant for successful treatment and survival of oral cancer. In addition, management of early stage oral cancer is often accomplished with less aggressive methods which can preserve vital organ function and physical appearance, resulting in a better quality of life for patients. Unfortunately, the majority of oral cancers exhibit advanced stage disease with spread to regional lymph nodes and/or distant metastases at the time of initial diagnosis suggesting that current detection methods, based upon visual examination alone, are insufficient for early tumor progression and molecular transformation.[4, 5]

Development of new diagnostic methods incorporating tumor biomarkers could enhance early detection by providing molecular-level insight into the biochemical and cellular changes associated with oral carcinogenesis.[6] A number of biomarkers (DNA, RNA and protein) demonstrating significant diagnostic, prognostic, and therapeutic potential have been characterized in oral cancer, including cyclins involved in cell cycle regulation; growth factors and their receptors; matrix metalloproteinases (MMPs) involved in cell attachment and migration; angiogenic factors; inflammatory mediators;

and apoptotic signaling molecules.[6-8] Given that molecular changes in these key cellular processes often occur prior to the histological changes associated with the clinical appearance of cancer, diagnostic tools for biomarker characterization offer new opportunities for oral cancer detection at early stages where treatment is most effective and survival is up to 85%.[6, 8, 9]

1.3 ORAL CAVITY ANATOMY AND STRUCTURE OF EPITHELIAL MUCOSA

Oral cancer encompasses all cancers developing in the oral cavity and pharynx.[10] The oral cavity includes the lips, tongue, minor salivary glands, gingiva, hard palate, buccal mucosa, and floor of the mouth. The oropharynx, located in the throat just behind the oral cavity, includes the base of the tongue, soft palate, tonsils, and throat walls. Approximately 90% of all oral malignancies are squamous cell carcinomas that originate in the epithelial mucosa lining the oral cavity and its tissues.[10] Oral squamous cell carcinoma (OSCC) is frequently the cancer-type referred to with the general term "oral cancer" and hereafter may be used interchangeably. Malignancies arising in the lymphoid tissue (lymphoma), salivary glands (adenocarcinoma), soft-tissues (melanoma), and skeletal tissues (sarcoma) account for the remaining 10% of oral tumors.

The oral mucosa is composed of two layers, an outer layer of epithelium and an underlying connective tissue layer (Figure 1-1). The epithelial layer is a stratified squamous epithelium that is either keratinized or nonkeratinized and functions as a protective barrier against mechanical, microbial, and chemical damage.[11] The underlying layer of dense connective tissue is known as the lamina propria and functions to provide mechanical support and nutrients for the epithelium.[11, 12] Beneath the lamina propria, a submucosa containing blood vessels, fat, and secretion glands may be present.[12] At various sites within the oral cavity, structural modifications in both the epithelial and connective tissue layers arise based upon the functional demands of each region.[12] The

three distinct histological types of oral mucosa which correspond to tissue function include: (i) the masticatory mucosa found on the gingiva and hard palate which possesses a mechanically tough, keratinized epithelium for protection against shear forces during mastication; (ii) the lining mucosa, with a nonkeratinized, flexible epithelium located on the lips, buccal regions, soft palate, floor of the mouth, and ventral surface of the tongue; and (iii) the specialized mucosa which is a mosaic of keratinized and nonkeratinized epithelia with specialized papillae located on the dorsal surface of the tongue.[11-13]

Similar to skin, the oral epithelium is arranged in multiple strata of densely packed epithelial cells that exhibit various patterns of differentiation.[11] The deepest layer is the basal epithelium consisting of undifferentiated mitotically active cells, often cuboidal or columnar in shape, which are responsible for cell production and division (Figure 1-1).[12] These basal cells are located directly above the basement membrane which anchors the epithelium to the underlying connective tissue. Upon cell division, basal cells migrate superficially into the spinous layer where they increase in cell size and volume, express differentiation-specific cytokeratins and take on a polyhedral appearance.[11, 12] As cells enter the granular (keratinized) or intermediate (nonkeratinized) layer, cells become flattened and densely packed with keratin filaments. In the surface layer of keratinized epithelium cells have thickened plasma membranes, compact arrays of condensed keratin filaments, no organelles and are surrounded by an external lipid matrix forming a permeability barrier.[11, 12] A similar progression occurs in nonkeratinized epithelium of lining mucosa, although organelles and nuclei persist in the outermost layer, here the superficial layer, and the permeability barrier formed is less effective than keratinized oral epithelium.[11, 12] Ultimately, the surface epithelial cells are sloughed off into the oral cavity and replenished from basal cell mitosis.

Cell production and turnover rates in oral mucosa differ at various anatomical sites, but typically occur rapidly (1 to 3 weeks) when compared to the epidermis of the skin (4 to 10 weeks depending upon site).[12] Thickness of the oral epithelium is also site-specific and ranges from 190 ± 40 μm in the floor of the mouth to 580 ± 90 μm in the buccal mucosa lining the cheek.[12] Additional non-epithelial cell types present in the oral mucosa include pigment producing melanocytes, Langerhans' cells, Merkel cells, and inflammatory cells such as lymphocytes, leukocytes, and mast cells. [11, 12] Together these cells can account for as much as 10% of the total cell population in the oral epithelium.[11]

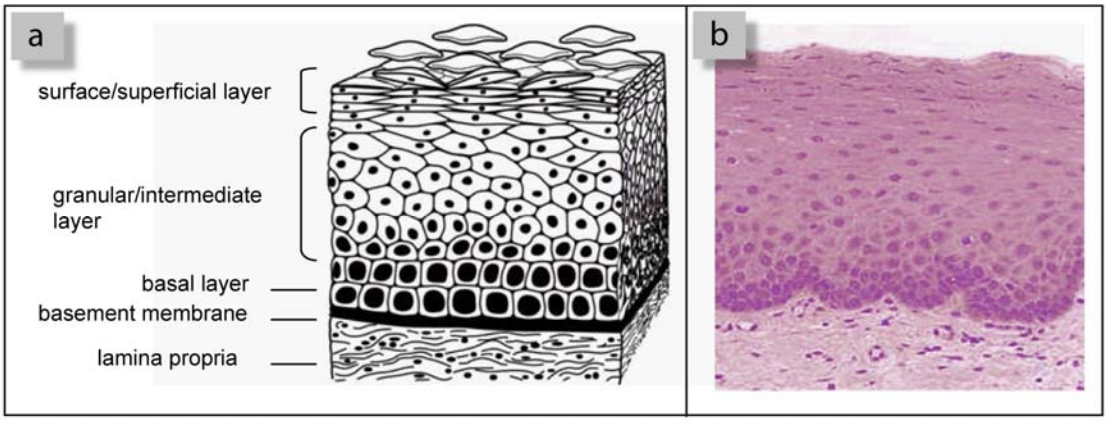

Figure 1-1. (a) Schematic drawing of the oral mucosa exhibiting the layers of stratified squamous epithelia; (b) Tissue section from the oral mucosa stained with hematoxylin and eosin. Figure reprinted with permission from Macmillan Publishers Ltd, Nature Reviews Cancer [14], copyright 2005.

1.4 ORAL CANCER BIOLOGY AND BACKGROUND

1.4.1 Epidemiology and Etiology

Oral cancer occurs predominately in adult males, aged 50 years and older with a history of tobacco and alcohol use, the primary risk factors for oral cancer. These risk factors account for the high incidence rates found in populations where cultural and

social use of tobacco and/or alcohol are common, such as Western Europe, Southeast Asia, and Melanesia (Table 1-1). In many regions, men exhibit greater prevalence than women, with incidence rates of 7.9 per 100,000 males versus 3.3 per 100,000 females in the US (Table1-1), due to higher proportion of smoking and drinking habits in men.[15-17] Interestingly, these factors appear to act individually or synergistically, with up to 100 times higher risk in heavy smokers and heavy drinkers.[10] Tobacco in all forms, including cigarettes, cigars, pipe tobacco, or smokeless tobacco such as chewing tobacco, snuff, and betel quid, increases the risk of oral cancer. Betel quid, common in India, Southeast Asia and the South Pacific islands, consists of a betel leaf that is wrapped around a mixture of areca nut and slaked lime with tobacco and sweeteners. In the past decade, there has been an alarming increase in the popularity of cheap, ready-packaged chewing tobacco that is often chocolate or mint candy flavored, among children in India over traditional betel quid. This trend has lead to an increase in malignant and pre-malignant lesions of the buccal mucosa in younger Indian populations, <50 years old.[16, 18, 19]

In addition, recent studies have linked high-risk HPVs (human papiloma virus-16 and 18) to oral cancer development in up to 25 % of all OSCC cases.[20, 21] HPV, one of the most common sexually transmitted diseases worldwide, may partially account for the increase in oral cancer among young adults 20-45, particularly those located on the tongue and tonsil.[22] HPV-associated OSCC may display distinct molecular, clinical, and pathological characteristics along with significantly improved prognosis (59% reduction in risk of death) versus non-HPV OSCC.[20, 21] Additional factors which may play a role in oral carcinogenesis include genetic susceptibility, diet, Epstein-Barr Virus infection and immunosuppression.[23]

Table 1-1. Oral cancer incidences for men and women according to geographic regions as reported in GLOBOCAN *2002* statistics.[3, 15] Patterns of cancer distribution can be traced to social and cultural use of tobacco and/or alcohol in specific geographic regions, including Melanesia, India, and Western Europe.

Region/Country	**Age-Standardized Incidence Rate of Oral Cancer (per 100,000)[15]**	
	Male	Female
North America	7.8	3.3
United States	7.9	3.3
Canada	6.9	2.9
Southern Africa	11.1	3.1
Botswana	23.1	9.5
Namibia	16.1	7.2
Lesotho	2.9	1.6
South African Republic	11.2	2.9
Swaziland	2.4	1.4
South Central Asia	12.7	8.3
Afghanistan	6.8	5.9
Bangladesh	13.4	16.8
Bhutan	12.8	8.4
India	12.8	7.5
Iran	2.9	1.7
Kazakhstan	14.9	2.7
Kyrgyzstan	8.1	1.7
Nepal	12.8	8.4
Pakistan	14.7	14.7
Sri Lanka	24.5	9.2
Tajikistan	2.6	1.3
Turkmenistan	12.9	3.3
Uzbekistan	9.3	2.3
Western Europe	11.3	2.7
Austria	11.3	1.7
Belgium	7.7	2.5
France	14.8	2.7
Germany	11.1	2.8
Luxembourg	9.0	2.7
The Netherlands	5.6	3.3
Switzerland	9.0	2.5
Australia/New Zealand	10.2	4.5
Melanesia	31.5	20.2
Fiji	1.9	1.4
Papua New Guinea	40.9	26.3
Solomon Islands	34.1	21.7
Vanuatu	3.7	2.0

1.4.2 Clinical, Histological, and Molecular Progression of Oral Cancer

1.4.2.1 Pre-malignant Lesions

Oral squamous cell carcinoma is often preceded by the emergence of clinically visible premalignant changes in the epithelial mucosa. These oral pre-malignant lesions (OPL) typically appear as white or red plaques know as leukoplakia and erythroplakia, respectively.[24, 25] Leukoplakia is by far the most common form of oral precancer, representing approximately 85% of all pre-malignancies.[24] Leukoplakia frequently occurs in the buccal mucosa, alveolar mucosa and lower lip with the majority of lesions exhibiting benign hyperkeratosis occurring in response to chronic irritation (eg, from dentures, lichen planus, tobacco, or cheek biting).[10, 26] However, a fraction of leukoplakias exhibit increased risk of malignant transformation at rates varying from 3% to 17.5%. [10, 25-28] While erythroplakia is less common than leukoplakia, there is a near total association of erythroplakia (90-100%) with either dysplasia or outright carcinoma at initial identification, reflecting significantly greater malignant potential.[10, 24, 25]

Since only a fraction of all OPLs actually progress to carcinoma, the clinical challenge is to identify which lesions possess a high-risk of malignant transformation and treat them accordingly. Assessment of malignant potential is influenced by factors such as clinical appearance (e.g. homogeneous versus non-homogeneous leukoplakias), etiology, and location, as well as the presence and degree of dysplasia. For example, non-homogeneous or "speckled" leukoplakias possess four- to five-times greater risk of malignant development than homogeneous ones.[26, 28, 29] In addition, several high-risk lesion sites have been identified that are more likely to harbor dysplastic or malignant changes, including the floor of the mouth and ventral/lateral surface of the tongue.[10] However, the most widely accepted predictor of cancer development is currently the presence and degree of dysplasia found upon surgical biopsy of the lesion tissue.

Table 1-2. Histological characteristics of epithelial dysplasia [29, 30]

Loss of polarity of the basal cells
The presence of more than one layer having a basaloid appearance
Increased nuclear-cytoplasmic ratio
Drop-shaped rete-ridges
Irregular epithelial stratification and differentiation
Increased number of mitotic figures, particularly in upper layers
Presence of abnormal mitoses
Cellular and nuclear pleomorphism
Nuclear hyperchramatism
Enlarged nuclei and prominent nucleoli
Loss of intercellular adherence

Dysplasia is a histologic term to describe the occurrence and extent of epithelial abnormality, often sub-divided into mild, moderate, or severe cases. Histological changes which may contribute to a diagnosis of epithelial dysplasia are listed in Table 1-2.[30] These include features of tissue architecture as well as individual cyto-morphological features, such as increased nuclear/cytoplasmic ratio, an increase in number of mitotic figures, and cellular and nuclear pleomorphism. Not all of these changes are necessarily seen in any one case and recognition/interpretation of their significance in various combinations is associated with considerable subjectivity.[30, 31] It should also be noted that some minor cellular atypia may be seen in epithelium due to inflammation and/or wound healing.[30]

In general, the risk of cancer development increases with the degree of dysplasia (Figure 1-2).[29] However, there are several major problems associated with the importance of epithelial dysplasia in predicting malignant development. First, the diagnosis and grading of dysplasia is ultimately a subjective process with high inter-observer variability.[32] Much of this variability is attributed to the lack of a well defined and universally accepted criterion for sub-dividing and grading of epithelial dysplasia.[31] In

addition, not all dysplastic OPLs will fully develop into carcinoma.[26, 29] Pindborg *et al.* reported spontaneous regression in nearly 15% of OPLs previously exhibiting dysplasia, often when tobacco use was reduced or eliminated.[27] Further, it appears that cancer development may occur from lesions diagnosed as non-dysplastic in previous biopsies.[26, 28] In order to overcome these limitations, novel strategies using clinical and histopathological data combined with molecular biomarker analysis, may be needed to improve prediction of cancer development from pre-malignant lesions.[29, 33]

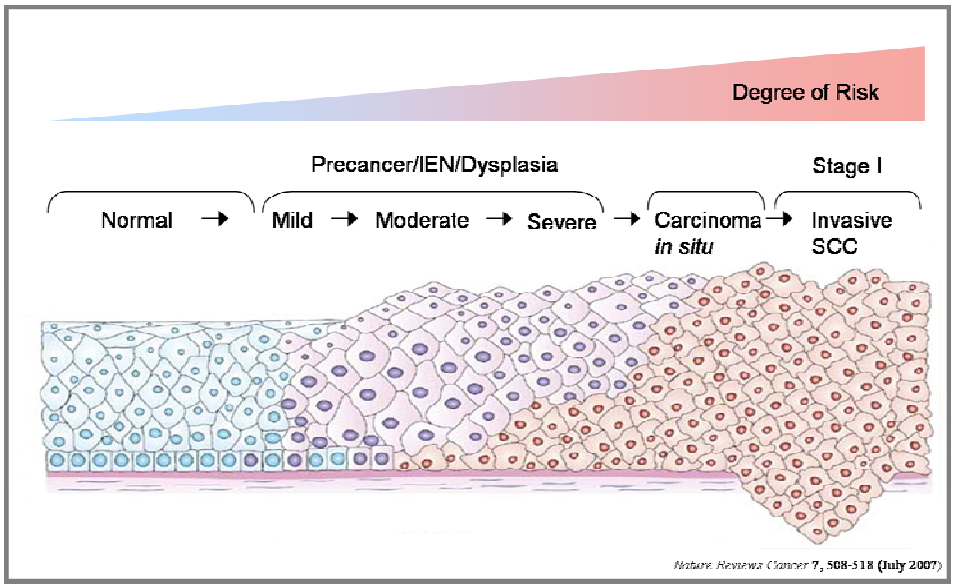

Figure 1-2. Schematic diagram of cellular and histological changes associated with oral cancer progression from mild, moderate and severe dysplasia to carcinoma in situ and ultimately invasive carcinoma. Figure reprinted with permission from Macmillan Publishers Ltd, Nature Reviews Cancer. [34]

1.4.2.2 Squamous Cell Carcinoma

Histologically, OSCC development may be viewed as an extension of the epithelial irregularity found in pre-malignancies through increasing degrees of dysplasia (mild → moderate → severe). When severe dysplasia is apparent throughout the entire

thickness of the epithelium, it is termed *carcinoma in situ*. Ultimately, the tumor cells breach the basement membrane and invade the underlying submucosa marking the defining transition into invasive squamous cell carcinoma (Figure 1-2).

OSCC is found most frequently in the lateral tongue, representing approximately 40% of all cases, and the floor of the mouth.[2, 10] The high-risk of malignancy at these sites is attributed to the pooling of saliva containing carcinogens in these areas, as well as the lack of protection afforded by the thin, non-keratinized epithelium present.[10, 29] A large number of squamous cell carcinomas also develop in the lower lip vermilion border due to excessive sun exposure, but typically possess low risk of metastasis.[10] Advanced metastatic spread of OSCC regularly encompasses multiple oral sites and/or cervical lymph nodes with greater than 50% of all OSCC cases showing regional lymph node involvement at initial diagnosis.[4, 16] Distant metastases can occur in any part of the body, but are seen most frequently in the lungs, bones, and liver.[10]

Approximately 9-14% of patients who have been diagnosed with oral cancer possess a second primary tumor in the upper aerodigestive tract at diagnosis.[35] Following treatment, oral cancer patients continue to exhibit significantly higher risk for development of second primary tumors at a rate of 3-7% per year, higher than any other malignancy.[36] This independent development of multiple primary tumors is attributed to widespread, chronic exposure of the mucosal epithelium to carcinogens such as tobacco and alcohol, through a process known as "field cancerization."[37] Originally proposed by Slaughter *et. al.* in 1953, the theory of field cancerization suggests that the exposed epithelium has been preconditioned for cancer development and may harbour sub-clinical changes related to carcinogenesis.[37] This theory has been supported by various clinical, histopathological[38] and molecular[39] evidence where normal appearing mucosa at the margin of an oral lesion or in a "mirror-image" biopsy exhibited distinct alterations

associated with cancer progression. Alternatively, it has been proposed that clonal expansion of initially transformed cells followed by micrometastasis may give rise to multiple primary oral tumors.[38]

1.4.2.3 Molecular Progression Model

Molecular development of OSCC occurs through a multi-step process of accumulated genetic, epigenetic, and biochemical alterations in tumor suppressor genes and proto-oncogenes.[40] These alterations manifest in the outward phenotypic changes in cellular and tissue morphology seen clinically or histologically. The presence of genetic changes in clinically normal or dysplastic tissue, particularly at the margin of OSCC tumors, suggests that molecular events occur early during tumorigenesis and may be used as indicators of disease and/or measurement of disease progression.[39, 41, 42]

Examination of the genetic changes associated with each histopathological stage, from pre-neoplastic lesions to invasive cancer, has helped to outline a model for the molecular progression of oral cancer, similar to colorectal cancer (Figure 1-3).[41] Here, loss of heterozygosity (LOH) in chromosomal region 9p21 is the most frequently observed genetic alteration and occurs early during tumorigenesis.[41, 42] As a consequence of this event, the *p16* gene which encodes a cyclin-dependent kinase inhibitor involved in cell cycle regulation, is inactivated.[41, 42] Subsequent events include LOH at the *p53* gene locus (17p13), cyclin D1 (11q13), and retinoblastoma (13q) whose gene products are key regulators of cell cycle progression, DNA repair, and apoptosis.[41, 42] Importantly, it is the accumulation rather than the order of genetic events that influences malignant progression. In a study by Rosin *et al.* risk of cancer development from OPLs was low in the absence of genetic alterations, increased moderately in the presence of genetic mutations on chromosomes 3p and 9p, and high when 3p and 9p mutations were accompanied by additional loss in one or more chromosomal regions (including 4q, 8p,

11q, 13q and 17p).[43] The continued accumulation in genetic mutations as a result of exposure to carcinogens, such as tobacco and alcohol, ultimately leads to wide-spread genomic instability associated with advanced cancer progression and metastasis.

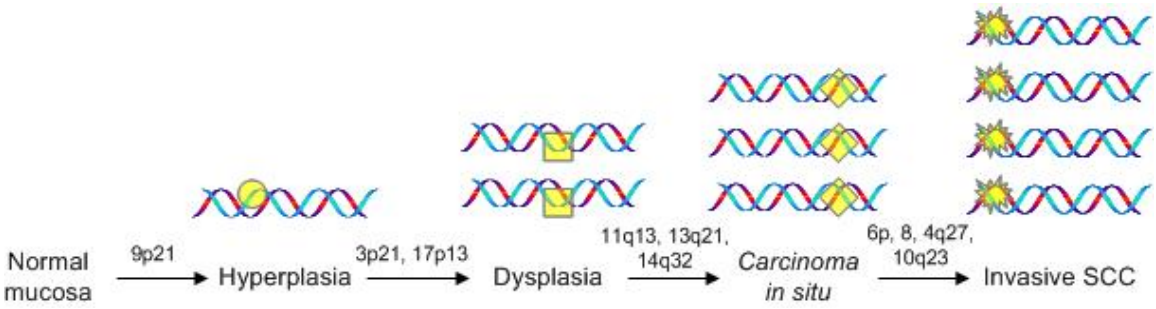

Figure 1-3. The molecular progression model for oral tumorigenesis proposed by Califano *et al.* demonstrates genetic events, such as the loss of heterozygosity in chromosomal regions encoding tumor suppressor genes and oncogenes, which are associated with histologically distinct stages of eary OSCC development. Figure modified from [41, 42].

Although this model provides a nice framework for understanding the genetic events associated with early development of oral cancer, it is far from complete and expresses a somewhat narrow view of tumorigenesis. Mechanisms involved in cancer development are not limited to genetic mutation only, but may include a variety of other epi-genetic and biochemical means to transform cellular function, including promoter hypermethylation and post-translational protein modifications effecting structure, function, enzymatic activity, localization, and expression.[44, 45]

1.4.3 Current Detection of Oral Cancer and Pre-malignant Lesions

Currently, detection of oral cancer and pre-malignant lesions relies upon visual inspection of the oral cavity for mucosal abnormalities in a process known as conventional oral examination (COE). Dental professionals and primary care physicians who see patients regularly are more likely to identify early-stage lesions through yearly

cancer related check-ups, as recommended by the American Cancer Society. However, only 13% of Americans report receiving an oral cancer examination in the past year and knowledge of the COE process among these clinicians may be inadequate.[46]

In a recent systematic review of seven studies evaluating COE as a method for detecting early cancerous lesions, sensitivity ranging from 60% - 97% and specificity ranging from 75% - 99% were reported, which are comparable to rates found in other cancer screening programs.[47] This suggests that COE may be an adequate screening method to identify oral lesions. Shortcomings of this method include the inability to detect sub-clinical abnormalities or discriminate between benign lesions and those with a high-risk of malignancy which may require the use of adjunctive diagnostic techniques.[48] Further, the effectiveness of COE screening to reduce disease-related mortality remains to be determined.[49, 50]

1.4.4 Clinical Diagnosis and Staging

Upon initial identification of a suspected pre-malignant lesion using visual examination, with or without adjunctive tests, clinicians typically pursue a two week follow-up approach for monitoring.[51] If the lesion persists in the absense of identifiable causes of local inflammation, a surgical biopsy is performed for definitive histopathological diagnosis. The decision to perform a surgical biopsy may be accelerated based upon clinical appearance of the lesion (e.g. presence of induration, erythematous component, and ulceration), location (e.g. floor of the mouth or tongue), size, patient history (e.g. past malignancy, smoking and alcohol use), and symptoms, such as numbness or pain.[51] In general, it is recommended that OPLs exhibiting moderate dysplasia or worse be removed by surgical excision, laser, or cryosurgery and monitored through follow-up every six months to one year.[10, 51, 52] Interestingly, surgical intervention does not appear to completely prevent malignant transformation in OPLs and

recurrence rates up to 35% have been reported.[52, 53] This relatively poor treatment success may be due in part to inadequately defined lesion margins during excision and/or the persistence of cancer stigmatized cells beyond the excision site as suggested by the field cancerization model.[53]

For patients with histologically confirmed invasive OSCC, further diagnostic tests such as physical examination, endoscopy, x-ray, CT, MRI, PET, and/or radionuclide scans are needed to assess the extent of tumor spread and presence of additional primary tumors. These test are utilized for staging in order to establish appropriate treatment and evaluate prognosis.[54] Tumors are most often classified according to the TNM, tumor-node-metastasis system updated by the American Joint Committee on Cancer in 2002, where (T) represents the primary tumor size, (N) indicates the status and extent of regional lymph node involvement, and (M) denotes the presence or absence of distant metastasis.[54, 55] The TNM stage grouping establishes an overall clinical stage (I-IV) that is closely related to survival (Table 1-3) according to an inverse relationship where the five-year survival rate for advanced stage disease (stage III-IV) is at or below 41%, whereas in early stage disease (stage I-II) five-year survival approaches 85%.[24, 54]

Table 1-3. Five-year survival rates of oral cancer according to tumor stage. [4, 24, 54]

Clinical Stage	TNM Classification	Five-year survival rate	Disease Status	% Cases at Diagnosis
0	T_{is} N_0 M_0	NA	Localized *in situ*	30-40%
I	T_1 N_0 M_0	68-85%	Localized	
II	T_2 N_0 M_0	53-66%		
III	T_{1-3} N_{0-1} M_0	41%	Advanced Regional Lymph Nodes	>50%
IV A/B	Any T_4,or T_{1-3} N_{2-3} M_0	9-27%		
IV C	Any T Any N M_1		Distant Metastasis	10%

1.4.5 Treatment and Prognosis

Extensive review of OSCC treatment and prognosis is beyond the scope of this dissertation and have been published elsewhere.[4, 56-59] Briefly, surgery and/or radiation therapy is the mainstay of treatment for early stage OSCC (stage I-II), where the tumor remains ≤ 4 cm in size and localized within the oral cavity.[23, 56] Treatment of locally advanced disease (stage III-IVA/B) requires a more extensive multidisciplinary approach using surgery, radiation, chemotherapy, or a combination of treatment modalities.[4, 56] The most widely used treatment approach includes surgery followed by adjuvant chemoradiotherapy or radiation to reduce locoregional failure, the most common cause of death among OSCC patients.[4] Alternatively, neoadjuvant chemoradiotherapy, with or without surgery as a salvage treatment, has become the dominant treatment strategy in some cancer centers due to improved organ preservation.[4] The emergence of molecular targeted therapeutics, such as the EGFR monoclonal antibody cetuximab (Erbitux®, Bristol Myers Squibb) may further enhance efficacy of current treatments with reduced treatment-related cytotoxicity.[4]

Lymph node status appears to be the most significant prognostic factor for OSCC with survival approximately cut in half when metastases are found in local or regional lymph nodes.[59] In these patients, the number of positive nodes and the presence of extracapsular spread contribute to a negative prognosis.[59] Other classic clinicopathological features including anatomical site, tumor size, grade, and maximal thickness have been shown to possess limited predictive value for the identification of patients with a high risk of disease relapse and death.[59]

1.5 ORAL CANCER BIOMARKERS

Recent advances in high-throughput "-omic" technologies has helped to unravel complex cellular mechanisms associated with tumorigenesis revealing a number of

molecular markers, or biomarkers, related to oral cancer initiation and progression.[14, 60-64] In the context of cancer research, biomarkers may be defined as "any substance or process that is indicative of the presence of cancer in the body."[65] However, the clinical role for biomarkers is not limited to detection. Biomarkers have been utilized in a range of clinical settings including screening, diagnosis, staging, prediction of treatment response, and monitoring of treatment and recurrence.[65, 66] Biomarkers directly involved in tumorigenesis and originating from the tumor itself, known as tumor-derived markers, have further served as targets for therapeutic intervention in an effort to reverse or inhibit disease development.[67]

The performance of a biomarker is measured by its sensitivity, specificity, positive predictive value (PPV) and negative predictive value (NPV) (Table 1-4). Sensitivity refers to the proportion of diseased individuals (confirmed using a diagnostic "gold standard" technique) whom test positive using the biomarker assay, whereas specificity refers to the proportion of non-diseased individuals with a negative biomarker result.[65] An ideal biomarker would exhibit 100% sensitivity and 100% specificity, i.e. everyone with cancer would test positive and everyone without cancer would test negative. In reality, acceptable sensitivity and specificity rates are dependent upon the intended use, for example diagnostic/monitoring tests place higher requirements on sensitivity while screening tests require higher specificity.[65] Biomarker performance may be measured further using predictive values which estimate the probability of disease according to a biomarker test result. Here, PPV indicates the percentage of individuals with a positive test that actually have the disease, while NPV is the percentage of individuals with a negative test who do not have cancer.[65]

		Confirmed Clinical Diagnosis	
		Diseased	Non-Diseased
Biomarker Test Result	Positive	True Positive	False Positive
	Negative	False Negative	True Negative

Sensitivity = TP/(TP+FN) Specificity = TN/(TN+FP)

PPV = TP/(TP + FP) NPV = TN/(TN + FN)

Table 1-4. Biomarker performance calculations of sensitivity, specificity, positive predictive value (PPV), and negative predictive value (NPV).

A number of biomarkers demonstrating significant diagnostic, prognostic, and therapeutic potential have been characterized in oral cancer. These biomarkers can be broadly classified according to their normal function in cell proliferation, differentiation, growth and signaling pathways, apoptosis, angiogenesis, and extracellular matrix degradation and migration.[6-8] Additional genomic markers include genetic alterations in tumor suppressor genes and oncogenes, which often result in dysregulation of the cell cycle, and markers of genetic/chromosomal instability, such as changes in DNA content (aneuploidy), micronuclei, microsatellite repeats, and allelic imbalance (LOH). [7, 8, 23, 67, 68]

As will be discussed later in the dissertation, the epidermal growth factor receptor biomarker was selected as a proof-of-concept biomarker for initial development of LOC sensor assays due to its overexpression in up to 90% of all OSCC and association with early tumorigenesis and aggressive cancer phenotypes.[69-71] Obviously, cancer development is a complex process disrupting a number of diverse cellular functions, therefore, it is unlikely that a single biomarker alone will provide sufficient sensitivity and specificity for conclusive cancer diagnosis. Instead a combination, or panel, of multiple biomarkers may be necessary for early detection and screening.[33] Nevertheless,

when utilized as an adjunct to current diagnostic methods, even a single biomarker has the potential to enhance early detection of oral cancer by reducing subjectivity associated with histopathological diagnosis and providing a molecular-level basis for risk assessment in primary or recurrent lesions.

Many OSCC biomarkers (DNA, RNA, and protein) have been identified in cancerous oral tissue or cells, as well as in extracellular fluids that drain from the oral cavity such as blood or saliva.[60, 62, 72-75] Particularly in the case of oral cancer, saliva presents an ideal fluid for biomarker identification due to the close proximity to the primary tumor site, availability of exfoliated cytology samples, and accessibility to the oral cavity. Li *et al.* examined the salivary mRNA transcript profile revealing seven putative biomarkers, including several inflammatory proteins and cellular enzymes, which could distinguish OSCC from healthy controls with high sensitivity and specificity.[72] Unfortunately, the absense of pre-malignant lesions and diseased controls (e.g. periodontitis or lichen planus) in this study leaves the role for such techniques in clinical diagnostics unclear.

Other approaches for cancer biomarker detection have directly examined oral epithelial cells, which can be found in whole saliva due to natural exfoliation of surface cells, oral rinses, or in brushings to selectively sample regions of the epithelium. Epithelial brushings or scrapings have been utilized for decades to screen for cervical cancer, but have traditionally provided inconsistent results in oral cancer detection due limited sampling of basal cells. Most dysplastic changes are visible first in the basal cells and may be lost in more mature keratinized cells located near the surface; therefore, full thickness sampling is essential to yield representative findings for diagnostic purposes.[6] Use of a cytobrush reportedly provides full trans-epithelial sampling for cytomorphological analysis as described below for OralCDx® testing.[6, 76] Exfoliative

cytology samples have also been subjected to molecular analysis, including LOH, microsatellite analysis, gene expression via RT-PCR, fluorescent *in situ* hybridization, DNA aneuploidy, and immunohistochemistry in an effort to improve OSCC detection and characterization.[73, 74, 77, 78] Alternatively, use of epithelial cells naturally exfoliated in saliva may also provide diagnostic information as reported by Xie *et al.* who catalogued over 1000 proteins and 30 bacterial species from whole cells in saliva of OSCC patients.[75] Many of the markers identified have been previously characterized in cell signaling and tumorigenesis pathways suggesting that whole cells in saliva may serve as a useful diagnostic medium, although the utility of this technique for early detection remains to be determined.[75]

Despite the availability of OSCC biomarkers with diagnostic and prognostic potential, none have successfully been translated into clinical practice. Barriers to the application of biomarkers include the high complexity of many biomarker assay formats.[79] For example, genomic and proteomic techniques require large instrumentation, extensive quality control, and highly skilled technicians that are often beyond the resources of many hospitals and smaller clinics. In addition, the majority of biomarker research has focused upon OSCC rather than pre-malignancies, possibly due to a lack of availability or access to these patients and samples, which limits the development and application of biomarkers for early detection. Further, there is an immense cost associated with the development, validation, and FDA regulatory approval process for either single or multi-biomarker assays.[79] Such issues should be considered in light of the fact that the final test must remain cost-effective for both the patients and insurance companies in order to be accessible to the general public.

1.6 ADJUNCTIVE TECHNIQUES FOR ORAL CANCER DETECTION AND DIAGNOSIS

The limitations of conventional oral examination and histopathology of OPLs has spurred the development of diagnostic aids and adjunctive techniques to enhance early detection of oral cancer. The clinical role for these adjuncts includes screening for evidence of occult disease or abnormal changes and assessment of the biologic potential in clinically apparent lesions.[48] The easy accessibility to the oral cavity permits the use of relatively non-invasive procedures, such as *in vivo* light-based methods to enhance visualization of abnormal mucosa or exfoliative cytology. In the following section, particular attention is paid to techniques that are currently in clinical use and a summary of clinical studies to define the sensitivity and specificity for each method is provided in Table 1-5.

1.6.1 OralCDx® Brush Biopsy

The OralCDx® brush biopsy with computer-assisted analysis (OralScan Laboratories Inc., Suffern, NY) is an exfoliative cytology technique which utilizes a cytobrush to obtain a trans-epithelial sampling of cells from an oral lesion for morphological analysis of atypia, similar in theory to a cervical Pap test.[76] The slide-based specimens are analyzed at a central laboratory facility in New York for abnormal cellular morphology, keratinization, and relative DNA ploidy.[76] Samples are classified into four categories: (i) positive, with definitive evidence of epithelial dysplasia or carcinoma; (ii) atypical, exhibiting abnormal epithelial changes of uncertain diagnostic significance; (iii) negative, where no epithelial abnormality is detected; or (iv) inadequate, due to insufficient specimen collection.[76] The OralCDx® procedure is not intended as a replacement to surgical biopsy, rather targets examination of innocuous appearing lesions that do not warrant surgical biopsy but may harbour high-risk of malignant transformation, such as leukoplakias of unknown clinical significance.[76, 80, 81]

In a large multi-centre study, the OralCDx® brush test demonstrated high sensitivity and specificity (100% and 93% respectively), with approximately 7% inadequate specimens, for detection of atypical epithelia as confirmed by scalpel biopsy.[76] Unfortunately, in this study scalpel biopsy was not performed for all, or even the majority, of OralCDx® "negative" or "atypical" specimens possibly resulting in over-estimation of the sensitivity/specificity for this test.[48, 76] In another study by Scheifele *et al.*, in which brush and surgical biopsies were performed on all subjects, 92% sensitivity and 94% specificity for detection of dysplasia and OSCC was reported.[81] However, both of these studies included a combination of both suspicious and non-suspicious lesions which may not accurately reflect the sensitivity and specificity in strictly non-suspicious or innocuous lesions for which the test is designed.[48, 76] As such, these studies focus on the ability of the OralCDx® methodology to confirm the presence of oral cancer in patients which exhibit overt signs of carcinoma or are known to be SCC positive bringing into question the weight that should be associated with the diagnostic performance values mentioned above. Potter *et al.* further underscore the importance of the selection of epithelial lesions appropriate for OralCDx® testing as false negative results in suspicious "speckled" lesions have been reported.[82, 83]

Despite promising results of the OralCDx® test and initial interest in this new technique, widespread clinical use by dental practitioners is waning due to high rates of false positive test results (personal communication). This trend is supported by Poate *et al.* reporting a 71% sensitivity and 32% specificity using the OralCDx® system.[82] Here, the low specificity may be due to flaws in the retrospective study design or the high occurrence of false positive results associated with benign inflammatory conditions, such as lichen planus.[76, 81] The latter suggests the need for additional disease-specific

biomarkers which may be used in conjunction with brush cytology to improve molecular-level characterization of oral lesions.[81, 82]

1.6.2 OraTest® - Toluidine Blue Staining

Vital tissue staining via topical application of toluidine blue (tolonium chloride), a metachromatic dye that preferentially stains cells with elevated DNA content, has been utilized for decades to assist in identifying oral cancer sites and/or delineating margins for excisional biopsy. The literature on toluidine blue is extensive and reviewed elsewhere.[48] In one study, examination of OSCC lesions using OraTest® (formerly OraScan®, Zila Pharmaceuticals, Phoenix, AZ), a ready-to-use tolunium blue kit, yielded a high sensitivity (100%) but low specificity (62%).[84] Interestingly, sensitivity decreased dramatically (80%) for the identification of lesions exhibiting epithelial dysplasia only.[84] Similar results have been reported elsewhere using generic toluidine blue[85, 86] and suggests that although toluidine blue staining yields high sensitivity in detecting SCC malignancies, its usefulness may be limited in characterizing mild-moderate epithelial dysplasia found in oral pre-malignant lesions.[6, 84, 87]

1.6.3 ViziLite® - Chemiluminescent Device

The ViziLite® device (Zila Pharmaceuticals, Phoenix, AZ) is an oral lesion identification system that involves an oral rinse with 1% acetic acid for 1 minute followed by visual examination under chemiluminescent light. In theory, acetic acid removes the glycoprotein barrier and slightly dehydrates the oral mucosa such that neoplastic cells with an increased nuclear/cytoplasmic ratio and density reflect more light than normal mucosa and appear “acetowhite.” This effect is enhanced when visualized under chemiluminescent light at 490-510 nm wavelengths; although, glare from the light has been reported to hinder visualization as well.[88, 89] Literature reporting the efficacy of

ViziLite® in detecting oral malignant and pre-malignant lesions and the benefit of this method over current techniques is somewhat limited.[88-91] One study suggests that ViziLite® is superior to toluidine blue for detection of OSCC and epithelial dysplasia with a reported sensitivity of 100%.[90] However, ViziLite® failed to differentially identify benign conditions showing excessive keratinization and/or inflammation, generating a high false-positive rate and low specificity of 14%, which is likely to result in numerous unnecessary biopsies during follow-up.[90] Interestingly, Huber *et al.* reported the identification of one subclinical lesion with ViziLite® "acetowhite" positive results, verified as atypical using the OralCDx system, suggesting possible utility in detection of occult epithelial abnormalities.[88] The clinical value and widespread acceptance of the ViziLite® system to enhance standard visual examination remains to be determined.

1.6.4 VELscope® - Autofluorescence Visualization

The VELscope® (LED Dental Inc. Vancouver, British Columbia, Canada) is an FDA cleared hand-held device for the direct visualization of tissue fluorescence in the oral cavity. Tissue autofluorescence is produced by naturally occurring fluorophores present in epithelial cells or tissue matrix after excitation at suitable wavelengths of light, typically in the ultra violet to blue light range (<450 nm).[92] Cell or matrix constituents contributing to autofluorescence include collagen, elastin, keratin, reduced nicotinamide adenine dinucleotide (NADH), flavins (FAD^+, FMN, and riboflavin) and aromatic amino acids (tryptophan, tyrosine, and phenylalanine). Autofluorescence emitted by these endogenous fluorophores is subjected to absorption and scattering events in the tissue prior to detection or visualization, which alters the measurable autofluorescence profile.[92] Under diseased conditions, fluorophore concentrations as well as the light scattering and absorption properties of the tissue are altered due to a variety of changes in cell metabolism, blood supply, and tissue architecture (e.g. nuclear size distribution, collagen

content, and thickness of the epithelium).[92] Analysis of tissue autofluorescence has been utilized to detect cancers of the lung, bladder, gastrointestinal tract, colon, cervix, and head and neck.[92-95]

The VELscope® utilizes blue excitation light (400-460 nm) to excite endogenous green-red fluorophores present in oral epithelium whose emission in the visible range (>475 nm) can be detected by the unaided human eye. Fluorescence visualization loss (FVL), or a decrease in visible autofluorescence in this wavelength range, is found in high-risk oral premalignant lesions and SCC.[93] In a clinical study examining 50 oral lesions, using histology as the diagnostic standard, the device exhibited a sensitivity of 98% and specificity of 100% when discriminating normal mucosa from high-risk premalignancy (severe dysplasia/CIS) or invasive carcinoma.[93] In addition, the VELscope® optical device has demonstrated potential for detection of occult oral lesions in pateints previously treated for OSCC to identify second primary and recurrent tumors, as well as assessment of tumor margins to aid surgical excision.[96, 97] Although the VELscope® shows significant promise, independent studies are lacking and the results of an eight-year longitudinal study are awaited to more accurately determine device sensitivity/specificity and value in characterizing FVL in subclinical epithelial abnormalities.

Table 1-5. Summary of FDA cleared oral cancer detection devices with representative studies reporting sensitivity and specificity of each technique.

Device	FDA Clearance	Detection Method	Sensitivity	Specificity	# Patients	Reference
OralCDx	No	Brush biopsy with computer assisted analysis	100%	93%	n = 945	Sciubba *et al.*[76]
	Released to market 2000		92%	94%	n = 103	Scheifele *et al.*[81]
			71%	32%	n = 112	Poate *et al.*[82]
VELscope®	July 2006	Direct visualization of tissue autofluorescence	98%	100%	n = 50; only SCC	Lane *et al.* 2006 [93]
ViziLite	Nov 2001	Acetic acid wash and chemiluminescence	100%	14%	n = 46; only SCC	Ram and Siar 2005[90]
OraTest®	Phase III	Toluidine blue	80% dysplasia 100% carcinoma	62%	n = 102	Warnakulsauriya *et al.*[84]
			92.5%	63%	n = 59	Epstein *et al.*[85]*
			77%	67%	n = 50	Onofre *et al.*[86]*

*study used generic toluidine blue

1.7 LAB-ON-A-CHIP SENSOR BACKGROUND

Over the past decade, research efforts in the McDevitt laboratory have led to the creation of a series of powerful microchip sensor systems that have the capacity to quantitate cellular antigens and diverse analytes within complex fluids, such as whole blood, saliva, and biopsy suspensions. These miniaturized lab-on-a-chip (LOC) systems could enable rapid, highly sensitive and cost-effective *in vitro* diagnostic tests to be completed at the point-of-care where patient care is most effective. Such systems hold strong promise for a variety of important diagnostic tests including HIV immune function monitoring, and cardiac risk assessment.[1, 98]

The lab-on-a-chip sensor system employs two basic methodologies for widespread application in clinical diagnostics; the membrane-based system which is optimized for cellular analysis[1, 99-101] and the bead-based sensor designed for biochemical detection of circulating analytes.[98, 102, 103] Developed initially as an “electronic taste chip”,

the LOC bead-based platform mimics the general structure and function of the human taste bud with chemically derivatized polymer microspheres as sensing elements. The microspheres, typically ~280μm porous agarose beads, serve as three dimensional substrates for sandwich type immunoassays designed for detection and quantitation of circulating disease biomarkers, such as C-reactive protein (CRP) for cardiac risk assessment.[104] In LOC bead-based immunoassays, sensitized beads are spatially positioned in a micro-etched array of wells on a silicon wafer/chip platform such that each bead within the array is a self-contained microreactor system, with its selectivity determined by the specificity of the antibody immobilized on the bead surface. The bead-filled microchip is placed between two optically transparent polymethyl-methacrylate (PMMA) inserts, with machined fluid inlet and outlet ports, and fitted within a custom metal housing or "flow cell". The trans-wafer openings allow for reagent and sample solutions to be delivered to each chamber as well as provide optical access to the chemically sensitive microspheres for fluorescent or colorimetric detection. Such bead-based sensor systems have been characterized for assessment of cardiac risk, acute myocardial infarction (AMI), and periodontitis using single or multiple biomarker panels with significant implications toward clinical diagnostics.[98, 104, 105] In addition, bead-based immunoassays are currently being explored for their capacity to detect and quantitate cancer biomarkers such as carcinoembryonic antigen (CEA) and cancer antigen-125 (CA-125) from serum and/or saliva as a non-invasive method for cancer detection and screening.

Along with the bead-based sensor arrays, a membrane-based sensor platform has been developed for analysis of whole cells. In this system, the microspheres and silicon microchip are replaced with a size-selective membrane, which functions as a micro-sieve to capture and screen cells from biological fluids or biopsy suspensions. Once captured,

cells are analyzed for protein and/or nucleic acids using assay-specific fluorescent labeling techniques. This novel mechanical entrapment approach has been employed in the context of online detection of bacillus spores in mail-handling facilities as well as for the enumeration of human CD4+ lymphocytes from whole blood samples.[1, 99]

Building upon the established tool-kit of diagnostic sensors, this dissertation outlines the development and application of membrane-based LOC sensor methodologies for single-cell analysis of OSCC biomarkers in exfoliative cytology specimens. This biological system presents unique challenges not previously encountered, particularly in the analysis of adherent epithelial cells which are irregularly shaped (non-spherical) and may remain in adherent clusters following collection. Although oral cancer is targeted, the techniques and methods developed here may be applicable toward screening other epithelial malignancies where exfoliative cytology or fine-needle aspiration specimens are available such as lung, breast, ovarian, and prostate cancer.

1.8 SUMMARY AND DISSERTATION OVERVIEW

The preceeding sections detail the clinical need and challenges associated with early detection of oral cancer and characterization of high-risk premalignant oral lesions, particularly leukoplakia. Ironically, oral cancer is well suited for early detection and advanced screening techniques due to the presence of pre-malignant changes that are visible in the oral epithelium and the easy accessibility to the oral cavity. Yet, visual examination alone is insufficient for early detection and while several adjunctive devices are currently available, they have demonstrated restricted, or in some cases un-tested, capacity to identify high-risk premalignant oral lesions. Suprisingly, none of these devices capitalize upon the diagnostic potential of emerging cancer biomarkers which may be detected during early stages of tumorigenesis and offer opportunities for increased sensitivity and specificity, particularly when used in multi-marker panels. The

high cost and complexity of many biomarker assay formats, along with the need for highly skilled technicians and long assay times, may deter their widespread application in cancer diagnostics and screening. Thus, new approaches toward OSCC biomarker detection are needed.

The membrane-based LOC sensor approach to early detection of oral cancer utilizes a combination of molecular and morphological markers of malignancy in non-invasive exfoliative cytology specimens. While morphological changes may occur relatively late during tumorigenesis, they form the basis for traditional cytopathologic examination which have long been established. This may allow potentially cancerous cells to be identified using standard morphological features and directly correlated with biomarker expression on a single-cell basis for discriminate analysis in a heterogeneous mixture. Further, this dual molecular and morphological approach encompasses a wide range of tumor phenotypes, potentially increasing sensitivity and specificity over conventional methods. As such, this dissertation strives to test the hypothesis that the membrane-based LOC sensor system can provide a suitable platform for detection of OSCC and high-risk oral pre-malignant lesions using well-established features of dysplasia, including increased nuclear size and nuclear-to-cytoplasm ratio, alone or in combination with the EGFR biomarker. The research objective here is not for discovery of new OSCC biomarkers, but to utilize previously characterized biomarkers in the LOC sensor as a validation tool that may facilitate clinical translation into effective diagnostics. Likewise, the overall aims of the work are two-fold: (1) to develop a general system for biomarker analysis that allows us to begin asking questions regarding the use of individual and multiple biomarkers to enhance early tumor detection and (2) to provide proof-of-concept support for the clinical application of the LOC sensor system in oral cancer diagnostics. With the development of a new diagnostic technique, a number of

questions must be addressed regarding the structure and design of the sensor, selection of biomarker inputs, detection modality, accuracy of detection by comparison with currently available techniques, and potential role in clinical practice. Points of focus for the dissertation include the following:

- Can microsensor systems be used to acquire useful information about the clinical status of oral cancer patients?
- What are the structure and design elements of cell capture systems that can be included in a microchip sensor systems targeted for oral cancer screening and diagnosis?
- What are the best modes to introduce the samples into the microchip?
- What are the best assay conditions to provide optimal sample visualization?
- What are the challenges and opportunities that are presented in the microchip cell analysis as applied to oral cancer diagnosis?
- Is it possible to include both morphological and molecular diagnostic information into the microchip cell analysis as applied to oral cancer diagnosis?
- What are the best biomarkers to be included in the microchip cell analysis as applied to oral cancer diagnosis?
- How do the microchip sensors systems compare to macro systems, like flow cytometry, for cell analysis?
- How do the microchip sensors systems compare to standard histopathology and cytopathology methods?
- What is the diagnostic accuracy of microchip cell assays as applied to oral cancer diagnosis?

- Can the microchip cell be used to screen for early signs of malignant transformation and cancer?
- Can these noninvasive devices be used to provide information about cancer field growth?

This research aims to contribute toward the science base that will enable the development of molecular diagnostic tools for early detection of oral cancer and other malignancies. The following chapter details the design and instrumentation employed for cellular analysis in the LOC sensor. In addition, the development and optimization of a proof-of-principle assay for the EGFR biomarker is described using *in vitro* tumor-derived cell lines as models of malignant transformation. Conventional assay techniques served as a standard for LOC assay development with respect to intensity, homogeneity, and cellular localization. The efficacy of the LOC sensor for characterization of EGFR overexpression in three oral cancer cell lines is examined and directly compared with the "gold standard" technique for protein expression analysis, flow cytometry. Quantitative flow cytometry further served to ascertain the absolute number of EGFR receptors per cell in each cell line, providing a basis for relating significant differences between oral cell lines identified using the LOC sensor.

Once it was established that the microchip sensor serves as a suitable platform for rapid, highly sensitive biomarker assays, the examination of cells from more clinically relevant sources was necessary. Chapter 3 serves to probe the conditions and adaptations necessary for the integration of exfoliative cytology specimens into the microchip sensor. The methods for obtaining and validating the quality of exfoliative cytology specimens were explored with particular considerations toward each phase of sample collection, processing, dissociation, and fixation in order to maintain compatibility with the previously established EGFR biomarker assay. In addition, factors affecting the capture

and dispersal of adherent epithelial cells across the membrane in the LOC sensor were investigated and optimized until a relatively homogeneous distribution was obtained. The supplemental use of Phalloidin and DAPI fluorescent stains as cytoplasmic and nuclear markers, respectively, served to expand the capacity of the LOC sensor for morphometric examination of cell and nuclear area, as well as nuclear to cytoplasmic ratio. These new markers presented additional requirements for multi-spectral imaging using X, Y, and Z-scan patterns which were further explored along with automated image analysis routines to obtain quantitiative measurements of biomarker expression and cytomorphometry. This work served to establish and refine the methods for cell-based assays in the microchip sensor using clinically relevant cytology specimens for the analysis of molecular and morphological parameters which could then be applied toward characterization of malignancy.

Chapter 4 presents the initial results of a collaborative pilot study to examine the clinical utility of the LOC sensor for identification of oral cancer and high-risk premalignant lesions. The differences in EGFR expression and cytomorophometry were examined in normal healthy mucosa, non-dysplastic benign lesions, pre-malignant lesions exhibiting mild/moderate/severe dysplasia, and in SCC tumors. Particular attention was focused upon the value of EGFR biomarker expression, as well as the nuclear area and distribution, in discriminating normal epithelium from dysplasia and SCC, either alone or in combination using logistic regression and ROC curve analysis. When contralateral or "mirror-image" brush biopsies were available, they served to provide insight regarding the presence of field changes in the mucosal epithelium and their relevance toward early detection and/or monitoring. The overall performance characteristics of the microchip sensor were evaluated, including sensitivity and specificity, for comparison with conventional oral examination and other diagnostic adjunctive devices to define the

clinical role of the LOC sensor assays described herein and the necessity for additional biomarker validation.

Collectively, the body of work in this dissertation lends itself to addressing the clinical need for new diagnostic methods targeting early OSCC tumor progression through the molecular evaluation of tumor biomarkers using a microchip sensor. Such biosensor systems may then be utilized as a clinical or translational tool to assess the strength of particular biomarkers, alone or in multi-marker panels, for detection of disease and possibly prediction of tumor behavior. Ultimately, this research aims to contribute toward the growing field of in vitro diagnostics using lab-on-a-chip and microfluidic techniques which may impact human healthcare by increasing the availability and access to diagnostic tests enhancing patient care and survival.

Chapter 2: Development of LOC Sensor Assay for Analysis of EGFR Biomarker Expression in OSCC Cell Lines[1]

2.1 INTRODUCTION

In the current chapter the development and optimization of an immunoassay for the epidermal growth factor receptor (EGFR) using LOC sensor techniques is presented. The purpose of this chapter is to evaluate and define the appropriate sensor design elements, as well as the assay and imaging parameters, relevant to the cellular analysis capability of the LOC sensor system. Toward this goal, *in vitro* tumor-derived cell lines are employed as models of malignant transformation in which EGFR expression can be characterized using standard immunophenotyping techniques for methods comparison and correlation with the microchip sensor. This chapter is organized in the following manner, beginning with background information on the function of the EGFR and its role in tumorigenesis. The LOC sensor platform is described along with the "on-membrane" EGFR assay development and optimization methods. The homogeneity, localization, and labeling times in the microchip sensor will be explored and directly compared with conventional immunolabeling techniques. The capacity of the LOC sensor for characterization of biomarker expression in OSCC tumor-derived cell lines will be evaluated by direct comparison and correlation with flow cytometry.

The epidermal growth factor receptor has emerged as a prominent biomarker whose overexpression has been characterized in a number of epithelial malignancies occurring in the lung, breast, head and neck, glioma, colon, bladder, and ovary.[106, 107] EGFR (also known as erbB-1 or HER1) is a 170-kDa transmembrane protein belonging

[1] Portions of this chaper have been published previously in Weigum, S.E., Floirano, P.N., Christodoulides, N., and McDevitt, J.T. 2007. Cell-based Sensor for Analysis of EGFR Biomarker Expression in Oral Cancer. *LabChip*. **7**(8), 995-1003.

to the *erbB*/HER family of receptor tyrosine kinases. Structurally, EGFR consists of an extracellular N-terminal ligand-binding domain with two cysteine rich regions, a membrane spanning domain, a juxtamembrane regulatory domain, and an intracellular C-terminal domain containing protein kinase activity and multiple phosphorylation sites.[108] A variety of ligands can bind EGFR receptors including epidermal growth factor (EGF), transforming growth factor-α (TGF-α), amphiregulin, heparin-binding EGF-like growth factor, betacellulin, and epiregulin.[109, 110] Upon ligand binding, the EGFR receptor dimerizes, forming either homo- or hetero-dimers with other *erbB*/HER family members, which in turn stimulates autocatalytic tyrosine kinase activity. Activated EGFR subsequently recruits and trans-activates cytoplasmic signaling complexes that initiate downstream signal transduction pathways, such as the *ras*-mitogen activated protein kinase (MAPK) pathway, signal transducers and activators of transcription (JAK/STAT) pathway, phosphatidylinositol-3-kinase (PI3K)-Akt pathway, and phospholipase C gamma (PLC-γ) pathway. These pathways regulate transcription of powerful oncogenes involved in cell proliferation, differentiation, survival (protection from apoptosis), angiogenesis, adhesion, and migration (Figure 2-1).[106, 108]

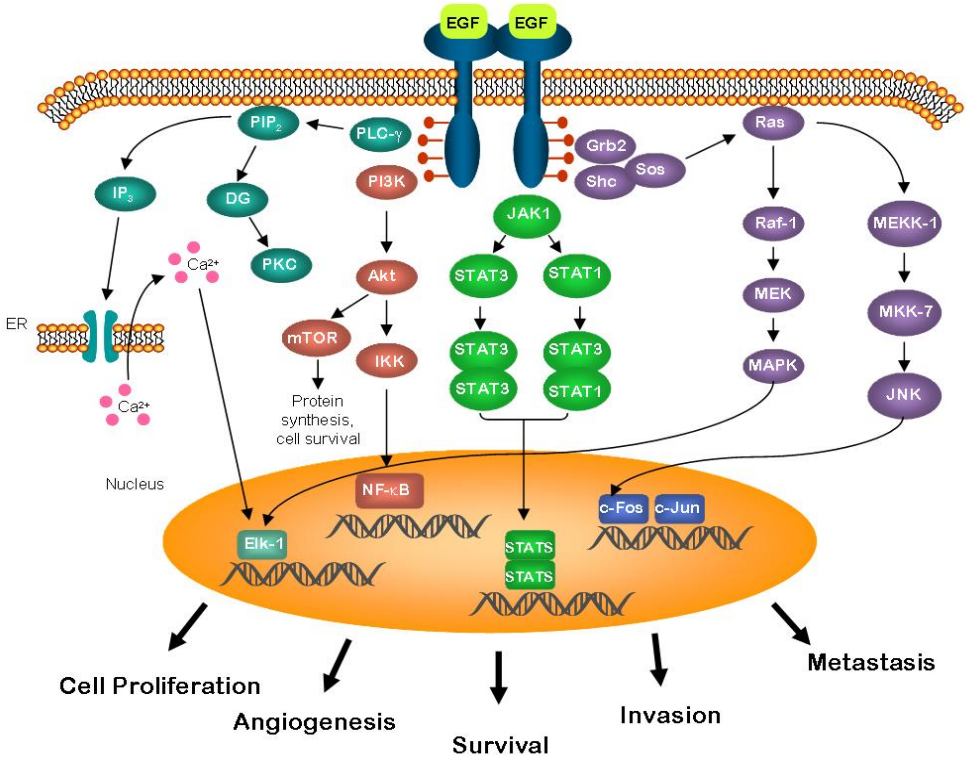

Figure 2-1. General schematic of EGFR signal transduction following ligand binding and receptor dimerization. Pathways involved include Ras/MEK/MAPK pathway (purple), JAK/STAT pathway (green), PI3K-Akt pathway (red), and PLC-γ pathway (blue) resulting in transcriptional activation of oncogenes promoting tumor cell growth and proliferation, angiogenesis, survival (anti-apoptosis), invasion, and metastasis.

Alterations in EGFR and its signaling pathways have been directly linked with malignant transformation and uncontrolled cell growth in a variety of epithelial and non-epithelial cancers.[106] Mechanisms include genetic mutation, over-expression of the receptor and/or ligands, structural rearrangement, or loss of inhibition and regulatory constraints. The oncogenic effect of these alterations is attributable to excessive EGFR activity in either a ligand dependent or independent manner. For example, a truncated EGFR mutant (EGFRvIII) containing a 268 amino acid deletion in the extracellular domain has been identified in up to 40% of glioblastomas, as well as cancers of the

breast, lung, ovary, and prostate.[111, 112] This EGFRvIII mutant exhibits constitutive activity functioning in the absence of ligand binding and has been associated with enhanced pathogenicity and chemotherapeutic resistance.[111, 112]

2.1.1 EGFR in Oral Cancer: Diagnostic and Prognostic Significance

EGFR has been extensively studied in the pathogenesis of oral cancer with significant implications toward diagnosis, prognosis, and treatment selection. Overexpression of both EGFR and its ligand, TGF-α, are common in head and neck squamous cell carcinomas (HNSCC) as demonstrated by elevated mRNA levels in 92% and 87% of tumors, respectively.[70] EGFR protein overexpression has also been reported in 34-80% of HNSCC tumors detected using immunohistochemistry (IHC).[58, 70] This overexpression is primarily due to epigenetic mechanisms where transcriptional activation becomes dysregulated resulting in increased mRNA synthesis and decreased downregulation.[70, 110] EGFR gene amplification appears to play only a minimal role in EGFR overexpression in HNSCC.[113] Site-specific differences in EGFR expression occur within the general category of head and neck SCC where laryngeal tumors demonstrate reduced EGFR expression compared to those in the pharynx and oral cavity.[108]

Two lines of evidence suggest that EGFR overexpression occurs early during tumorigenesis: (i) presence in pre-malignant or dysplastic lesions and (ii) presence in clinically normal tissue adjacent to SCC tumors. Shin *et al.* demonstrated a two-step increase in EGFR protein expression where EGFR was elevated 2-fold in dysplastic, hyperplastic and normal tissue adjacent to SCC tumors above healthy control tissue.[114] A second significant increase was observed at the transition from dysplasia to SCC.[114] In agreement with this finding, Grandis *et al.* reported 29-fold increase in EGFR mRNA in histologically normal tissue from SCC patients and up to 69-fold increase in SCC tumors compared to normal control mucosa. Here, EGFR expression increased according to the

degree of epithelial dysplasia and distance from the primary tumor site suggesting that EGFR may be a useful diagnostic marker of early tumor progression. These findings also provide support for field cancerization where tobacco and alcohol "pre-condition" the epithelium toward hyperproliferation or high-risk reactive changes mediated via EGFR activity.

Due to the central role of EGFR in promoting cell growth, it is reasonable to think that elevated EGFR activity could be related to aggressive tumor growth and repopulation following treatment. Therefore, EGFR has also been investigated as a prognostic marker for identification of OSCC patients with a high-risk of disease relapse and death, as well as therapeutic resistance. Indeed, several studies have associated EGFR overexpression with a reduction in disease-free survival and overall survival, suggesting utility as negative prognostic indicators either alone or in combination with additional markers.[71, 115-118] However, other studies have not found EGFR expression to be correlated with clinicopathological features or survival leaving the prognostic utility of EGFR unclear.[119, 120]

Interestingly, upregulation of EGFR activity has also been shown to occur in response to ionizing radiation such that tumors overexpressing EGFR may demonstrate increased resistance to chemotherapeutic agents and radiotherapy. This implies that EGFR status may aid in the selection of the optimum treatment and radiation scheduling. In HNSCC patients with high EGFR expression, Bentzen *et al.* reported a significant benefit in locoregional control from accelerated hyperfractionated radiotherapy, which in theory allows less time between treatments for tumor repopulation, over conventional fractionated therapy.[121] Thus, as a biomarker EGFR may not only provide useful diagnostic information but enhance prognostic evaluation and treatment selection in patients with SCC, particularly for new EGFR molecular therapeutics in development.

2.1.2 EGFR-Targeted Treatment

The pivotal role of EGFR in promoting tumor growth and malignant transformation make EGFR an excellent target for therapeutic intervention. EGFR targeted cancer therapies currently under investigation utilize immunotoxins, monoclonal antibodies, tyrosine kinase inhibitors, and antisense oligonucleotides to inhibit EGFR activation and signaling.[69, 106, 122] In fact, the monoclonal antibody cetuximab (Erbitux, ImClone Systems Inc., New York, NY) is the first new drug to receive FDA approval for treatment of OSCC in over 45 years.[123] Cetuximab is a chimeric mouse and human IgG_1 antibody that attaches to the extracellular domain of EGFR, thereby inhibiting ligand binding and receptor activation. In combination with radiotherapy, cetuximab increased the duration of locoregional control by 11 months and improved overall survival by 20 months, thereby increasing the 2-3 year survival rates in patients with locoregionally advanced HNSCC without significantly increasing the incidence of severe (grade 3-5) toxicities.[124, 125] Although this treatment appears promising, efficacy of cetuximab plus radiation as compared to standard chemoradiotherapy (CRT) remains to be determined.[125, 126] Further, challenges remain to identify patients who may benefit most from this targeted therapy (i.e. patients with tumors that overexpress EGFR).

2.1.3 Clinical Role for EGFR Biomarker Detection

EGFR is one of the most well characterized biomarkers in OSCC that holds enormous diagnostic potential for early tumor detection and characterization of high-risk pre-malignant lesions. In addition, its association with poor prognosis suggests that EGFR characterization at the time of diagnosis may help to identify patients with high risk of recurrence and metastasis who may benefit from more aggressive treatment. Thus, EGFR biomarker detection in OSCC may fill multiple roles in cancer diagnostics, not only for early detection but at the time of diagnosis for prognostic evaluation and

treatment selection. The research presented herein describes the development of a lab-on-a-chip sensor assay for EGFR biomarker detection using a novel membrane-based immunoassay technique and quantitative fluorescent image microscopy/analysis. Using EGFR as a proof-of-principle biomarker, general methods will be established that may be applied toward detection of additional clinically relevant OSCC biomarkers. Ultimately, this research program aims to impact human healthcare by providing a rapid, cost-effective molecular diagnostic tool for early detection, assessment of risk, and prediction of therapeutic response in OSCC tumors which may improve patient prognosis and survival.

2.2 EXPERIMENTAL METHODS

2.2.1 Sensor Design and Instrumentation

The cell-based LOC sensor is a multi-layered structure built upon a 22 x 30 x 8.6 mm poly-methyl methacrylate (PMMA) base containing a 1mm diameter, round fluid inlet and outlet port (Figure 2-2a) (design and machining specifications are provided in Appendix A). A polycarbonate track-etched membrane, or screen filter, with 0.4μm pores (#HTBP01300, Isopore™ Millipore, Billerica, MA) (Figure 2-2c) and underlying support were embedded within the base, sealed with laminate adhesives containing a precision cut fluid delivery channel and topped with a glass coverslip. Laminate cut-out structures were created using SolidWorks® 3D CAD software and cut at 25 μm resolution using a SummaCut D-60 vinyl plotter cutter. Dimensions of the fluidic channel are 1 mm wide by 125 μm high by 8.2 mm long generating a channel volume of 1.1 μl. The circular membrane capture area and imaging window is 5 mm in diameter by 200 μm high resulting in a reaction volume of 3.9 μl above the membrane surface. Fluid and sample delivery was facilitated by a peristaltic pump with 6-port injection valve at flow rates

between 250µl/min-725µL/min. Cells retained on the surface of the membrane using this straightforward filtration mechanism were analyzed for protein and/or nucleic acids using assay-specific fluorescent labeling techniques as described below. Efficiency of membrane capture is dependent upon the ratio of particle size, or in this instance cell size (typically 10 µm), to membrane pore size (0.4 µm). According to the manufacturer, greater than 99% capture efficiency is obtained for particles exceeding the membrane pore size of 0.4 µm.

Digital micrographs were obtained in an (X, Y) membrane scan using a 20X (0.4 NA) or 10X (0.3 NA) objective, on an automated Olympus BX-61 modified epifluorescent microscope with motorized X,Y,Z stage (Prior, Rockland, MA), and 12-bit monochrome CCD camera (Q-Imaging, British Columbia) controlled via Simple PCI software (Compix Inc., Sewickley, PA). Automated image analysis was performed using ImageJ (v1.38e)[127] open-source software with custom written macros for quantitative intensity standardization and cell contouring to identify and define the boundaries of individual cells for measurement. As field illumination with Hg light sources is often non-uniform, the field uniformity was measured using FITC/GFP Fluor-Ref reference slide (Microscopy Education, Allen, TX) with homogeneous intensity. Typically the variation in field uniformity was 5.5% (mean intensity 145.4 ± 8.34) with the brightest intensity located at the center of the field and slightly dimmer at the edges. Thus, all fluorescent images were shade corrected to eliminate these variations according to Varga *et al.*[128] using the equation:

$$I'_{x,y} = I_{x,y} * W_{mean}/W_{x,y}$$

where I' and I are the corrected image and the original image respectively; W is the bright (or white) reference image and x,y denotes the pixel location in each image. Relevant objects in each field were then identified using a basic screen according to size and

intensity to generate individual 8-bit single-object images. Next, auto-segmentation with an Otsu thresholding algorithm was performed to define the intensity contour and area-of-interest (AOI) of each object followed by local background subtraction and watershed algorithms to separate touching objects. Measurement parameters included AOI area, perimeter, circularity, minimum and maximum intensity, mean, standard deviation, mode, and integrated intensity. For statistical analysis, data was exported to Microsoft® EXCEL® with Analyse-It® (Analyse-It Software Ltd., Leeds, UK) software and SigmaPlot 9.0 (Systat Software Inc., San Jose, CA) for graphical representation.

2.2.2 In vitro cell culture

Three human oral tumor-derived cell lines were utilized in this study including A253 adenocarcinoma from the submaxillary saliva gland, obtained from the American Type Culture Collection (ATCC); SqCC/Y1 from the bucal mucosa; and UMSCC-22A from the hypopharynx, both squamous cell carcinomas generously provided by Dr. Rebecca Richards-Kortum at Rice University. Cells were maintained in recommended culture media (McCoy's 5A, DMEM-F12, and EMEM respectively) containing 1.5 mM – 2.5 mM L-glutamine, 10% fetal bovine serum and 50μg/mL penicillin/streptomycin at 37^{O}C with 5% CO_2 in a humidified environment. Two breast adenocarcinoma cell lines, MDA-MB-468 and MDA-MB-435S (ATCC), were maintained in Leibovitz's L-15 media, supplemented as above, at 37^{O}C under atmospheric conditions. All cells were seeded at 0.5-1x10^4cells/cm^2 in T-75 flasks and allowed to grow for 3-5 days until cells reached ~80% confluency. Adherent cells were harvested using 0.25% Trypsin/EDTA solution, washed twice in 3mL PBS (BupH™ Modified Dulbecco's Phosphate Buffered Saline, #28374, Pierce/Thermo Fisher Scientific, Rockford, IL) by centrifugation at 150g for 5 minutes and fixed in 1mL Histochoice™MB fixative (Electron Microscopy

Sciences, Hatfield, PA) for 20 minutes at room temperature then stored at $4^{O}C$ for up to two weeks.

2.2.3 Flow cytometry and pre-labeling EGFR protocol

EGFR labeling was performed using an indirect flow cytometry protocol for cell surface antigens as previously described by Hsu *et al.*[129] Briefly, 1-2x10^6 cells were incubated in anti-EGFR mouse monoclonal antibody (10µg/ml in PBS with 0.1% BSA, LabVision/Thermo Fisher Scientific Inc., Waltham, MA) for 1 hr. at room temp. followed by goat anti-mouse IgG $F(ab')_2$ conjugated to AlexaFluor®488 (20µg/ml in PBSA, Molecular Probes, Eugene, OR) for 45 minutes. Intermediate washing was carried out twice in 2 mL PBSA by centrifugation at 150xg for 5 minutes. Negative controls replaced anti-EGFR with an irrelevant antibody of the same isotype (10µg/ml Mouse IgG_1 in PBSA, Sigma, St. Louis, MO). Optimal primary and secondary antibody concentrations for use in flow cytometry and LOC assays were determined by titration. All labeled cell samples were analyzed on a Beckman Coulter FC500 flow cytometer or delivered directly to the LOC sensor serving as "pre-labeled" samples for comparison of immunoassay techniques.

2.2.4 Assay development in LOC sensor

In order to determine the optimal assay parameters for "on-membrane" labeling within the LOC sensor, an intensity curve was generated using A253 cells incubated for various time periods (0.2-2 minutes) in primary and secondary antibodies with a 2 minute intermediate buffer wash. Incubation time was manipulated by increasing the antibody sample loop size from 50-500µl while maintaining a constant flow rate of 250µl/min to avoid introducing variations in flow dynamics within the microfluidic channels and membrane chamber. Mean EGFR intensity was expressed as a percentage of the intensity

obtained from pre-labeled A253 cells imaged and analyzed in LOC sensor under the same conditions. All assays were performed in triplicate with matched isotype controls.

In order to ensure homogeneous labeling across the membrane surface, the sample distribution and variation in integrated intensity of bead standards labeled in LOC sensor versus those pre-labeled in centrifuge tube was examined. Bead standards were obtained from QIFI quantitative flow cytometry kit (see below) set solution. Data acquisition and analysis was performed as described using a 10X objective with a 4x4 raster pattern scan of 11.4 mm^2 of the membrane surface area. Events were gated according to ROI area and max pixel intensity followed by single-parameter histogram analysis of log-transformed integrated intensity values to obtain the geometric mean and CV of each population.

2.2.5 EGFR in tumor cell lines

Capacity of the LOC sensor to detect EGFR overexpression was examined in oral tumor cell lines using the membrane-based sensor immunoassay protocol above. The MDA-MB-486 cells known to overexpress EGFR at approximately $1x10^6$ receptors/cell[129, 130] served as a positive immunolabeling control while MDA-MB-435S cells which express no or low levels of EGFR served as a negative control.[130-132] Data acquisition and analysis was performed as described using a 20X objective with a 5x10 scan pattern covering 9.12 mm^2 membrane area. Integrated intensity data was not normally distributed; therefore, log transformation was applied to data prior to statistical analysis and presented in original scale for convenience. Mean integrated intensity values of triplicate biomarker assays were reported and 1-way pairwise ANOVA performed to determine statistically significant ($p < 0.05$) differences among cell populations. Parallel cell samples were labeled and analyzed via standard flow cytometry. Correlation of mean fluorescent intensity (MFI) obtained from flow cytometry and LOC sensor (calculated as

the mean of all integrated intensity values for a single cell population in LOC data) was assessed using linear regression with 95% confidence interval.

2.2.6 Quantitative flow cytometry

Quantitative flow cytometry using QIFIKIT® (#K0078, Dako Cytomation, Denmark) was performed on all cell lines to determine how many receptors per cell were being labeled. The QIFIKIT® consists of a series of bead standards with defined amounts of anti-CD5 monoclonal antibody immobilized on the surface to mimic cells labeled with primary antibody to surface antigens. Binding of fluorescently labeled secondary antibodies generated an intensity calibration curve from which the number of receptors per cell was interpolated. Bead standards and cell samples were labeled in parallel under the same conditions according to the flow cytometry protocol above. Data acquisition and analysis, including linear regression of calibration curve and calculation of antigen density, was completed according to manufacturer's instructions.

2.3 RESULTS

2.3.1 Membrane Cell Capture

The LOC sensor utilized an embedded size-selective membrane, functioning as a microsieve, to capture and screen epithelial cells from culture suspensions (Figure 2-2a). The flow-through design allowed cell samples and reagents to enter through the side inlet in the PMMA base; from here, fluid traveled up to the adhesive layers where a narrow channel directed fluid over the membrane then out using a bottom drain (Figure 2-2b). Cell capture was verified by scanning electron microscopy (SEM) of the membrane surface (Figure 2-2c). Once captured, cells retained on the membrane were available for protein expression analysis using assay-specific fluorescent labeling. This simple yet

elegant integrated microfluidic system is shown to be functional for both cell collection and cell staining steps as described below.

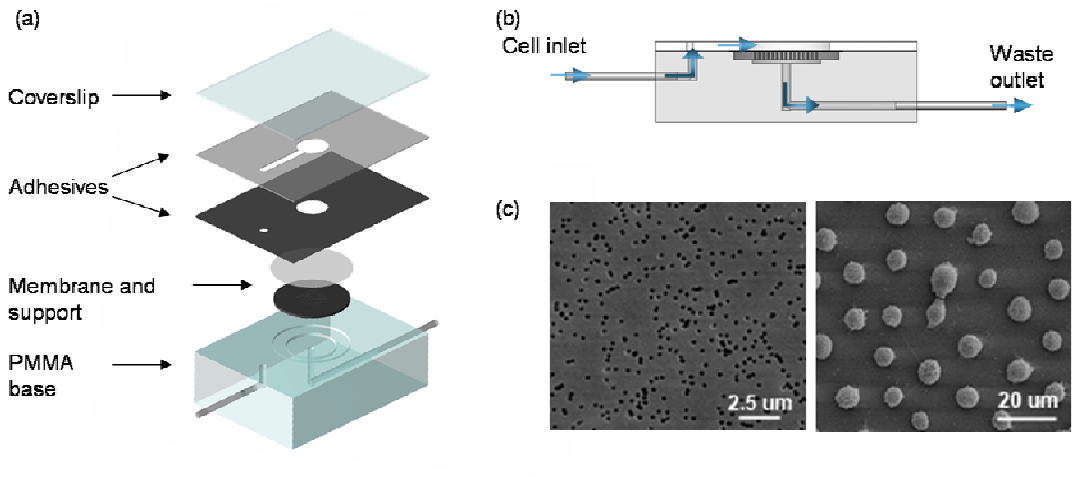

Figure 2-2. Structure of membrane-based LOC sensor. (a) Schematic diagram of layered LOC device with embedded track-etched membrane designed for cellular capture, imaging and analysis. (b) Cross-section view shows continuous fluid flow path supporting cell capture and delivery of reagents for "on-membrane" assays. (c) SEM micrograph of a LOC sensor 0.4μm track-etched membrane section before (left) and after (right) cell capture.

2.3.2 EGFR Biomarker Assay in LOC Sensor

Mean fluorescence intensity of oral cancer cells immunolabeled in the LOC sensor for EGFR biomarker at increasing antibody incubation times under saturating conditions is demonstrated in Figure 2-3a. At a constant flow rate of 250μl/min, 2 minutes of sequential primary and secondary antibody incubation resulted in an EGFR labeling intensity of 110 ± 10 percent of pre-labeled EGFR intensity. Thus, these conditions were established as the optimal sensor immunolabeling parameters comparable to standard protocols. Ultimately, the EGFR assay was established in the LOC sensor as follows: (1) cell capture of 5,000-10,000 cells at 725μl/min for 1 min.; (2)

PBS wash for 2 min.; (3) 10μg/ml anti-EGFR at 250μl/min for 2 min.; (4) PBS wash for 2 min.; (5) 20μl/ml AlexaFluor-488 conjugate at 250μl/min for 2 min. immediately followed by automated imaging and analysis.

A surface plot of cell subsets from the LOC sensor assay at 2 min. and pre-labeled cells further demonstrates equivalent EGFR intensity obtained using the "on-membrane" sensor immunolabeling technique (Figure 2-3b). In addition, the surface contour reveals cellular localization of EGFR primarily at the cell surface, as expected for a membrane-bound receptor, using both methods. Direct comparison of immunolabeling schemes exhibits a greater than 10-fold reduction in assay labeling time using the integrated microfluidic cell collector-detector methodology. Here EGFR biomarker detection was completed in 9 minutes, which accounts for cell capture, antibody incubation, and brief buffer washes between reagents, whereas the pre-labeling/flow cytometry protocol required 2 hrs and 5 min (Figure 2-3c).

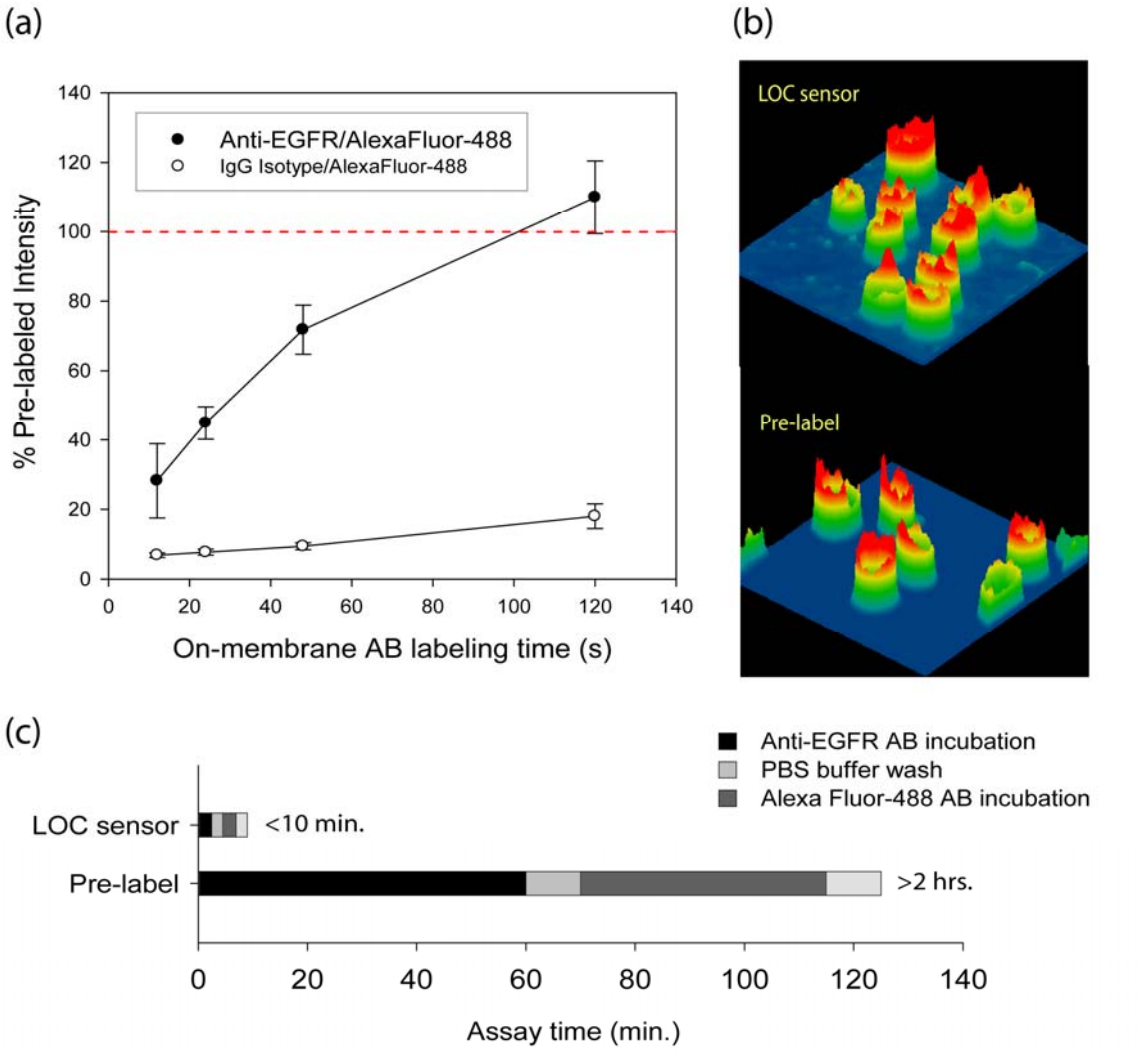

Figure 2-3. Optimization of EGFR immunoassay in LOC sensor. (a) Line graph of EGFR fluorescent labeling intensity obtained using LOC sensor "on-membrane" staining of A253 cells at various antibody incubation times from 10-120 seconds. Results are expressed as a percentage of the EGFR intensity found when cells were pre-labeled according to a standard flow cytometry protocol. (b) A surface intensity plot of select cells from the LOC sensor assay at 120 seconds (top) and pre-labeled cells (bottom) shows relative EGFR intensity and membrane localization. (c) Bar graph comparing stepwise immunolabeling time in LOC sensor and pre-label protocol.

2.3.3 Homogeneous Labeling in Sensor

With the "on-membrane" sensor immunoassay technique it is important that all cells are adequately labeled regardless of their spatial location on the membrane. In order to assess labeling spatial homogeneity, single-parameter intensity histograms of EGFR pre-labeled bead standards versus those labeled within LOC sensor were examined (Figure 2-4). A gating scheme, similar to those utilized in flow cytometry, was implemented according to visual observation of a 2-D scatter plot using area and maximun pixel intensity parameters as demonstrated in Figure 3 inset. Here, a large cluster of measured objects are clearly seen near an area of 200 pixels with a smaller cluster found at 400 pixels, approximately double, suggesting the presence of bead doublets that were not separated during image processing. This finding was confirmed by tracing individual measurements in each of these two populations back to the original LOC images as shown. Thus, data was filtered according to user-established area and max pixel intensity thresholds in order to exclude these doublets and higher level aggregates along with debris, from each data set for further calculations. Comparison of the histogram CVs, which provide a measure of variation within each sample population, shows narrow peak distributions with a slightly lower CV found for the LOC sensor labeled beads (1.7%) versus beads pre-labeled in centrifuge tube (2.1%) (not analyzed for statistical significance). Hence, the LOC sensor provided homogeneous immunolabeling of the bead population across the membrane surface comparable to current in-tube labeling methods.

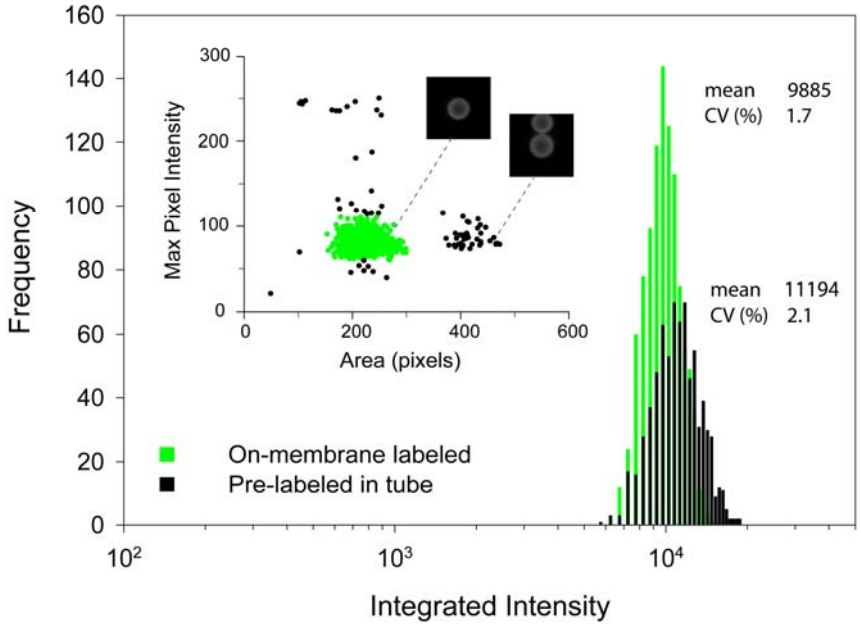

Figure 2-4. Frequency histograms of bead standards labeled "on-membrane" in LOC sensor (green) and pre-labeled in centrifuge tube (black overlay) for comparison of immunolabeling homogeneity in the microchip sensor versus conventional methods. A rectangular gate according to object area and max pixel intensity (inset) was utilized in order to eliminate debris and bead doublets from histogram analysis and statistics which was verified using raw images of events, or in this case beads. The geometric mean and CV are reported for each population containing approximately 1000 events each.

2.3.4 EGFR in OSCC Cell Lines

Fluorescent micrographs of EGFR detected in tumor cell lines using the LOC sensor are presented in Figure 2-5a. Visually, EGFR expression was demonstrated in all oral cancer cell lines (ii-iv) and in MDA-MB-468 cells (i) known to overexpress EGFR. The MDA-MB-435S cells, previously reported to express no or very low levels of EGFR, demonstrated slight staining intensity (v) while isotype controls were indistinguishable from background fluorescence (vi). Subsequent automated image analysis revealed quantitative differences in EGFR intensity with significantly elevated levels found in

MDA-MB-468, A253, SqCC/Y1, and UMSCC-22A cells compared to MDA-MB-435S negative control cells (Figure 2-5b). The three oral cancer cell lines appeared to cluster at similar EGFR expression levels, although A253 cells exhibited a significant increase 1.5-fold over UMSCC-22A cells. In order to validate the LOC sensor assay methodology, parallel cell samples were stained and analyzed using flow cytometry, the gold standard in cellular protein expression analysis. The lab-on-a-chip sensor EGFR immunassay results displayed a high degree of correlation ($r^2 = 0.98$) with 95% confidence interval to conventional flow cytometry (Figure 2-5c).

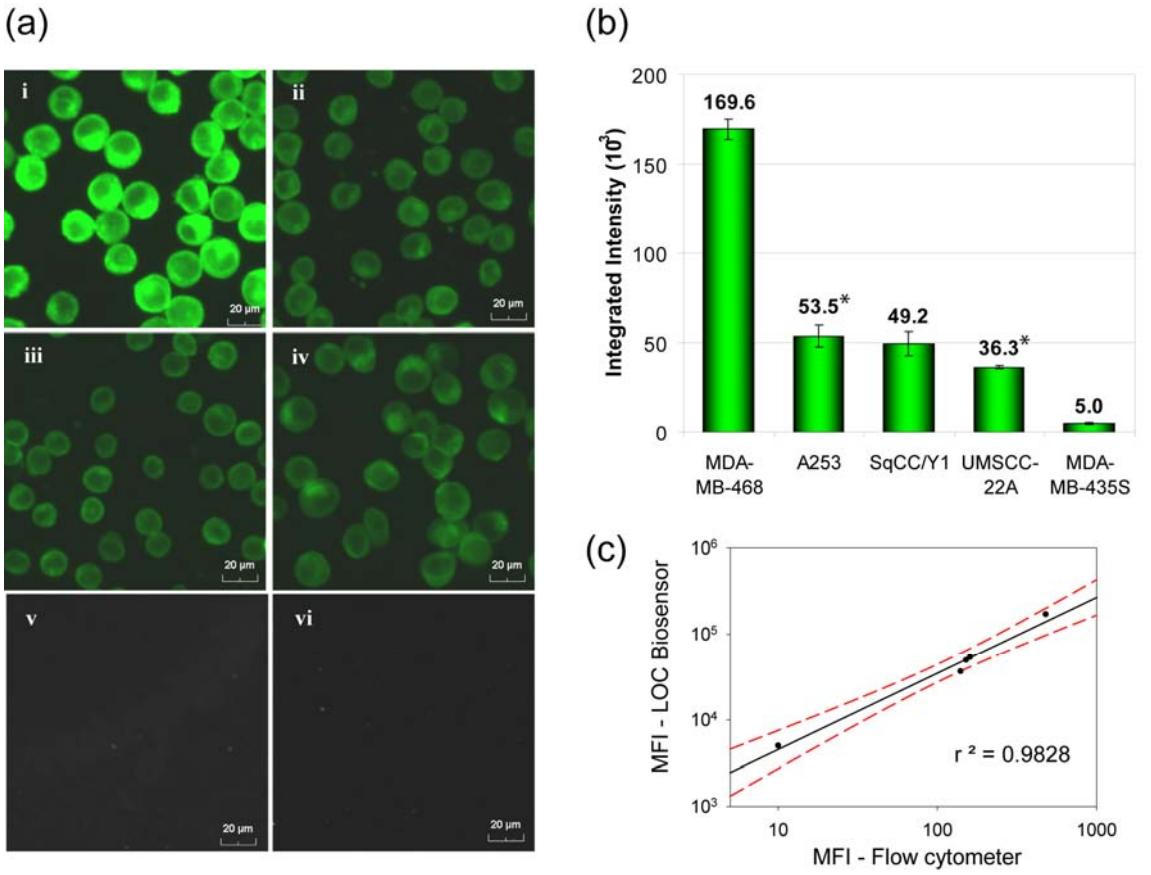

Figure 2-5. Detection of EGFR overexpression using LOC sensor. (a) Fluorescent micrographs of EGFR sensor immunoassays in cancer cell lines (i) MDA-MB-468; (ii) A253; (iii) SqCC/Y1; (iv) UMSCC-22A; (v) MDA-MB-435S; and (vi) isotype control. (b) Examination of EGFR expression using automated image analysis macros shows mean integrated intensity ± SD of triplicate EGFR assays with statistical differences found between all cell lines and MDA-MB-435S negative control ($p < 0.05$). Among the oral cancer cell lines, A253 and UMSCC-22A also exhibited statistical differences in EGFR expression ($p < 0.01$) denoted with *. (c) Correlation of mean fluorescent intensity (MFI) obtained from LOC expression analysis with standard flow cytometry shows a high degree of correlation ($r^2 = 0.98$) at the 95% confidence interval (dashed lines).

2.3.5 Quantitative Flow Cytometry

In order to further understand the cellular differences detected by the LOC sensor, the number of EGFR receptors per cell was determined in all cell lines by quantitative

flow cytometry using QIFIKIT® analysis (Figure 2-6). In agreement with the results achieved on the LOC system, MDA-MB-486 cells exhibited the highest EGFR expression at a density of $8.1x10^5$ receptors per cell, followed by A253 ($2.7x10^5$ EGFR/cell), SqCC/Y1 ($2.5x10^5$ EGFR/cell), UMSCC-22A ($2.3x10^5$ EGFR/cell), and MDA-MB-435S cells with less than $0.2x10^5$ EGFR/cell. Although normal oral epithelium was not examined in this study, previous investigators have reported ~$0.3x10^5$ EGFR binding sites per cell in normal cervical squamous epithelium[131] similar to MDA-MB-435S cells presented here. Thus, MDA-MB-435S cells more closely model a "normal" control rather than a true EGFR negative control as does the isotype. Attempts at EGFR quantitation in the LOC sensor using QIFI standards was unsuccessful as presented in Appendix C.

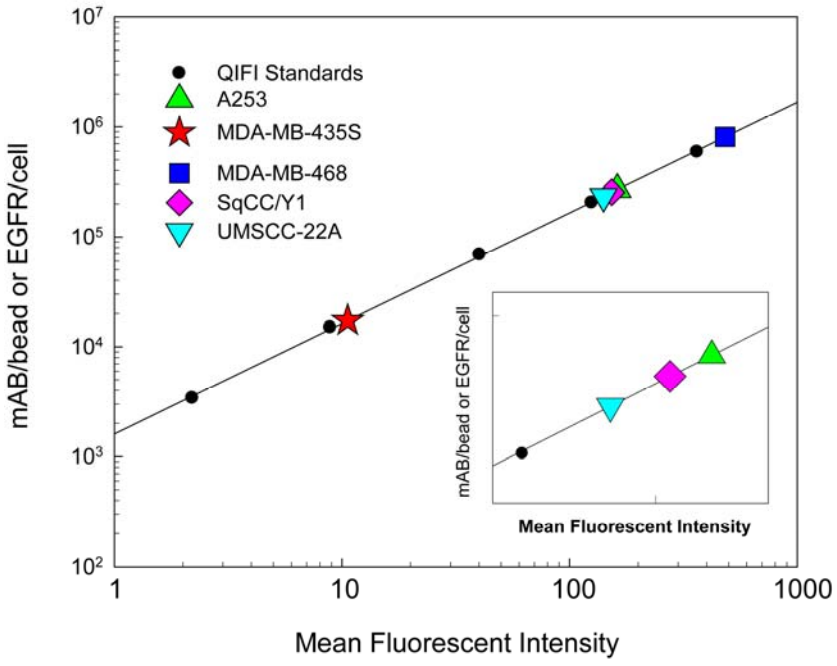

Figure 2-6. Quantitative flow cytometry. Standard curve generated from flow cytometric analysis of QIFI bead standards for interpolation and quantification of EGFR receptors per cell in tumor-derived cell lines ranging from 0.2-$8.0x10^5$ EGFR/cell.

2.4 DISCUSSION

In the present study, we describe the development of a cellular biomarker assay for EGFR towards the establishment of a lab-on-a-chip sensor for early detection of oral cancer. Current methods for detection of cellular biomarkers, such as slide-based immunohistochemistry and flow cytometry, require extensive sample preparation, long incubation periods and repeated washing steps which may result in sample loss. In contrast, the optimized LOC sensor assay was completed in less than 10 minutes using a constant flow "on-membrane" staining technique while maintaining labeling intensity and homogeneity comparable to standard protocols. These results support the use of the LOC sensor platform for rapid cellular immunoassays, in less than one-tenth the labeling time of conventional techniques, which is highly desirable for diagnostic testing devices and point-of-care applications.

Using *in vitro* tumor cell lines to serve as a model for the biomarker expression levels found in healthy and diseased patients, we have demonstrated successful characterization of EGFR overexpression in OSCC cells. As shown in Figure 2-5, MDA-MB-468, A253, SqCC/Y1 and UMSCC-22A, with a mean EGFR range from $36.3x10^3$ to $169.6x10^3$, exhibited EGFR intensities significantly above control MDA-MB-435S cells with a mean of $5x10^3$ and EGFR expression similar to normal squamous epithelium.[131] Thus, there is roughly a 7- to 10- fold difference between MDA-MB-453S cell intensity and the three oral cancer cell lines, UMSCC-22A, SqCC/Y1, and A253. With respect to the MDA-MB-468 cell line, known to strongly over-express EGFR, this factor goes up to as high as 33. For each of these cell lines, an analysis of the sample distribution of cell fluorescence intensities shows a log-normal distribution with the coefficient of variation (CV) values in the range of 3% to 5%. Since the differences in the mean intensity values far exceed the population differences as manifested in their modest CV values, the

prospect for differentiating the various cell phenotypes based upon EGFR expression is quite good for the method herein described.

Furthermore, if a threshold for normal EGFR expression is established based upon the sample distribution and variance for the MDA-MB-435S cell line located 2 standard deviations above the mean EGFR intensity ($8.84x10^3$), then all cells intensities above this threshold could be classified as EGFR over-expressed. Using this criteria, the oral cancer cell lines A253, SqCC/Y1 and UMSCC-22A in addition to MDA-MB-468 are characterized as over-expressing the EGFR biomarker.

The LOC sensor assays were well correlated to flow cytometry, the current clinical standard in cell-based protein expression analysis with $r^2 = 0.98$. Corresponding quantitative flow cytometry revealed a mean EGFR/cell of $2.5x10^5$ among the OSCC cell lines, far exceeding the expression level found in MDA-MB-435S cells (0.2x105 EGFR/cell) similar to normal squamous epithelium, but below MDA-MB-468 cells ($8.1x10^5$ EGFR/cell) known to strongly over-express EGFR. In agreement with LOC results, quantitative flow cytometry suggests that EGFR is over-expressed in these OSCC cell lines, although to a lesser extent than MDA-MB-468 cells. Taken together, these results support the lab-on-a-chip sensor system as a suitable platform for analysis of EGFR cellular biomarker expression. Further validation via a small pilot study examining OSCC patients versus normal healthy controls is warranted and necessary to establish the sensitivity and specificity of this EGFR biomarker assay in clinical applications.

Although tumor cell lines make excellent models for assay development, there are fundamental differences likely to be encountered in clinical samples from cancer patients. In particular, heterogeneous cell populations containing both normal and cancerous cells are expected, compared to the relatively homogeneous cell line populations utilized in the current study. Should this be the case, future clinical measurements may rely on the

identification of cell sub-populations and percentage of cells over-expressing EGFR. In addition, the presence of EGFR negative cells may necessitate the use of secondary cellular fluorophores labeling cytoplasmic and/or nuclear structures independent of EGFR expression in order to identify cells for measurement. This multi-spectral labeling strategy could further exploit the image cytometry capabilities of the sensor system to incorporate cytomorphological analyses such as cell size and nuclear-to-cytoplasm ratio which are often altered during tumorigenesis. Thus, potentially cancerous cells could be identified using traditional pathological features and directly correlated with specific biomarker expression on a single-cell basis.

Ability of the LOC sensor to characterize cell samples based upon intrinsic EGFR biomarker expression, or in combination with other cytomorphological markers, is governed by the quality of cell labeling and fluorescent imaging. Each of these areas must be considered carefully and optimized in a systematic manner in order to extract meaningful information regarding cellular phenotype during image analysis procedures. While it is beyond the scope of this manuscript to provide an exhaustive discussion of these areas, some of the more key issues related to the LOC sensor are discussed briefly here.

The flatness of the membrane and the associated support is one of the most important variables affecting cell imaging. If the membrane deflects under the influence of the fluid flow, some of the cells will move out of the plane of focus. In order to minimize this effect the LOC sensor utilizes a planar track-etched membrane with a smooth glass-like surface which maintains captured cells on the surface of the membrane at similar heights as compared to the uneven fiber matrices found in depth-type filters. In addition, application of microscope-based autofocusing on each field of view further compensates for focal variations due to minute fluctuations in membrane flatness.

Alternatively, acquisition of multiple Z-plane images for selection of the best focused image or deconvolution may be utilized for similar purposes in future analyses.

The amount of acceptable deviation from the ideal planar geometry depends on the depth of field and the numerical aperture of the optical objective used. While higher NA affords better light collection, the lower NA values provide increased depth of field enabling all cells within the field of view to be imaged in a single focal plane. The microscope objective utilized in these studies had a 10X magnification with a low numerical aperture of 0.3 yielding a depth of field of 5.8 μm. Although this depth of field is less than the typical cell size of 10 μm, in practice the LOC sensor appears to adequately represent fluorescent intensities obtained from the entire cell as demonstrated by the excellent correlation of LOC EGFR analysis with flow cytometry. Further use of deconvolution and extended-depth-of-field algorithms may enable more quantitative image analysis applications in future analyses.

Background fluorescence intensity is another factor that is important to successful cellular analysis. Here the choice of materials to construct the imaging chamber and membrane support is essential. Low fluorescence plastics like PMMA and glass slides are used for the current studies and found to be adequate for this purpose. For the cell line with the lowest EGFR expression level (i.e. MDA-MB-453S), an estimate of the number of copies of EGFR per cell for this protein is 20,000. Even with this cell system having the lowest number of fluorophores thereon, a signal (on cell) to background (off cell) ratio of 0.6 and a signal-to-noise ratio of 10.5 was obtained. For the other cancer cell lines, signal-to-background (S/B) ratios in the range of 4 to 20 were obtained. These values serve to establish a contrast level that is readily exploited for the recognition of the cellular objects from the digital images.

2.5 CONCLUSIONS

This body of work demonstrated the design and development of a cell-based lab-on-a-chip sensor supporting rapid immunoassays for biomarker expression. Using EGFR as a proof-of-principle biomarker, the sensor demonstrated capacity to characterize EGFR overexpression in less than one-tenth the time of traditional methods and to discriminate between closely related sample populations. As a clinical tool, such assays may fill multi-functional roles in cancer diagnostics (i) as an early detection device screening pre-malignant oral lesions and (ii) as an adjunct to surgical pathology providing a molecular basis for prognostic evaluation and therapeutic selection.

Chapter 3: Integration of Exfoliative Cytology in LOC Sensor Assays

3.1 INTRODUCTION

In the previous chapter, the membrane-based lab-on-a-chip sensor was shown to support cellular biomarker assays which may aid in the early detection of oral cancer using *in vitro* tumor-derived cell lines. While these cell lines serve as an excellent model for tumorigenesis, further development of the LOC sensor system for diagnostic and translational purposes must employ cells from more clinically relevant sources. The use of exfoliative cytology offers a rapid, non-invasive method to obtain a sampling of epithelial cells from mucosal membranes which may be subjected to microscopic or molecular examination for signs of malignancy. This chapter strives to develop the practical methods for analysis of exfoliative cytology using the LOC microchip technique. The chapter is organized in the following manner beginning with background information regarding the current methods and applications of exfoliative cytology followed by the specific challenges existing in the imaging and analysis of once adherent epithelium in the LOC sensor. The optimal cell sampling and processing methods, including the necessity for cell dissociation, fixation, and permeabilization, will be critically evaluated along with the appropriate conditions for sample introduction and capture on the sensor membrane. A variety of cytoplasmic and nuclear markers will be examined, as well as the requisite z-scan imaging parameters. In addition, a detailed description of the data extraction and analysis approach employed with this new automated cytology technique will be provided. Implications of such techniques in disease diagnostics will be discussed with the overall goal of establishing the precedent for Chapter 4 in which the clinical utility of these new automated cellular analysis methods will be explored.

Cytopathology has been successfully utilized for cervical cancer screening for over 50 years and has also been applied toward detection of malignancies in the lung and respiratory tract, breast, female genital tract, digestive tract, oral cavity, urinary tract and the prostate.[133] However, traditional cytopathology for early detection of oral cancer has long been viewed unfavorably with limited diagnostic ability and low sensitivity. This has frequently been attributed to poor or inadequate cell sampling and subjectivity associated with cytologic interpretation and diagnosis.[134] Recent improvements in specimen collection and quantitative image analysis techniques, including cytomorphometry and DNA aneuploidy, have helped to overcome these past limitations stimulating a renewed interest in cytology for detection of oral malignancies.[135] In addition, exfoliative cytology has emerged as an excellent, non-invasive method to obtain cellular material for DNA-, RNA-, and protein-based analysis of tumor biomarkers shifting the clinical impact of oral cytology toward molecular diagnostic techniques.[135] Bringing these two approaches together on a single microchip platform for molecular and morphological analysis in oral cytology may further enhance their role and utility in clinical diagnostics.

3.1.1 Exfoliative Cytology Sample Collection Techniques

Exfoliative cytology cells may be found naturally in biological fluids, such as sputum and saliva, or collected by brushing, scraping, or rinsing of the tissue surface. A cytobrush, such as the OralCDx® brush biopsy instrument (OralScan Laboratories Inc., Suffern, NY), is used most frequently and appears to provide an full trans-epithelial sampling of cells from the basal, intermediate and superficial layers.[76] Sampling through the entire thickness of epithelium, particularly the basal cells, is crucial for early detection of oral cancer because dysplasia or other signs of malignancy are first apparent in the basal epithelium while morphology of the upper layers may appear cytologically

normal. Poor or inadequate cell sampling limited to the superficial cell layers is frequently associated with the low sensitivity originally found with oral cytopathology.[136]

Characterization of oral cytology is typically based upon available features of dysplasia including variations in cell size and shape, presence of enlarged and irregular nuclei, increased nuclear-to-cytoplasm ratio, hyperchromatism, presence of mitotic figures, and irregular keratinization (Table1-2).[133, 134] Thus, cytopathology suffers similar limitations as histology where subjectivity exists in determining the extent of abnormality present and the significance of individual dysplastic features, particularly in pre-malignant stages, which has restricted the clinical value of oral cytology in the past. Attempts to reduce subjectivity of cytopathologic diagnosis have implemented computer-assisted image analysis techniques, quantitative measurement of cellular and nuclear morphometry, DNA cytometry, and/or tumor biomarkers. [76, 137, 138]

3.1.2 Exfoliative Cytology Applications

3.1.2.1 OralCDx® with Computer-assisted Analysis

As described previously, the OralCDx® system is a slide-based cytopathology test with computer-assisted analysis utilized for screening and detection of high-risk oral lesions. According to Sciubba *et al*., the OralCDx® test employs a neural network-based image-processing system to identify epithelial cells with abnormal cellular morphology and keratinization, indicative of malignancy.[76] As few as two abnormal epithelial cells are reported to be detectable among thousands of cells in a brush biopsy specimen.[76] These "abnormal" cells are then reviewed by a trained pathologist who interprets cytologic images and makes a final diagnosis.[76] Although the OralCDx® system shows promise, numerous discrepancies have been described regarding the true sensitivity and

specificity of this technique for identification of high-risk pre-malignant lesions with a number of false-negative and false-positive test results having been reported.[83]

3.1.2.2 Cytomorphometry and DNA Aneuploidy

Application of other quantitative techniques, such as cytomorphometry and image-based DNA cytometry, have also shown efficacy for characterization of malignant change in exfoliative cytology specimens. Morphometric features examined often include nuclear and cytoplasmic area, diameter, or perimeter, and the nuclear-to-cytoplasmic ratio (N/C ratio). Using image-based cytomorphometry to assess cellular and nuclear diameter, Ramaesh *et al.* demonstrated a progressive decrease in mean cell diameter, from 51.8 μm in normal epithelia to 38.6 μm in SCC lesions.[137] This coincided with an increase in nuclear diameter, found to be highest in SCC and dysplasia (10.1 μm and 9.0 μm, respectively) compared to non-dysplastic lesions and normal epithelia (8.3 μm).[137] These studies suggest that a reduction in cellular size and increase in nuclear size are valuable indicators of malignant transformation. However, using cytomorphometry alone a rather low sensitivity of 77% was reported for identification of pre-malignant leukoplakia lesions. It remains unclear if this low sensitivity is truly representative of the technique or a result of the absense of basal cells when using a wooden spatula for cytology collection, frequently seen in these earlier studies.[139]

Additional research further suggests that a combination of cellular/nuclear morphometry and DNA ploidy profiles can help to discriminated malignant and pre-malignant lesions from normal cytology specimens with a low rate of false negatives, which has plagued oral cytology in the past.[138, 140] Change in DNA content or chromosome number, also known as aneuploidy, results from unbalanced chromosomal segregation during mitosis and is thought to be the most prevalent genetic alteration reported in over 20,000 solid tumors analyzed to date.[141] High sensitivity and specificity

have been reported using DNA image cytometry for tumor characterization with strong implications toward early identification of lesions with a high-risk of malignant progression.[142-144] While there is a very solid research based for the use of DNA ploidy as an indicator of malignancy, much of the literature focused upon DNA cytometry in oral cancer authored by J. Sudbo is not considered to be reliable, leaving the role of DNA ploidy in oral cancer uncertain and in need of further validation.[145]

3.1.2.3 Immunohistochemistry

The identification of tumor biomarkers in exfoliative cytology has generated considerable interest toward early detection of oral cancer.[146] In particular, the profile of cytokeratin expression, which provides useful information on cell differentiation status, has been widely examined, but with limited diagnostic success due to the complexity of cytokeratin expression patterns and presence in normal epithelia.[146] Nonetheless, Ogden *et al.* have shown cytokeratin-8 and -19 to be useful indicators of malignancy, particularly when assessed in conjuction with DNA content or ploidy status.[146, 147] The p53 immunoreactivity has also shown diagnostic value in oral cytology, although, immunoreactivity is not necessarily indicative of p53 mutation which has been reported in approximately 50% of OSCC tumors. Further, p53 expression may be associated with advanced stage disease restricting its utility for early detection and diagnosis.[148] Other tumor-related proteins detectable by immunohistochemistry in exfoliative cytology with varying degrees of success include laminin-5,[74] tenascin-C,[149] and minichromosome maintenance proteins (Mcm-2/Mcm-5).[150] While immunohistochemistry is a very useful technique, many of the markers present in oral tumors are also present at various expression levels in normal mucosa and/or benign conditions necessitating the use of more quantitative biomarker approaches and advanced image analysis techniques.[146]

3.1.2.4 Molecular Analysis

Over the past 20 years, a shift from histopathology toward molecular methods has occurred in disease diagnostics, and exfoliative cytology has emerged as a rapid, non-invasive method to obtain cellular material for such analyses.[146] Molecular techniques applied toward exfoliated cytology have included fluorescent *in situ* hybridization (FISH),[78] analysis of genomic instability via loss of heterozygosity (LOH) and microsatellite markers,[73] gene expression,[77] and proteomic profiling.[75] There appears to be a high correlation between the molecular changes present in tumor biopsy tissue and those found in exfoliated cells.[6] In one study by Rosin *et al.* LOH, or allelic loss, was evaluated in brush cytology specimens with a nearly identical pattern of loss seen in corresponding biopsy tissue at the same site.[6, 151] As stated earlier, molecular-level changes can occur prior to the appearance of microscopically or clinically apparent abnormalities. Thus, examination of exfoliated cells for molecular or protein biomarkers opens new opportunities for early detection and diagnosis, as well as monitoring the progress of lesions during treatment and follow-up.[6]

The purpose of this chapter is to develop the practical methods for analysis of exfoliative cytology using the LOC microchip technique. The integration of exfoliative cytology into the microchip sensor presents a number of opportunities as well as a number of significant new challenges for sample processing and imaging of these naturally adherent cells. Relative to the simple non-adherent cell suspensions examined in the previous chapter, it is clear that additional cytoplasmic and nuclear markers are required for the microchip analysis of the cytology samples as demonstrated in Figure 3-1. This example highlights the approach described in this chapter for transitioning sensor assays and methods from tumor cell lines to more complex epithelial cytology specimens. The origin of this challenge can be seen in Figure 3-1(a) and (b), i, where cultured cells

are readily apparent based soley upon EGFR labeling intensity (Figure 3-1(a), i) while cytology cells are not (Figure 3-1(b), i). With the addition of a cytoplasmic marker (red) (Figure 3-1,(b), ii), cells present in the cytology specimen materialize allowing digital recognition of individual cells. However, when cells are touching, as is often found in these cytology specimens, the cytoplasmic marker alone poorly delineates the appropriate divisions between cells due to the irregular cell shape and borders. Thus, the nuclear marker serves to identify the number of cells present, which provides additional information from which to define the divisions between adherent cells. These new modes of data collection, made necessary with the more difficult sampling and imaging challenges, provide an opportunity to explore morphological features of malignancy which have been well established in cytopathology for decades.

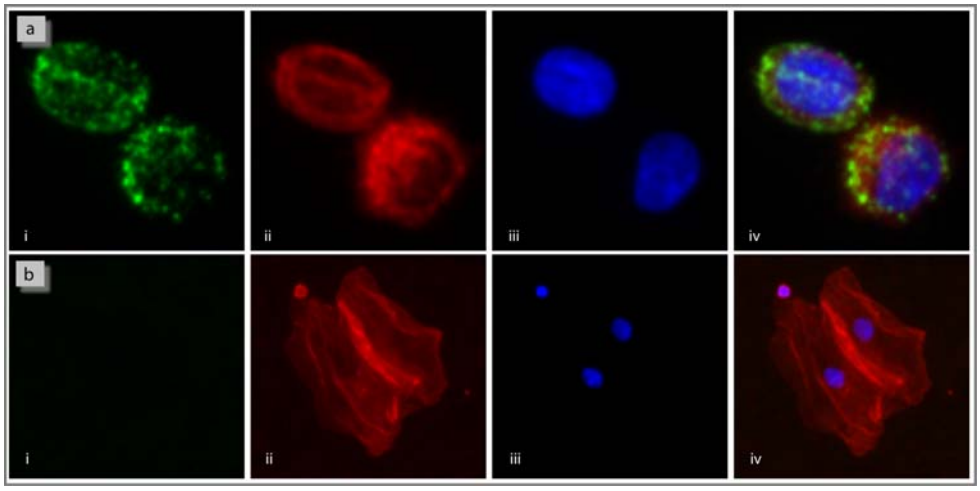

Figure 3-1. Representative cells from *in vitro* tumor-derived cell line SqCC/Y1 (a) and healthy exfoliated brush cytology specimen (b) for analysis of EGFR expression (panel i) and cytomorphometry, using dual cytoplasmic (phalloidin, panel ii) and nuclear (DAPI, panel iii) markers. The combination of nuclear and cytoplasmic markers (RGB, panel iv) allows identification and separation of each epithelial cell for measurement.

3.2 EXPERIMENTAL METHODS

3.2.1 Exfoliative Cytology Sample Collection, Dissociation and Fixation

Exfoliative cytology specimens were collected using the OralCDx® biopsy brush according to manufacturer's protocol. Briefly, the nylon brush was placed firmly against the buccal mucosa of healthy volunteers and rotated 10-15 times while applying moderate pressure. The appearance of pinpoint bleeding signified breach of the basement membrane and biopsy depth through the full-thickness of the epithelium. Cells were released from the biopsy brush and suspended in 5 mL cold Eagle's Minimum Essential Media (EMEM) culture media supplemented with 2 mM L-glutamine and 10% fetal bovine serum using vigorous agitation for 15-30 seconds. Culture media was removed by centrifugation at 1200 rpm for 5 minutes. Cells were then washed twice in 3 mL PBS buffer (BupH™ Modified Dulbecco's Phosphate Buffered Saline Packs #28374, Pierce/Thermo Fisher Scientific, St. Louis, MO) by centrifugation at 1200 rpm for 5 minutes.

Cell dissociation was investigated using a variety of mechanical and enzymatic methods. Mechanical methods included vortexing (Vortex-Genie 2, setting 7.0) for 5 minutes, shear stress with a 27 ½ gauge needle (approximately 10 aspirations), and straining through 35 μm mesh built into the cap of a 12 x 75 mm flow cytometry tube (BD Falcon #352235). Enzymatic treatments included 0.025%-0.25% trypsin-EDTA (Gibco #25200-056), Versene™ (Gibco #15040), 50 U/mL – 100 U/mL Collagenase Type-1 (Gibco #17100-017), and 0.5 U/mL – 1.0 U/mL Dispase (Gibco #17105-041) at durations ranging from five minutes to one hour. Following dissociation, cells were stained with 0.4% Trypan blue solution (#T8154, Sigma-Aldrich, St. Louis, MO), using a 1:1 mixture of staining solution and cell suspension, for evaluation of viability and dissociation efficiency using a bright field hemacytometer. The relative ranking of each

method was based upon the presence of intact squamous cells, moderate clustering (<10 cells each), extra-cellular debris, isolated nuclei, and extent of membrane folding using an arbitrary scale of (+) poor, (++) fair, (+++) good, and (++++) excellent. The effect of fixation on EGFR biomarker immunolabeling was examined by flow cytometry in the OSCC cell line, SqCC/Y1, cultured *in vitro* and labeled for EGFR biomarker according to previously established protocols.[152] Fixation was typically carried out prior to immunolabeling in 1 mL of 0.5% - 4% formaldehyde in PBS buffer at 4^0C for 20 minutes to 1 hour or in commercially available fixatives according to manufacturer's instructions. These included Histochoice™-MB fixative (#64115) from Electron Microscopy Science, Hatfield, PA; Cyto-Chex® Cell Preservative (#213350) from Streck, Omaha, NE; and Cytofix/Cytoperm™ (#554714) from BD Biosciences, San Diego, CA. Following fixation, cells were washed twice in PBS buffer, immunolabeled with anti-EGFR mAB followed by AlexaFluor®-488 fluorescent secondary antibody as described using in-tube flow cytometry protocol, and analyzed on an FC500 Beckman Coulter flow cytometer.[152] Negative controls replaced anti-EGFR antibody with an irrelevant antibody of the same IgG_1 isotype. Flow cytometry data was collected in the FS (linear), SS (linear) and FL-1 (log) channels then exported to WinMDI2.9 software, available from the Scripps Research Institute (http://facs.scrips.edu), for analysis. Events were gated upon forward and side scatter parameters and analyzed via single-parameter EGFR intensity histograms with user-defined region markers roughly centered on each peak allowing statistical evaluation of the mean intensity and coefficient of variation. Signal to background (S/B) ratios were calculated by subtracting the mean of the isotype, or background, from the mean EGFR signal, divided by the background also represented as [(mean M2 – mean M1)/mean M1]. Fixed cells were stored in PBS with 0.1% BSA (PBSA) at 4^0C for up to 1 week.

3.2.2 Labeling of Basal Cells

Brush cytology specimens were collected and processed as described above then labeled in the LOC sensor using either 10 μg/mL AE1 (#ab3117, Abcam Inc., Cambridge, MA) in PBSAT followed by a secondary fluorescent staining cocktail containing 20 μg/mL goat anti-mouse/AlexaFluor®-488 conjugate in PBSAT or 1:30 dilution of cytokeratin-14 Ab (#2001-1, Epitomics Inc., Burlingame, CA) in PBSAT followed by 20 μg/mL goat anti-rabbit/AlexaFluor®-488 secondary antibody conjugate in PBSAT. Counter-stains were added to the secondary antibody solution at a final concentration of 0.33 μM Phalloidin/AlexaFluor®-647 and 5 μM DAPI in PBSAT. The use of phalloidin and DAPI as cytoplasmic and nuclear markers is discussed in further detail below. Negative controls for AE1 and cytokeratin-14 labeling replaced primary antibodies with an irrelevant antibody of the same isotype or normal rabbit serum, respectively.

3.2.3 Cell Capture and Dispersal in LOC Sensor

Cell capture and dispersal on the membrane surface were optimized through a series of experiments altering the flow rate, from 250 μL/min – 2 mL/min, and viscosity of the cell suspension fluid with the addition of 0%, 20%, 40%, 50% and 60% glycerol in PBSA. The sample volume delivered to the membrane remained constant at 500 μL with a concentration of $1x10^3$ – $1x10^4$ cells/mL, capturing approximately 2,500 – 5,000 cells total. Visual assessment of cell dispersal was facilitated by the addition of DAPI (5 μM in PBSAT) directly to cell suspensions and manual 2 x 2 epifluorescent imaging of the entire membrane surface at 2.5X magnification. Alignment of images for full membrane representation was performed in Adobe® Photoshop®CS8.0.

3.2.4 Z-Scan Imaging

A z-scan image sequence of DAPI stained nuclei (see below for details) was collected over a range of 50 μm at 1.0 μm intervals above and below the ideal focal plane, determined using autofocus routines in SimplePCI microscope software (z = 0 with z-scan ±25 μm). Ten well-focused nuclei were selected at random and regions of interest (ROI) were manually drawn to encircle each nucleus for mean intensity measurement in the full z-sequence of 51 images. Images at 5 μm intervals (z = 0, +5, +10, +15, and +20 μm) were extracted from this z-scan sequence and recombined, using a stack focusing algorithm in ImageJ, in progressive cycles generating a single "focused" image consisting of one to five focal planes. Using a simple intensity thresholding and segmentation procedure, the total number of nuclei detectable in each focused image was calculated and superimposed onto the corresponding focused image in a cell subset.

3.2.5 DAPI Nuclear Staining

DAPI (4',6-diamidino-2-phenylindole) (#D3571, Molecular Probes Invitrogen) (Ex/Em 358/461 nm) stock solutions were prepared in 2 mL deionized water yielding a stock concentration of 5 mg/ml or 10.9 mM. DAPI staining was performed simultaneously with the EGFR assay, such that DAPI was directly added to the EGFR secondary antibody labeling solution at a final concentration of 5 μM in PBSA with 0.1% Tween-20 (PBSAT) and delivered to the microchip sensor at 250 μL/min for 2.5 minutes followed by a brief buffer wash as outlined below. DAPI filter set (#31000v2, Chroma Technology, Rockingham, VT) was used for imaging.

3.2.6 Staining/Labeling with Cytoplasmic Markers

Cell samples were collected according to the brush biopsy protocol above and fixed in either Histochoice-MB® or 0.5% formaldehyde fixative, or left unfixed. When

possible, cytoplasmic staining was performed in conjunction with the established EGFR assay using brush biopsy cells as detailed below. Briefly, cell capture of ~2,500 cells was accomplished at 2 mL/min (50% glycerol in PBSA) followed by primary anti-EGFR antibody labeling, and fluorescent secondary antibody labeling with intermittent buffer washes. Secondary antibody solution contained 5 μM DAPI for identification of nuclei. Imaging was carried out in a four by four X, Y raster scan of the membrane surface collecting three consecutive 12-bit monochrome images of the red/green/blue (RGB) fluorescent channels with the corresponding filter sets.

3.2.6.1 Sulforhodamine 101

Sulforhodamine 101 (SR101, #S359 Invitrogen Corp., Carlsbad, CA) is a rhodamine derivative (Ex/Em 576/593 nm) that has been reported to bind ionically and non-specifically to proteins enabling measurement of total cellular protein in flow cytometry applications.[153-155] A 1 mg/mL SR101 stock solution was prepared in PBS with sodium azide and stored at 4^0C protected from light for up to six months. In the LOC sensor assay, the SR101 stain was directly added to the goat anti-mouse/AlexaFluor®-488 secondary antibody solution at a final concentration of 20 μg/mL in PBSAT, in the presence of 5 μM DAPI forming a three-color fluorescent staining cocktail. The Texas Red® (#41004, Chroma) filter set was utilized for epifluorescent imaging of SR101.

3.2.6.2 FM®4-64 Lipophilic Dye

The FM®4-64 (#T13320, Invitrogen Corp.) reagent is a lipophilic styryl dye (Ex/Em 565/744 nm) that becomes strongly fluorescent upon insertion into plasma membranes. The FM®4-64 stock solutions were prepared in 1 mL deionized water at a concentration of ~100 μg/mL and stored at -20^0C for up to two weeks. Similar to SR101, FM®4-64 was directly added to the AlexaFluor®-488 secondary antibody solutions

during the EGFR assay, at a final concentration of 10 μg/mL in PBSAT. Filter set #11007v2 (Chroma) containing a 535/50 nm excitation filter, 565 nm dichroic filter, and 590 nm long pass filter was used for imaging of FM®4-64.

3.2.6.3 Pan Cytokeratin

For cytokeratin immunolabeling, a rabbit anti-human pan cytokeratin antibody (#C9097-48D, US Biological, Swampscott, MA) was selected for indirect labeling which could be performed simultaneously with the EGFR assay due to the difference in antibody species of origin and no known cross-reactivities. As such, 10 μg/mL of anti-cytokeratin was added to the primary anti-EGFR antibody solution in PBSAT followed by 20 μg/mL of goat anti-rabbit IgG secondary antibody conjugated to AlexaFluor®-594 (#A110037, Invitrogen, Ex/Em 590/617 nm) to the secondary antibody solution in PBSAT. Texas Red® filter set was utilized for imaging.

3.2.6.4 β-Actin

As one of the most abundant and universally expressed proteins in eukaryotic cells, β-actin, serves as an attractive cytoplasmic marker for use in the LOC sensor assay. Here, a rabbit monoclonal antibody to β-actin (#NB110-55433, Novus Biologicals, Littleton, CO) was used in parallel with EGFR labeling similar to cytokeratin, at a dilution of 1:50 (concentration unreported) in PBSAT. Goat anti-rabbit IgG/AlexaFluor®-594 (#A110037, Invitrogen, Ex/Em 590/617 nm) was added at a final concentration of 20 μg/mL to the secondary staining cocktail in PBSAT. Texas Red® filter set was utilized for imaging.

3.2.6.5 Phalloidin

Phalloidin is a naturally occuring toxin isolated from the *Amanita phalloides* mushroom that binds to F-actin in the cell cytoskeleton. Two fluorescent conjugates of

phalloidin were tested including AlexaFluor®-594 (#A12381, Invitrogen, Ex/Em 581/609 nm) and AlexaFluor®-647 (#A22287, Invitrogen, Ex/Em 650/668 nm). Phalloidin stock solutions were prepared in 1.5 mL methanol at a concentration of approximately 6.6 μM and stored in single-use aliquots at -20^{0}C for up to one year. Since phalloidin is directly conjugated to a fluorophore, it could also be mixed into a cocktail with the secondary antibody/DAPI solution in PBSAT during the microchip assay sequence. Concentrations ranging from 0.165 μM to 1 μM were examined in order to determine the optimal dilution.

3.2.7 Image Analysis and Data Extraction using Custom Macros

Two open-source software programs were utilized for oral cytology image analysis and data extraction, ImageJ (version 1.38e)[127] and Cell Profiler™ (version 1.0.4684).[156] Programming for custom macros/modules were written in JavaScript and MATLAB®, respectively, in order to identify and discriminate individual cells from the background, as well as each other in adherent cell clusters. The overall image processing steps and sequences were implemented as described in Figure 3-2. Ultimately, two regions of interest (ROIs) were created for each cell, the whole cell ROI and the nuclear ROI, which serve to define the cellular regions for measurement. Measurement parameters related to morphometry include ROI area, Feret's diameter, perimeter, and circularity for both the whole cell and nucleus generating eight measurements (4 parameters in 2 ROIs, whole cell and nucleus), plus the calculated nuclear-to-cytoplasm ratio for a total of nine morphological parameters examined in each cell. An additional seven intensity parameters, including the mean intensity, standard deviation, mode, minimum, maximum, median, and integrated density are also measured for each ROI pair from the three separate red (phalloidin), green (EGFR), and blue (DAPI) images, yielding a 42 total intensity parameters related to the individual cell's physiological staining

pattern. For statistical analysis, data was exported to Microsoft® EXCEL® with Analyse-It® software and SigmaPlot 9.0 for graphical representation.

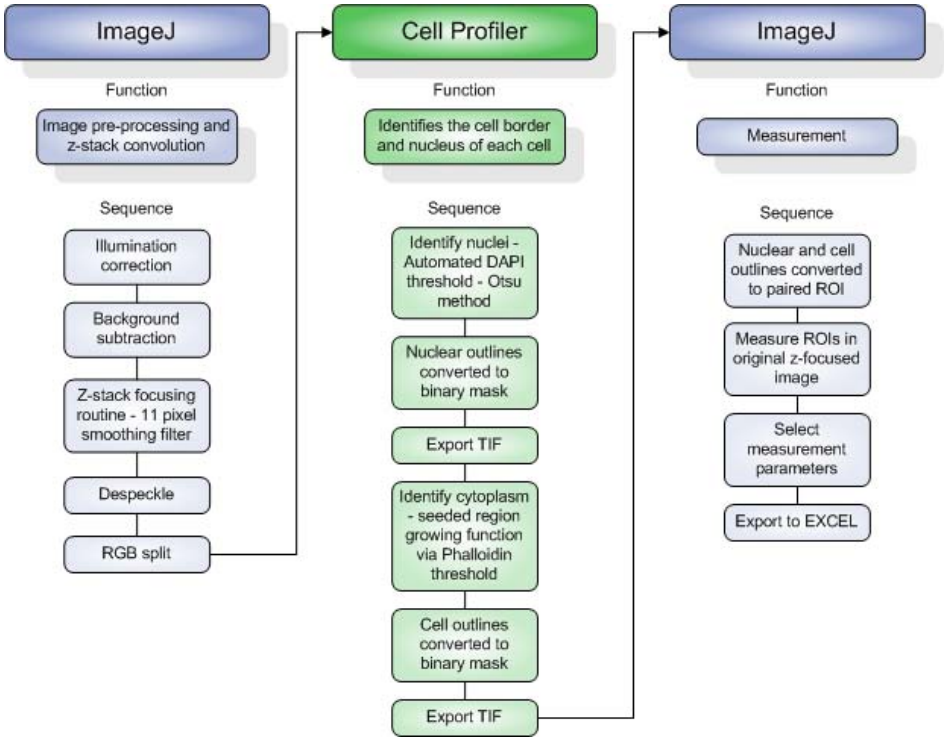

Figure 3-2. Flow diagram demonstrating the overall image analysis sequence using custom macros and processing routines optimized for cytologic analysis in the LOC sensor assays.

3.3 RESULTS

3.3.1 Specimen Collection and Adequacy of Basal Cell Sampling

In the current study, the OralCDx® cytobrush was selected for collection of oral cytology specimens based upon literature support for trans-epithelial sampling from the basal, intermediate, and superficial layers of epithelium, as well as from the suggestion of clinical collaborators.[76] Further, the design of the OralCDx® brush enabled sampling using either the brush tip or the side surface for added comfort in the oral cavity. In order

to integrate this technique into the LOC sensor system, two important criteria must be met; (1) a sufficient number of cells for the microchip assay must be collected, and (2) cells from all layers of epithelium must be present. Using the OralCDx® brush technique in ten isolated instances, an average of 1.4×10^5 total cells (range $2.0 \times 10^4 - 3.0 \times 10^5$) were collected from a brush sample of the buccal mucosa of healthy volunteers. However, this measurement provides only a rough estimate of total cell number due to the inherent inaccuracy of cell counting with a hemacytometer, particularly in the presence of clumped cells. Nevertheless, given that each microchip sensor assay requires only 2,500 – 5,000 cells, the volume of sample obtained with the brush cytology method was more than enough for multiple sensor assays.

Next, the ability to obtain trans-epithelial sampling of cells was examined. Adequate cell sampling through the full thickness of epithelium is crucial if cytology is to provide representative diagnostic findings, particularly in pre-malignant cases exhibiting mild or moderate dysplasia. This is evidenced by the low sensitivity associated with past cytopathology efforts where sampling was typically limited to the superficial layers of epithelia. Here, two cytokeratin makers, AE1 and cytokeratin-14, were utilized to identify the presence of basal/suprabasal cells in brush cytology specimens (Figure 3-3). Immunolabeling with the AE1 monoclonal antibody resulted in positive staining in a fraction of the cells as shown in Figure 3-3(a) (green), with a diffuse labeling pattern in the cell cytoplasm counterstained with phalloidin (red) and DAPI (blue). The AE1 negative cells exhibited phalloidin and DAPI staining only. A similar labeling pattern was seen with cytokeratin-14 (Figure 3-3(b), green), where a combination of positively and negatively stained cells was observed throughout the specimen. While AE1 and cytokeratin-14 have been utilized as basal cell markers in a number of prior studies, these markers have also been identified in suprabasal layers, albeit to a lesser extent.[157, 158]

Thus, the results presented herein cannot definitively identify basal cells, but rather suggest the presence of basal and/or suprabasal cells in these brush cytology specimens.

Further examination of brush cytology used slide-based cytospin preparations and Papanicolaou (Pap) staining, as shown in Figure 3-3(c), where mature epithelial cells from superficial layers were stained pink, intermediate cells were stained green, and immature basal/parabasal cells exhibited a blue-green color. In such preparations, basal cells may also be identified by a difference in morphology when compared to mature squames due to their smaller size, slightly larger nuclei, and somewhat cuboidal shape. While certain cellular features may be recognizable in cytology smears by an untrained eye, true interpretation requires a highly trained specialist in the field of cytopathology or oral diagnostics. Therefore, the final assessment of the quality of cytological sampling was made through consultation with clinical pathologists from the University of Texas Health Science Centers in Houston and San Antonio. Using standard cytopathology criterion and the AE1 and cytokeratin-14 staining methods above, the presence of basal cells were confirmed in OralCDx biopsy specimens by these experts in the field of cytopathology and oral diagnostics, verifying the adequacy of cell sampling using the brush cytology protocol.

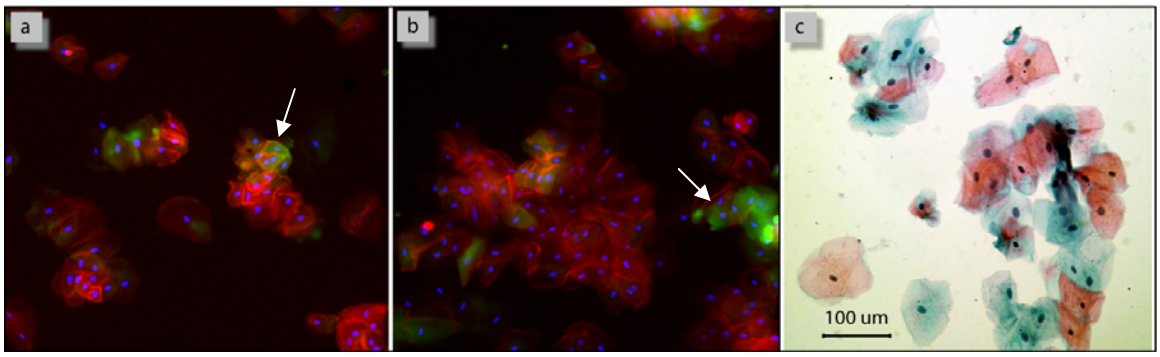

Figure 3-3. Identification of basal/parabasal cells in healthy brush cytology specimen. Cells were immunolabeled in the LOC sensor using two basal cell markers, (a) AE1 monoclonal antibody/AlexaFluor-488 (green) or (b) cytokeratin-14/AlexaFluor-488 (green), and counterstained with phalloidin (red) and DAPI (blue), cytoplasmic and nuclear markers, respectively. Basal/parabasal cells with positive AE1/cytokeratin-14 labeling are marked with arrows. (c)* Slide-based cytospin preparations stained with Papanicolaou further confirm the presence of mature squamous cells (pink), intermediate cells (green), and immature basal/parabasal cells (blue-green). *Image provided by courtesy of N. Vigneswaran at UTHSC Houston.

3.3.2 Mechanical and Enzymatic Dissociation of Adherent Cells

One of the main challenges associated with cellular analysis in exfoliative cytology is the use of naturally adherent cells, which, when significantly clustered, may obstruct visualization and imaging of rare or subtle signs of disease that are particularly important for detecting early cancerous or pre-cancerous conditions. Therefore, a variety of mechanical and enzymatic methods were evaluated in an attempt to dissociate large cell clusters in exfoliative cytology specimens, as listed in Table 3-1. Each method was compared to untreated cells which exhibited a high degree of cell clustering with approximately 50-60% of all cells touching at least one other cell estimated using a hemacytometer. Unfortunately, none of the enzymatic methods or conditions tested provided adequate or even acceptable results. For example, treatment with Trypsin-EDTA resulted in fewer cell clusters, but also generated a large amount of debris and isolated nuclei indicative of cell lysis. While treatment with collagenase or dispase either

had no effect on cell dissociation or again resulted in extensive cell lysis. Interestingly, nearly all of the treated and untreated cells stained positive with Trypan blue indicating disruption or perforation of the cell membrane, which likely occurred during the collection process when cell-cell and cell-ECM contacts were disrupted. Thus, it is possible that these enzymatic treatments were ineffective because the epithelial cell membranes did not remain intact following the brush biopsy procedure. This surprising occurrence provided a significant advantage in later microchip assay development, enabling intracellular staining/labeling in the absence of additional cell permeabilizing agents.

The only method with somewhat reasonable outcome was the 35 μm cell strainer which generated a very nice distribution of individual cells and small clusters, typically with less than five cells per cluster. This method was utilized for a brief period during the initial testing of normal and diseased cytology specimens, but was later discounted due to unacceptable levels of cell loss. In fact, it was pointed out by our collaborators in oral pathology that these clusters may contain the majority of basal cells and be the most relevant for assessment of malignancy. Therefore, no dissociation treatment was ultimately adopted and rather than eliminating the cell clusters, a multi-Z-plane imaging approach to image throughout the clusters was implemented as described below.

Table 3-1. Comparison of mechanical and enzymatic methods used for dissociation of exfoliative cytology specimens.

Treatment	*% Cells Touching*	*Comments*	*Relative Performance*
Untreated	59%	All cells trypan blue positive; few isolated nuclei; clear background with no debris	
Mechanical			
Vortex, 5 min.	NC	Severe clumping and cell debris prevented counting	Poor (+)
Shear stress – 27½ gauge needle	13%	Significant cell loss (~½)	Fair (++)
Mesh filter – 35 μm	24%	Majority of cells appear as intact squames; significant cell loss	Good (+++)
Enzymatic			
Trypsin-EDTA 0.25%	18%	Significant fibrous debris; and large number of isolated nuclei	Poor (+)
Versene (EDTA)	52%	Cell debris and isolated nuclei seen after 10 min.	Poor (+)
Collagenase 100U/mL	NC	Significant cell debris, fragments and isolated nuclei	Poor (+)
Collagenase 50U/mL	NC	Large clumps still present	Fair (++)
Dispase 1U/mL	NC	Minimal cell damage, but only moderate effect on dispersal	Fair (++)
Dispase 0.5U/mL	NC	No effect	
Dispase 0.5U/mL and collagenase 100U/mL	NC	Extensive cell lysis and debris	Poor (+)

3.3.3 Effect of Fixation on EGFR Immunolabeling

Cell fixation, while unwanted in a true point-of-care LOC sensor assay intended for clinical practice, is preferred during development due to decreased biohazard risk and prolonged sample utility. However, aldehyde-based fixatives are known to disrupt secondary alpha helical protein structure, which may in turn affect antibody binding at certain epitopes, particularly in membrane-bound receptors such as EGFR.[159] For this reason, the selection of fixative is very important to overall sensor performance and immunolabeling sensitivity. In this experiment, a variety of fixatives were tested to determine their effect on EGFR immunolabeling intensity as shown in Figure 3-4. Here,

unfixed cells demonstrated a mean EGFR intensity of 790, while the mean isotype control was 6.8 yielding a S/B ratio of 115, which served as the standard by which other methods were compared (Figure 3-4(a)). Fixation in 0.5% formaldehyde resulted in peak channels for EGFR and isotype of 880 and 7.8, respectively, with a S/B ratio of 110 (Figure 3-4(c)) while 4% formaldehyde fixation exhibited slightly higher EGFR and isotype means (1150 and 20, respectively), but with significantly lower S/B ratio of 57 (Figure 3-4e). The three commercially available fixatives yielded S/B ratios of 53 for Cytofix/Cytoperm®, 102 for CytoChex® and 465 for Histochoice-MB® (Figure 3-4(b, d, and f)). Although the exact chemical composition of the commercially available fixatives is proprietary, Cytofix/Cytoperm® is reported to contain 4% paraformaldehyde and demonstrated very consistent S/B ratio as the 4% formaldehyde solution prepared in-house. Suprisingly, the Histochoice-MB® fixative exhibited nearly 4 times greater S/B ratio over any other method. The manufacturer reports that the use of Histochoice-MB® fixative often enhances signal intensity, yet the mechanism for this phenomenon is unknown. These results initially directed attention toward the use of Histochoice-MB® for EGFR assays in the LOC sensor. However, it was later discovered that this fixative is incompatible with one of the cytoplasmic markers investigated, which raised doubts regarding the overall compatibility of Histochoice-MB® fixative in the development of future sensor assays. In the end, fixation using a low percentage of formaldehyde (0.5%) was selected due to the high similarity to unfixed cells.

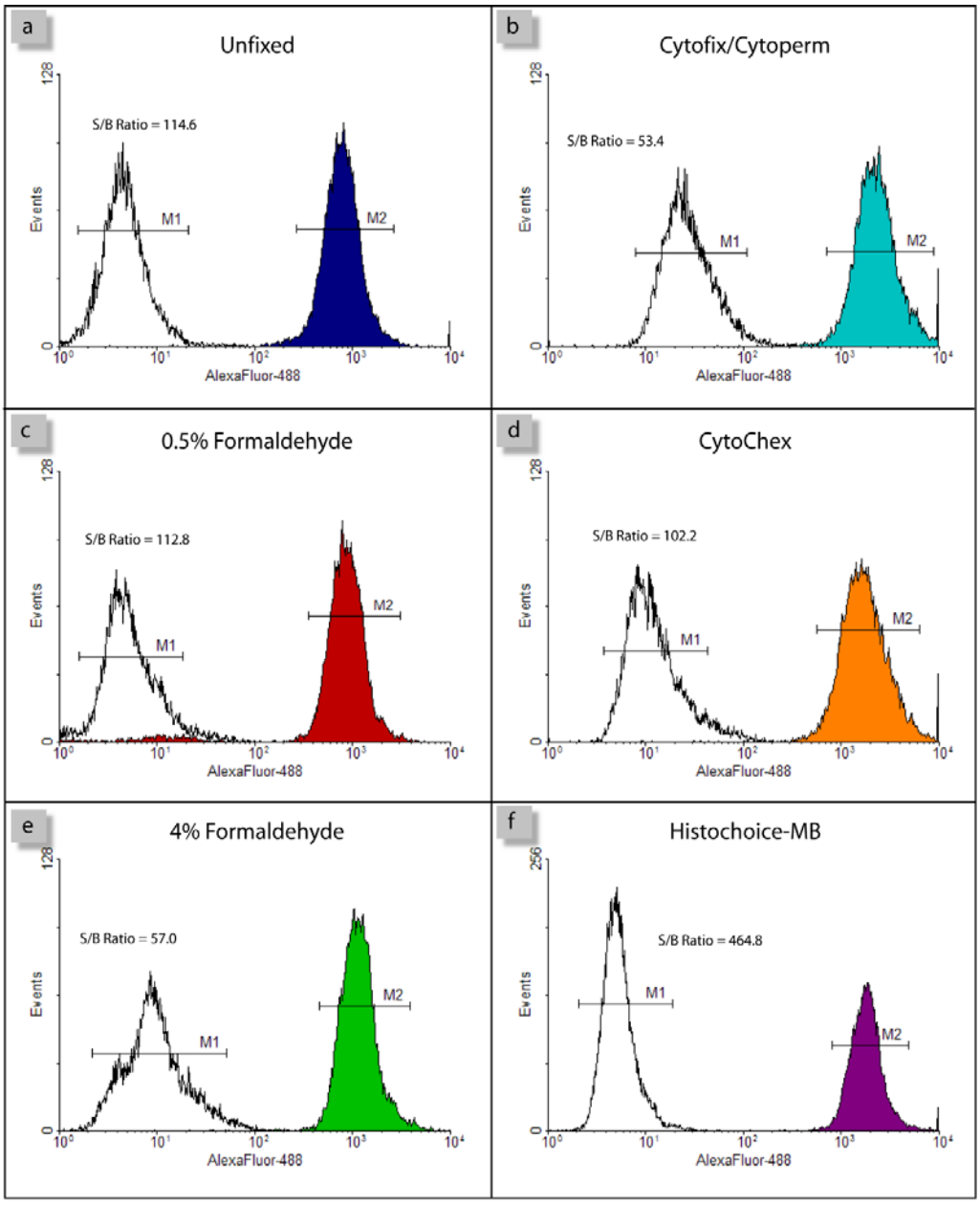

Figure 3-4. Effect of fixation of EGFR immunolabeling. Single-parameter EGFR intensity histograms, obtained by flow cytometry, of SqCC/Y1 tumor cells (a) unfixed, (b) fixed in Cytofix/Cytoperm, (c) 0.5% formaldehyde, (d) CytoChex, (e) 4% formaldehyde, and (f) Histochoice-MB. Matched isotype controls are overlayed as black outline histograms and are typically located in the first decade along the X-axis. User-established region markers centered on each peak generated statistics for calculation of the signal to background ratio using the equation [(mean M2 – mean M1)/ mean M1].

3.3.4 Optimization of Cell Capture and Dispersal in Microchip Sensor

Another important factor affecting cellular analysis in the LOC sensor is the dispersal of cells across the membrane surface. Under ideal conditions, cells would be distributed homogeneously throughout the membrane forming a dispersed monolayer, such that no excessive cell accumulation occurred in any one membrane region compounding the challenges associated with imaging and analysis of aggregated or clumped cells. Influencing this dispersal is the size and shape of the cells, the viscosity of the fluid, the dimensions of the fluidic channels, and the flow rate. In the current experiment, the size and shape of the cells, as well as the fluidic channels, remain relatively fixed, while the flow rate and viscosity of the fluid were adjusted to find the optimal parameters for cell capture and dispersal. Starting at an initial flow rate of 725 μL/min, previously optimized for tumor cell lines, brush biopsy cells suspended in PBSA buffer tended to gather at the left border of the membrane near the fluidic channel entrance with very few cells reaching the center and/or right edge, suggesting the need for higher flow rates (data not shown). Subsequent cell capture trials at 1.0, 1.5, 2.0, and 2.5 mL/min demonstrated that a flow rate of 2 mL/min provided the best improvement in cell dispersal with cells found throughout the membrane, albeit at a higher density near the exterior edges and somewhat sparse in the center of the membrane (Figure 3-5(a)).

Further improvement in cell dispersal was obtained by increasing the viscosity of the cell suspension fluid with the addition of glycerol as shown in Figure 3-5. At a constant flow rate of 2 mL/min, low percentage glycerol solutions resulted in the same general pattern of accumulation near the edges of the membrane with sparse patches located in the interior (Figure 3-5(a-c)). However, at 60% glycerol cell dispersal appeared much more even across the entire membrane surface with no overt regions of high or low cell density (Figure 3-5(d)). Further experiments revealed that 50% glycerol provided

similar dispersal patterns as 60% glycerol, but with greater reproducibility and less risk of sensor failure under high pressure (data not shown); therefore, cell capture at 2 mL/min in 50% glycerol/PBSA was implemented in all subsequent LOC cytology assays.

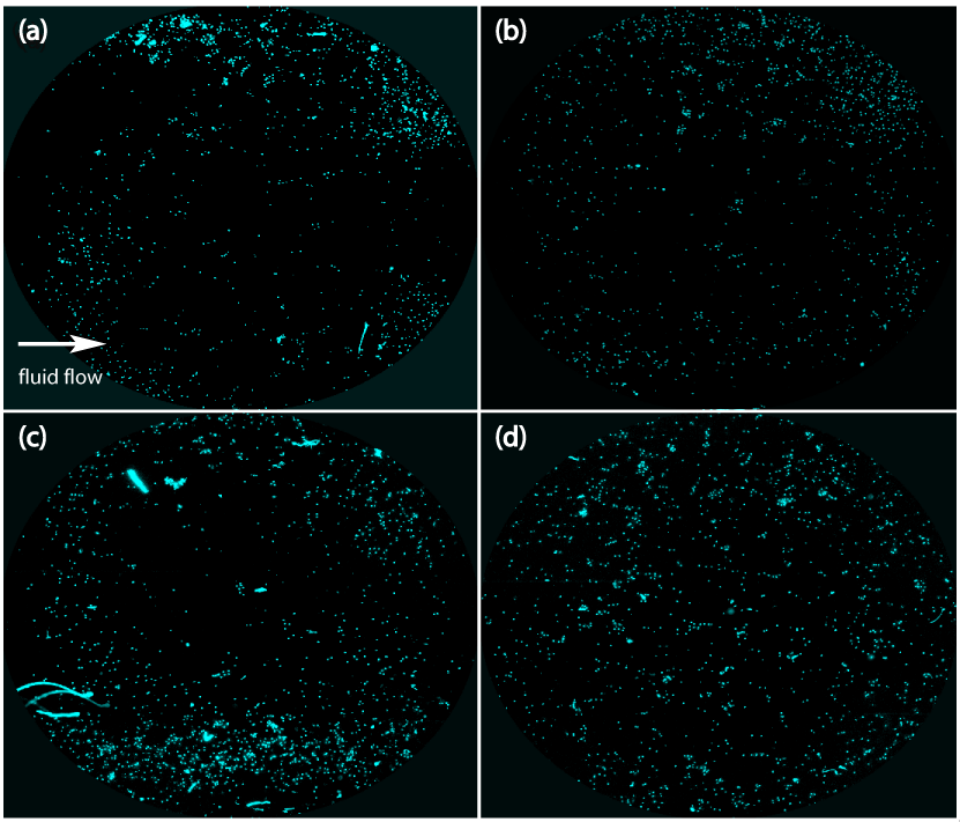

Figure 3-5. Evaluation of optimal conditions for cytology dispersal. Pseudo-color image montages of healthy brush biopsy cells stained with DAPI captured on the LOC membrane surface at a flow rate of 2 mL/min. in (a) 0% glycerol, (b) 20% glycerol, (c) 40% glycerol, and (d) 60% glycerol in PBSA solutions.

3.3.5 Parameters for Z-Scan Imaging of Cell Clusters

In order to circumvent the challenges, and ultimately failures, associated with cell dissociation, a z-scan imaging approach was adopted to collect multiple focal planes which could be recombined into a single "focused" image using convolution algorithms. With this methodology, two parameters must be defined including the z-axis step size and

the total number of z-planes necessary to image cell clusters. The appropriate step size was determined by examining the distribution in mean intensity values of ten randomly selected nuclei as a function of z-position in a 50 μm z-scan sequence as shown in Figure 3-6(a). The maximum intensity was seen at the z = 0 position, which was the "ideal" focal plane selected using autofocusing algorithms built into the microscope software. A sharp decrease in intensity was apparent as the z-position moved ±25 μm above or below the ideal focal plane. Using this intensity curve, the full width at half maximum intensity of approximately 12 μm was measured indicating that ±6 μm from the ideally focused z-plane resulted in a 50% decrease in intensity, beyond which intensity losses were unacceptable. This value closely approximates the size of a typical nucleus (~5 μm) and the calculated depth of field for the microscope objective (5.8 μm). Thus, as an underestimate, a step size of 5 μm was selected for z-scan imaging.

Next, the minimum number of focal planes necessary to image through a typical cluster of 20 or more cells was explored. Here, a total of five z-planes were extracted from the full 50 μm z-sequence at 5 μm intervals above the autofocus plane, generating a stack of z-images which were recombined sequentially using an ImageJ stack focusing algorithm. Figure 3-6(b) presents a subset of cells found in an adherent cluster at z = 0 in a single focal plane (i), followed by the combined image of two focal planes, z = 0 and 5 μm (ii), three focal planes, z = 0, 5, and 10 μm (iii), four focal planes, z = 0, 5, 10, and 15 μm (iv), and all five focal planes, z = 0, 5, 10, 15, and 20 (v). Using these combined images, a simple image threshold and segmentation macro was established to count the number of individual cells/nuclei which could be identified in each processed image as presented in Figure 3-6(c). Here, a total cell count of 129 was obtained for the single z = 0 focal plane identified via autofocus routine, while 142 cells could be identified using two focal planes, 152 cells in three focal planes, and 153 cells in four or five focal planes.

These differences were further demonstrated by overlaying the outline of individually identified nuclei in the cell cluster found in Figure 3-6(b). Obviously, a number of nuclei present in this cluster were poorly focused in the z = 0 focal plane which prevented their clear identification and subsequent measurement (Figure 3-6(b), i). The combination of two focal planes enabled identification of several more nuclei which were undetectable in the previous single image (Figure 3-6(b), ii). This trend continued with the addition of a third focal plane, but leveled off thereafter with the extra fourth and fifth focal planes (Figure 3-6(b), iii-v). Thus, in this instance three focal planes were sufficient to provide the maximum number of cells/nuclei that could be identified in the cluster, as well as the full field of view.

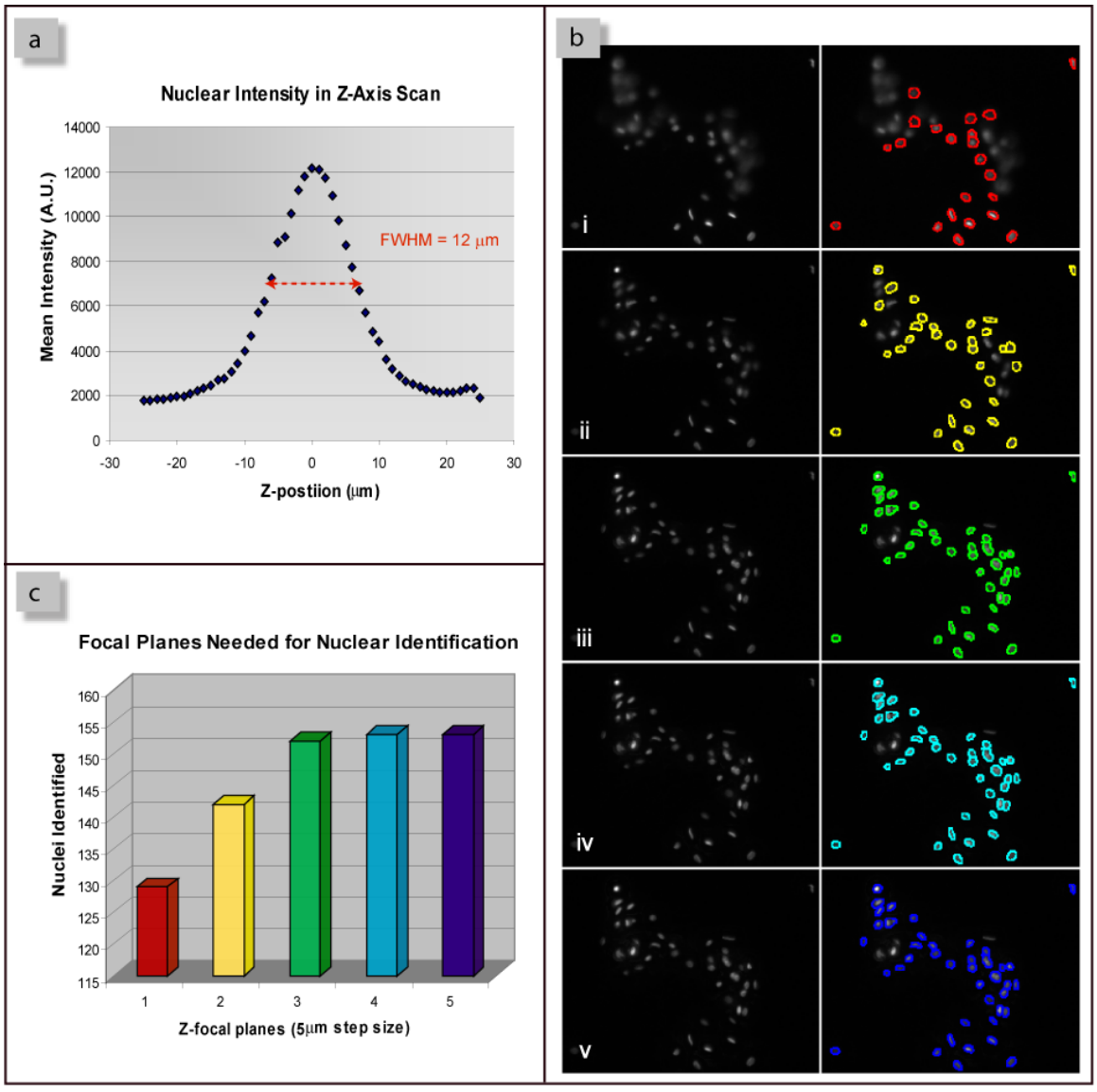

Figure 3-6. Examination of z-scan imaging parameters in DAPI-stained healthy cytology specimen with (a) nuclear intensity plotted as a function of distance along the Z-axis at 1 µm intervals exhibiting a 50% decrease in intensity approximately 6 µm above and below the ideal focal plane. (b) Using stack focusing algorithms, multiple image planes were recombined with the ideal focal plane, 0 µm (panel i) in progressive sequence at 5 µm intervals consisting of two focal planes, 0 and 5 µm, (panel ii); three focal planes, 0, 5, and 10 µm (panel iii); four focal planes, 0, 5, 10, 15 µm, (panel iv); and 5 focal planes, 0, 5, 10, 15, and 20 µm (panel v). "Focused" images of a typical cell cluster are shown at left with contours of nuclei detectable using automated image segmentation overlayed at right. (c) Graphical representation of the number of nuclei identified in progressive stacks of multiple Z-focal planes demonstrates that three focal planes are sufficient for maximum detection of nearly all nuclei.

3.3.6 Selection of Nuclear and Cytoplasmic Markers for Cytomorphometry

In order to measure biomarker expression on a single-cell basis, the entire cell must be recognizable and distinguishable from the background by the image analysis software. This was easily achieved with the EGFR biomarker alone in the tumor derived cell lines, even at very low levels in the MDA-MB-435S cells.[152] However, it was apparent very early that this was not the case for oral brush biopsies, particularly from healthy mucosa. Here, low EGFR expression and diffuse cytoplasmic/membrane labeling was insufficient to define the cellular area for measurement. This necessitated the investigation of cytoplasmic and nuclear counter-stains for identification of oral epithelial cells regardless of EGFR expression level and disease state. Ideally, these stains would be found in all cells with a relatively homogeneous intensity throughout the cell, and would be compatible with previously established cell processing techniques and EGFR assay.

Representative images of the five cytoplasmic markers examined in conjunction with the EGFR immunoassay (green) and DAPI staining (blue) in brush biopsy specimens are presented in Figure 3-7. Sulforhodamine 101, FM®4-64, and cytokeratin (Figure 3-7(a-c), red) all exhibited positive cytoplasmic labeling, but with rather heterogeneous or punctate staining patterns and poorly defined cell boundaries. Furthermore, FM®4-64 lipophilic dye was found to be incompatible with Histochoice-MB® fixation and generated a high fluorescence background emanating from the frit support underlying the membrane as a result of interaction with the black frit coating (data not shown). Immunolabeling with β-actin/AlexaFluor®-594 resulted in relatively low cytoplasmic intensity (Figure 3-7(d), red), but with somewhat higher EGFR (green) signal intensity. It appears as if non-specific binding or fluorescence bleed through may contribute to the higher EGFR intensity seen here as a result of overlapping emission spectra between AlexaFluor®-488 and AlexaFluor-®594. Phalloidin yielded positive

cytoplasmic staining in nearly all of the cells present with a moderately homogeneous labeling pattern that distinguishes individual cells from each other and the background (Figure 3-7(e), red). Based upon these results, phalloidin/AlexaFluor®-647 was chosen as a suitable cytoplasmic marker and subsequent dilution studies established an appropriate concentration of 0.33 μM for future assays (data not shown).

In all of the samples tested, DAPI exhibited excellent nuclear staining (Figure 3-7, blue). The presence of several small, faintly stained nuclei in Figure 3-7(a) and (b) may be indicative of superficial surface cells found in non-keratinized epithelium, whose nuclei often appear pyknotic. Interestingly, DAPI was also found to interact with the black coating applied to the frit support underlying the membrane (data not shown). This generated a relatively high background in the absence of the membrane or in combination with certain membranes which were not dyed black and/or possessed large pore sizes (~ 3 μm). The influence of this background fluorescence toward DAPI signals is not appreciable with the 0.4 μm black membranes utilized in the current study as evidenced by the extremely low background found in DAPI channel (mean 3.0 ± 1.0, range 1 - 33 in 8-bit scale). This is likely due to the increased thickness and surface area of the blackened 0.4 μm membranes and the low exposure times.

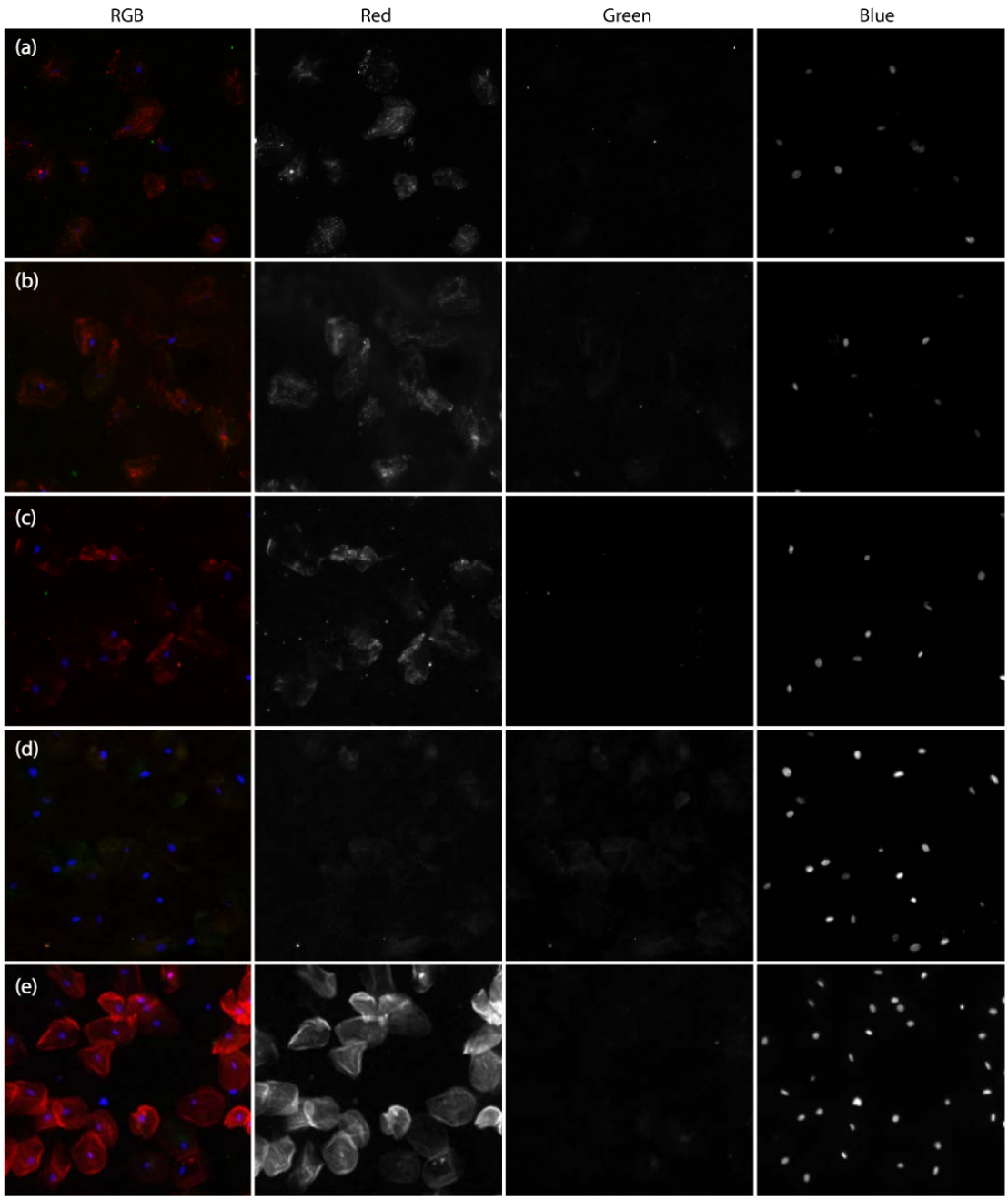

Figure 3-7. Comparison of cytoplasmic staining/labeling employing (a) sulforhodamine 101 total protein stain (0.2 s. exposure and 1.0 camera gain); (b) FM®4-64 lipophilic dye (0.2 sec, 1.0 gain); (c) pan cytokeratin/AlexaFluor®-594 antibody (0.5 sec., 2.0 gain); (d) β-actin/AlexaFluor®-594 antibody (0.5 sec., 1.0 gain); and (e) phalloidin/AlexaFluor®-647 (1.0 sec., 10.0 gain). Staining was perfomed in conjunction with EGFR assay (green) and DAPI staining (blue) in 0.5% formaldehyde fixed specimens. Brightness and contrast settings have been adjusted for visualization and printing purposes.

3.3.7 Digital Image Analysis

With the integration of exfoliative cytology specimens, the necessity for multiple z-focal planes and multi-spectral detection of EGFR/phalloidin/DAPI required development of a new, more complex image analysis strategy than previously described for tumor cell lines. In addition, the irregular shape of the epithelial cells and their adherent nature further complicated the image analysis process. Using a variety of image analysis tools, custom routines were developed to automatically detect individual cells and define the regions of interest (ROI) for EGFR biomarker measurement. This was achieved by strategic nuclear and cytoplasmic dye selection based upon the assumption that each cell must possess a nucleus and a surrounding cytoplasm. As such, when cells are closely clustered or adherent, their nuclei are less likely to overlap than the surrounding cytoplasm, thus, the DAPI stained nuclei serve to identify the presence of each cell regardless of clustering, while cytoplasmic phalloidin staining serves to identify the boundary of the cell surrounding each nucleus. Therefore, both dyes are necessary to identify the whole cell ROI for measurement of EGFR biomarker intensity. Early in the development of these methods, it became very apparent that the techniques necessary for measurement of biomarker expression in cytology cells could be used in parallel for cytomorphometric analysis, offering additional parameters in which to characterize malignancy.

An example image sequence is presented in Figure 3-8 showing the digital inputs and outputs at each stage of this process. Here, illumination corrected digital micrographs consisting of three z-focal planes were convolved using ImageJ stack focusing algorithms as shown in Figure 3-8(a), i-iv. These focused images were then utilized to define the nuclear and cytoplasmic outlines based upon intensity threshold and segmentation in DAPI and phalloidin images, respectively (Figure 3-8(b), v-xi). Touching cells were

separated based upon weighted parameters of intensity and distance from adjacent nuclei. Binary masks of primary (nuclei) and secondary (whole cell) objects were generated from which the regions of interest (ROI) outlining each paired cell and nucleus were drawn for measurement on the original focused image. All together nine morphological parameters and seven intensity parameters were extracted from three separate RGB channels for a total of 30 measurement parameters and one calculated parameter, nuclear-to-cytoplasm ratio (N/C ratio), per sample.

Examination of the Cell Profiler™ output image (Figure 3-8, xi) with outlines overlayed onto the original focused images demonstrates successful discrimination of the cell cytoplasm and borders between overlapping or adjacent cells. Although, this is by no means perfect and discrepancies between automated separation borders and visual interpretation may exist, but this method exhibits the best capability for cytologic analysis examined so far. As such, cytomorphometric measurements obtained from fifteen random cells in Figure 3-8, iv were as follows: mean cellular area, 2261 μm^2; mean cellular diameter, 70.9 μm; mean nuclear area, 55.2 μm^2; mean nuclear diameter, 11.1 μm; and mean nuclear-to-cytoplasm ratio, 0.027. Thus, using this combination of cellular dyes and image analysis sequence, we have identified an automated method for cellular examination and in the processes expanded the capacity of the LOC sensor assay for analysis of cytomorphometry, which has widely been demonstrated as a useful indicator of malignancy.

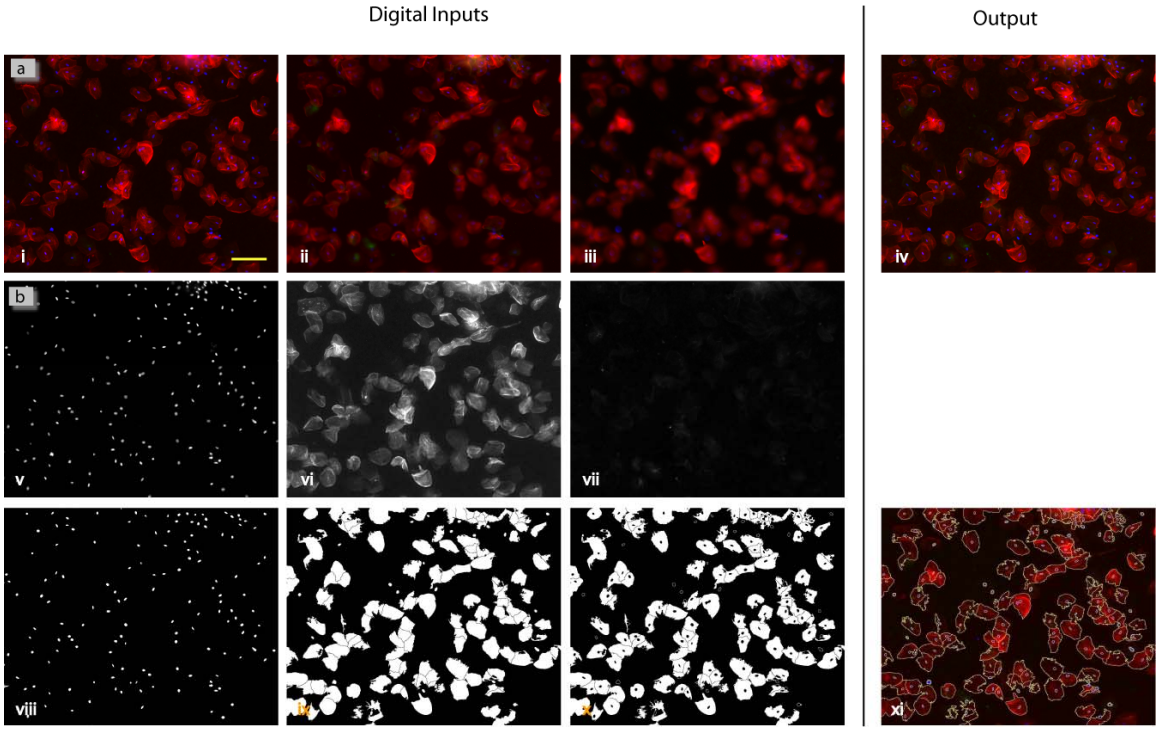

Figure 3-8. Digital image analysis was performed in ImageJ using custom macros and sequences for combining three z-focal planes, collected at 5 µm intervals, into a single convoluted or "focused" image (a, panels i-iv). This focused image served as the input for Cell Profiler (b) in separate RGB channels where the blue or DAPI channel (panel v) was utilized for primary identification of a cell followed by secondary identification of the cell cytoplasm surrounding each nucleus according to phalloidin staining intensity (panel vi). Binary masks of these objects are shown in panel viii and ix, respectively, and in a combined mask, panel x. The outlines of individual nuclei and cell boundaries generated from these masks (panel xi) were exported back to ImageJ for measurement and digital filtering to eliminate debris and non-cellular material. Scale bar is 100 µm.

3.4 DISCUSSION

The integration of exfoliative cytology into the LOC sensor methodology offers a number of opportunities as well as challenges for oral diagnostics. Advantages include the quick, non-invasive nature of cell sampling which could enable examination of lesions which do not call for surgical biopsy or in cases where surgical biopsy is not feasible. In addition, the relatively painless procedure could allow for repeated sampling

for monitoring purposes in high-risk individuals, response to treatment, and follow-up in OSCC patients. Challenges related to oral exfoliative cytology stem from the direct relationship between diagnostic capacity and the quality of the specimen collection and preparation, such that individual cell and nuclear characteristics should be visible in a monolayer of cells from all epithelial layers.

While the adequacy of sampling with the OralCDx brush technique has previously been reported, in the current application further verification was sought using the modified suspension-based protocol described herein.[76] Two basal cell markers, the AE1 monoclonal antibody and cytokeratin-14, were utilized for this purpose with positive cellular staining seen in both instances as demonstrated in Figure 3-2. The AE1 monoclonal antibody recognizes shared epitopes on all acidic (Type 1) cytokeratins including cytokeratin-10, -14, -15, -16, and -19, and has previously been shown to localize in basal/suprabasal cells in complex mucosal epithelium, such as the oral mucosa.[157, 158] In clinical applications, AE1 has also been employed in an antibody cocktail, in combination with AE3 mAB recognizing the basic (Type 2) keratins, to identify metastatic tumors of epithelial origin. Due to the multiple proteins recognized by AE1, an antibody specific to cytokeratin-14 only was further used to assess the presence of basal cells in cytology specimens (Figure 3-2b). All basal cells in stratified squamous epithelia have been shown to express cytokeratin-14, though expression may persist in upper stratified layers where differentiation-specific keratins are also expressed.[157] Despite the fact that cytokeratin-14 is not restricted to the basal epithelium, it may still serve as a useful basal cell marker due to higher intensity seen in basal versus suprabasal layers.[157]

While AE1 and cytokeratin-14 may be useful indicators of basal/parabasal cells, the cells with positive staining in Figure 3-2 do not all appear as small cuboidal cells with

slightly larger nuclei, characteristic of true basal cells. Therefore, the final classification was completed using the standard procedures employed by trained pathologists using H&E stains of paraffin tissue sections.[160] Based upon standard cytology techniques, as well as the AE1 and cytokeratin-14 staining profile, basal cells were confirmed in OralCDx brush specimens collected with the current protocol (Figure 3-2(c)). In addition, it was pointed out that the proportion of basal cells expected in a cytology sample, in relation to the intermediate and superficial cells, is rather low such that basal cells may not be visible in every 20X field of view. Taken together, the evidence and expert opinions support the use of brush cytology to provide an adequate sampling of cells representative from the basal, intermediate, and superficial layers of oral epithelium for application in the microchip sensor system.

Besides obtaining an adequate sampling of cells, one of the intrinsic challenges associated with exfoliative cytology is the examination of naturally adherent cells, which, when significantly clustered, may prevent clear visualization and imaging of infrequent or subtle signs of disease that are particularly important for detecting early malignancies. Of the methods investigated for cell dissociation, including both mechanical and enzymatic treatments, none provided satisfactory results (Table 3-1). For example, methods which successfully dissociated the cell clusters, such as 35 μm mesh filter or trypsin, were also accompanied by unacceptable levels of cell loss and/or cell lysis generating cellular fragments and isolated nuclei. As an alternative to these harsh cell dissociation techniques, capability of Z-scan imaging to enhance the detection and measurement of clustered cells was examined. Here, digital convolution or de-blurring of three z-focal planes at 5 μm intervals enabled detection of 19 additional nuclei present in a typical adherent cell cluster (Figure 3-6(b)) and 23 additional nuclei in the full field of view (Figure 3-6(c)). The subsequent convolution of an additional fourth or fifth focal

plane yielded only one more detectable nucleus in the full field of view (Figure 3-6(c)). Based upon these results, the acquisition of three focal planes at a z-step size of 5 μm served as the most appropriate parameters for z-scan imaging in exfoliative oral cytology specimens. Of course, the size of cell clusters encountered in oral cytology varies by specimen and may be larger or smaller than the one examined here. However, there is an important trade-off between the potential benefits of acquiring additional z-focal planes with sample photobleaching which must be considered. With this in mind, the minimum number of focal planes applicable to the majority of cell clusters was sought. As such, it is likely that a fraction of cells in clusters larger than the one in Figure 3-6 may remain undetectable. The effects of photobleaching were also minimized with the use of relatively stable fluorophores such as the Alexa series of molecular dyes.

During development of the LOC microchip assay using oral exfoliative cytology, cell fixation was performed in order to decrease the biohazard risk associated with human tissue and preserve sample integrity for delayed analysis. This is likely an unnecessary and unwanted step in a true point-of-care LOC sensor assay due to the additional time required and potential for sample loss during centrifugation and washing. Nevertheless, fixation serves a useful purpose during development of this new sensor technique, unfortunately, not all fixatives are suitable for immunocytochemistry. Therefore, the effect of various fixatives on EGFR immunolabeling intensity was examined in order to identify an appropriate method for LOC sensor assays as demonstrated in Figure 3-4. Based upon S/B ratio, Histochoice-MB® appears to be the best fixative with a S/B ratio nearly 4 times greater than any other method, including unfixed cells. This effect was also seen in the LOC sensor where tumor cell lines fixed in Histochoice-MB® exhibited appreciably stronger EGFR intensity (data not shown). While this phenomenon has been reported elsewhere and by the manufacturer, the mechanism remains unexplained and the

formula proprietary, leaving a number of variables essentially unknown. In addition, it was later discovered that this fixative is incompatible with FM®4-64 membrane staining, which raised doubts regarding the cellular effect and overall compatibility of Histochoice-MB® fixative in the development of future sensor assays. Thus, rather than the highest S/B ratio, the fixation method which was most similar to unfixed cells, 0.5% formaldehyde, was identified as the least disruptive method and most appropriate for LOC sensor assays, now and in future applications in the absence of fixation. Fixation in 0.5% formaldehyde exhibited mean EGFR intensity and signal to background ratio values closest to unfixed cells (112.8 and 114.6, respectively), followed by CytoChex® fixative (102.2). Other fixatives with a higher percentage of formaldehyde, particularly 4% and Cytofix/Cytopem® known to contain 4% formaldehyde, resulted in a slight shift of both the isotype and EGFR histogram peaks to the right with appreciably reduced S/B ratios (approximately 50). The affect is primarily seen on the isotype control indicating increased background fluorescence. Typically, fixation in 4% formaldehyde is performed after labeling of surface antigens and the higher level of cross-linking generated with 4% formaldehyde, versus 0.5% formaldehyde, may account for an elevation in non-specific antibody binding.[159] Although a variety of fixatives were examined, it is by no means exhaustive and additional fixatives and/or cell storage solutions may serve the purposes of the microchip sensor equally or better than 0.5% formaldehyde.

Another important factor to consider in the integration of exfoliative cytology into the LOC sensor is the dispersal of cells across the membrane surface. Under ideal conditions, cells would be distributed homogeneously throughout the membrane forming a well-dispersed monolayer. Under sub-optimal conditions, regional accumulation of cells may compound the challenges associated with imaging and analysis of aggregated or clumped cells, while regions devoid of cells prevent effective utilization of the full

membrane area. During the transition from cultured cell lines toward exfoliated cells, the change is cell size and shape significantly affected membrane dispersal such that re-optimization of the cell capture conditions was necessary. Here, a high flow rate of 2 mL/min and high viscosity of the cell suspension fluid (>50% glycerol/PBSA) improved cell dispersal over other methods generating a relatively even density of cells across then entire membrane capture area (Figure 3-5). The influences of flow rate and viscosity on cell dispersal may be elucidated by tracing the path of fluid flow through the LOC sensor and the forces acting upon suspended cells. Naturally, fluid will travel the path of least resistance, so as soon as the fluid enters the membrane chamber it exits through the first available membrane pores leaving behind the suspended cells. At high viscosity, the path of least resistance may result in fluid filling the entire membrane chamber before it is pushed through the membrane pores allowing cell capture in all regions of the membrane equally. Similar influences of viscosity have previously been seen in the membrane-based LOC sensor system for enumeration of $CD3^{+}CD4^{+}$ lymphocytes. In this instance, whole blood, with a viscosity of 4 mPa·s at 20^{0}C and 2.7 mPa·s at 37^{0}C, enhanced the dispersal of white blood cells enabling assay and sampling of the entire membrane area.[1] Interestingly, a 50% glycerol solution in water is reported to possess a viscosity of 6.0 mPa·s at 20^{0}C and 3.1 mPa·s at 40^{0}C, somewhat similar to whole blood.[161] While viscosity obviously has a strong affect on cell dispersal, sensor to sensor variations in fluidic channels created by mis-alignment of laminate adhesives during assembly may also contribute to altered dispersal patterns. Further development toward a clinical device should explore additional techniques to generate well-dispersed monolayers, such as liquid-based preparation and thin-prep techniques employed in slide-based cytopathology, and their applicability in the microchip sensor.[162]

Next, the incorporation of cytoplasmic and nuclear markers into the LOC sensor assay was explored. The need for these markers stems from the poor identification of cellular boundaries in exfoliative cells using the EGFR signal intensity alone, particularly in normal healthy mucosa. Five putative cytoplasmic markers were identified targeting diverse cellular structures or physiology, including one total protein stain, one lipophilic dye, and three cytoskeletal proteins as represented in Figure 3-7. Not suprisingly, all markers analyzed exhibited positive cytoplasmic or membrane staining to a certain extent. Although, only phalloidin staining appeared relatively homogeneous throughout the cytoplasm with well defined cell boundaries important toward identification of individual cells, and particularly separation of touching cells, during automated image analysis routines. Thus, phalloidin was selected as the cytoplasmic marker to be implemented in subsequent LOC sensor assays. In addition, DAPI provided superb staining of nuclei in all samples tested (Figure 3-7) thus serving as an excellent nuclear marker in microchip sensor assays. Overall, the integration of these cytoplasmic and nuclear markers into the LOC sensor system served to enhance cell identification and discrimination independently of biomarker expression level, analogous to the forward/side scatter parameters available in flow and image cytometry. Unlike traditional flow cytometry, these markers enable direct measurement of cellular morphology, including cell and nuclear size, area, perimeter, and nuclear to cytoplasm ratio which may provide additional information regarding the presence and progression of disease.

The extra complexity of z-scan imaging and cytomorphometry in irregularly shapped and adherent cells presented a number of unique challenges for image analysis. Foremost, among these was the difficulty associated with the separation of adherent or touching cells. While the z-stack focusing plugin in ImageJ sufficed for detection of nuclei in clustered cells, the focused cytoplasms remain overlapped due to their larger

size and direct cell-cell contacts as seen in Figure 3-8(a). Typical methods for separation, such as watershed technique, often resulted in over or under segmentation in larger cell clusters where the borders of cells were not very well defined, even with the use of phalloidin staining. Therefore, a combined approach was taken where each cell could first be identified by its nucleus and then by the cytoplasm surrounding each nucleus. In other words, the number of nuclei present in a cell cluster served to define the number of cells into which the cluster was expected to be divided. Cell Profiler™ routines were well suited for this type of approach with the dual identification of primary and secondary objects based upon DAPI and phalloidin intensity, respectively. During identification of secondary objects, separation of overlapping or adjacent cells was based upon a propagation algorithm according to weighted factors of intensity of phalloidin staining and distance to primary objects (Figure 3-8(b)). This method provided suitable identification and separation in the majority of cells as judged by visual examination (Figure 3-8(b), xi) which further enabled cytomorphometric measurement of cell and nuclear area, diameter, and nuclear-to-cytoplasm ratio. Unfortunately, this method requires the assumption that there exists one nucleus for each cell which may not always be the case, particularly in malignancies where bi-nucleated cells may occur. In addition, instances where individual nuclei are overlapping would improperly result in identification of a single cell cytoplasm suggesting the need for verification of proper segmentation and filtering of unwanted events in the final measurement data.

While Cell Profiler™ software was particularly useful for identification of individual cells; the program is relatively new, released in 2006, and a number of problems with its functionality were encountered during analysis which prevented its utility throughout the image analysis process. Therefore, initial image processing was performed in ImageJ prior to Cell Profiler™ analysis, such as illumination correction and

z-stack focusing, and image masks generated from Cell Profiler™ were exported back to ImageJ for final measurement. Through these image analysis tools, it was possible to achieve the objective of an integrated lab-on-a-chip analysis of cellular morphology and biomarker expression associated with oral cancer brush biopsy samples.

Taken as a whole, the studies presented in this Chapter have successfully defined new methods for examination of exfoliative cytology using the lab-on-a-chip sensor technique. The complete microchip assay sequence, with integrated cell capture, staining, and imaging/analysis routines, has been established as illustrated in Figure 3-9. In this overall process, each step builds upon the one before it, such that suboptimal conditions in any one step have significant implications toward the overall sensor analysis capability and output. This cumulative effect underscores the importance of the studies presented herein to characterized and isolate the key influences and requirements for cytologic analysis at each step, establishing the framework for diagnostically relevant assays applied in Chapter 4. As such, the major accomplishments in assay development and optimization of LOC sensor methods are further outlined in Table 3-3.

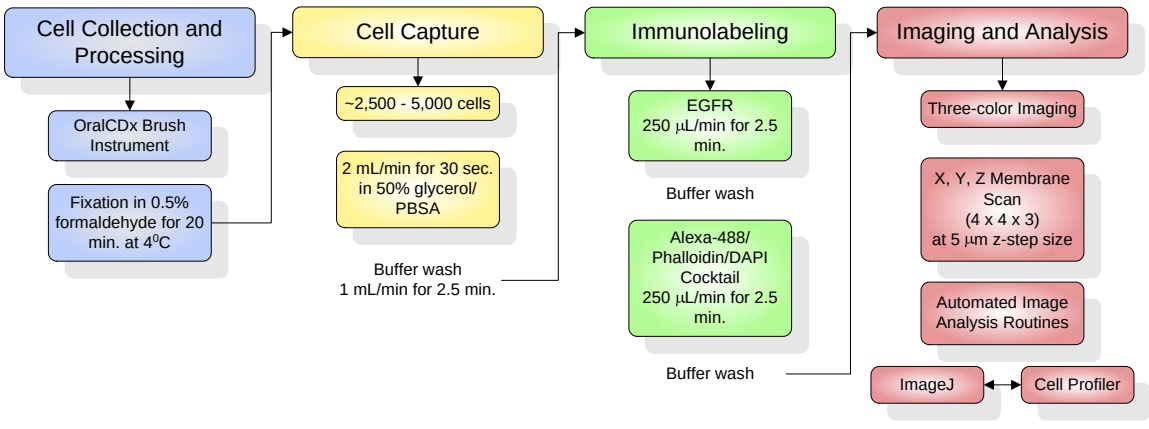

Figure 3-9. Schematic diagram of the full LOC sensor assay as described for EGFR biomarker detection and cytomorphometry from cell collection and processing, through cell capture on the sensor membrane, immunolabeling and staining with EGFR/Phalloidin/DAPI, fluorescent imaging and analysis.

Table 3-3. Accomplishments toward LOC cellular analysis methods

- Identified appropriate nuclear and cytoplasmic markers
- Developed compatible three color EGFR/Phalloidin/DAPI labeling protocols
- Optimized cell capture and dispersal conditions
- Established z-scan imaging approach for imaging of adherent cell clusters
- Developed custom image analysis routines for EGFR biomarker expression
- Incorporated cytomorphometry into LOC sensor analysis
- Determined the cell dissociation is unnecessary
- Demostrated intracellular staining without need for additional cell permeabilization
- Identified adequate sampling of oral epithelium using OralCDx brush instrument

3.5 CONCLUSIONS

In this Chapter, the dynamic influences and issues associated with LOC sensor assays integrating exfoliative cytology were examined and defined for the first time. Here the OralCDx brush cytology protocol was shown to provide an adequate sample of cells from the oral mucosa that can be introduced directly into the LOC device. The need for cell dissociation was discounted and overcome using a z-scan imaging approach. The parameters for sample introduction and capture on the sensor membrane were characterized, yielding a relatively homogeneous distribution of cells across the membrane surface critical for imaging and analysis. Cytoplasmic and nuclear markers were shown to be compatible with the EGFR assay and aid identification of individual cells for measurement; while new image analysis techniques and sequences were developed for examination of cytomorphometry in exfoliative cytology cells within the LOC sensor. Taken together, this research demonstrates capability of the LOC sensor system for dual molecular and morphological examination of clinically relevant exfoliative cytology tissue. Such biosensor systems may then be utilized to assess the strength of particular biomarkers, such as EGFR and/or cytomorphometry, for detection of disease and possibly prediction of tumor behavior.

Chapter 4: Preliminary Results of Pilot Study to Identify Clinical Utility of LOC Sensor Assay and Technique for Detection of OSCC

4.1 INTRODUCTION

In the preceding chapter, the important influences and imaging methods for expansion of LOC sensor assays integrating exfoliative cytology were defined. The next step toward development of a clinically relevant device was to initiate a pilot study whereby the sensor methods could be challenged with diseased and non-diseased samples to determine efficacy in characterizing oral malignancy. In the current chapter, the capacity of the LOC sensor system, with dual molecular and morphological assays, to serve as a suitable diagnostic platform for detection of OSCC and high-risk pre-malignancies is tested. Toward this goal, two overall objectives may be delineated; (1) examination of the sensor methodology itself in order to establish clinical viability and value of such lab-on-a-chip sensor devices, and (2) assessment of the established assay for detection of OSCC using a combination of EGFR biomarker expression and cytomorphometry.

Although oral cancer is a pressing medical issue, it is less prevalent than many other cancers occuring in the breast, ovary, prostate, or colon. Thus, the availability and access to oral cancer patients and tissue is far more limited. For this pilot study, an initial sample size of 25 – 30 participants, including healthy controls, was targeted in an effort to balance the number of OSCC patients which could be identified within a reasonable time-frame (~ 1 yr.) and the requirements for statistical inference. Patients were enrolled in the study by clinical collaborators at the University of Texas Health Science Center (UTHSC) at San Antonio and Houston Dental Branch and colleagues at M.D. Anderson Cancer Center. Eligibility criteria for inclusion in the study included presentation of a

clinically suspicious oral lesion in patients undergoing surgical biopsy. These lesions included leukoplakia or erythroplakia pre-malignancies, or overt lesions with signs and symptoms of suspected carcinoma within the oral cavity, with or without prior history of oral cancer. All oral lesions underwent surgical biopsy for histopathological diagnosis, which served as the "gold standard" for comparison with the microchip sensor technique. Tissue sections and/or cytospin preparations from these patients were submitted for immunohistochemical analysis for the epidermal growth factor receptor in order to provide comparison and possibly correlation between standard staining methods and the LOC sensor assay. When available, contralateral control brush cytology specimens taken from the "mirror image" of the lesion site served for assessement of wether or not the microchip sensor could provide useful information regarding cancer field growth.

4.2 EXPERIMENTAL METHODS

4.2.1 Study Participants and Demographics

A total of 31 participants were enrolled in this study from May 2007 to June 2008. Eleven of these volunteers were healthy individuals with no known oral diseases or signs of epithelial abnormality within the oral cavity. Nine of these healthy subjects were recruited from the student population at UT Austin, while two were from the laboratory of Dr. N. Vigneswaran from the Dental Branch at the University of Texas Health Science Center, Houston. An additional 20 clinical participants were identified by collaborating physicians located at UTHSC at San Antonio (n = 9) and Houston (n = 11). Eligibility criteria included patients presenting with a visible oral lesion(s) with suspicion of carcinoma who would be undergoing surgical biopsy or removal. Informed consent was obtained from all participants and the study guidelines were approved by the Institutional Review Board at each institution.

The demographic data and pathological diagnosis available from clinical participants is provided in Table 4-1. Of the 20 cases, 75% were male, 85% had a history of tobacco use, 42% also reported moderate to heavy alcohol consumption, and 70% were ethnically Caucasian. The average age in this clinical group was 57 (40 – 75 years). The majority of lesions occurred in the tongue or floor of the mouth (12 of 20, 60%), with two cases from the soft palate, two from the hard palate, one alveolar ridge, one retromolar trigone region, and one from the gingiva. Diagnosis was established for each patient by surgical biopsy of the lesion site and standard histopathology by board certified oral and maxillofacial pathologists at their respective institutions. These included fourteen squamous cell carcinomas, one lymphoma, three dysplasias (mild, moderate, or severe), and one benign hyperkeratosis. Ten of the SCCs were moderately differentiated and one was poorly differentiated, while the remaining were undetermined. The group of eleven healthy participants consisted of 55% males, 64% of which were ethnically Caucasian, with an average age of 33 (21 – 53 years). Only one of the healthy participants reported a history of smoking.

Table 4-1. Demographic data and pathological diagnosis for study participants enrolled at UTHSC San Antonio and Houston clinics.

Patient ID	*Age*	*Sex*	*Ethnicity*	*Smoking History*	*Lesion Location*	*Pathological Diagnosis*
UTSA-001	48	M	Hispanic	1pack/day	Floor of mouth (L)	Moderately differentiated, keratinized SCC
UTSA-002	56	M	Caucasian	37 pack years	Base of tongue (R)	Poorly differentiated SCC
UTSA-003	57	M	Caucasian	45 pack years	Soft palate	Mild-moderate dysplasia
UTSA-004	44	M	Caucasian	24 pack years	Soft palate and tonsil	Moderately differentiated SCC
UTSA-005	40	M	Caucasian	30 pack years	Lateral tongue	SCC
UTSA-006	48	M	Asian	No	Hard palate (R)	Benign hyperkeratosis and submucosal fibrosis
UTSA-007	45	F	Hispanic	No	Ventral tongue	SCCA
UTSA-008	44	M	Hispanic	Yes	Alveolar ridge	Lymphoma
UTSA-009	64	M	Caucasian	Yes	Retromolar trigone	SCCA
UTH-001	56	M	Caucasian	30 pack/yrs.	Hard palate	Invasive SCC, moderately differentiated, ulcerated
UTH-002	68	M	Indian	½ pack/day; betel nut use	Hard palate	Invasive SCC, moderately differentiated, ulcerated
UTH-003	53	M	Caucasian	31 pack/yrs.	Tongue	Invasive SCC, moderately differentiated, ulcerated
UTH-004	52	M	Caucasian	1 ½ x 30 yrs	Tongue, floor of mouth	Invasive SCC, moderately differentiated, ulcerated
UTH-005	74	F	Caucasian	Quit > 40yrs. ago	Tongue	Residual SCC - ulcerated
UTH-006	47	M	Asian	10-15/day for 25 yrs.	Tongue, floor of mouth	Invasive SCC, moderately differentiated, ulcerated
UTH-007	75	F	Caucasian	40 pack/yrs.	Tongue	Moderate dysplasia
UTH-008	50	M	Caucasian	30 pack/yrs.	Tongue	Invasive SCC, moderately differentiated, ulcerated
UTH-009	79	F	Caucasian	No	Tongue	Invasive SCC, moderately differentiated, ulcerated
UTH-010	69	M	Caucasian	1 ½ pk/day for 55 yrs.	Tongue	Focal superficially invasive SCC, moderately differentiated, ulcerated
UTH-011	62	F	Caucasian	40 pack/yrs.	Gingiva	Leukoplakia – severe dysplasia

4.2.2 Sample Collection and Processing

Exfoliative cytology specimens were collected using the OralCDx® biopsy brush by placing the nylon brush firmly against the epithelial surface and rotating 10-15 times, while applying moderate pressure, till pinpoint bleeding was attained. Cells were then released from the biopsy brush and suspended in 5 mL cold EMEM culture media in a 15 mL centrifuge tube using vigorous agitation for 15-30 seconds. Culture media was removed by centrifugation at 1200 rpm for 5 minutes. Cells were then washed twice in 3 mL PBS buffer (BupH™ Modified Dulbecco's Phosphate Buffered Saline Packs #28374, Pierce/Thermo Fisher Scientific, St. Louis, MO) by centrifugation at 1200 rpm for 5 minutes. Following the final wash, the supernatant was discarded and the cell pellet was resuspended in cryopreservative, consisting of fetal bovine serum with 10% dimethyl sulfoxide (DMSO), and frozen at -80^0C in order to allow for long-term storage and transport to Austin for LOC sensor analysis. In preparation for analysis, frozen samples were thawed rapidly in a 37^0C water bath, fixed in 0.5% formaldehyde in PBS for 20 minutes at 4^0C as described and then stored at 4^0C for up to two weeks. All pre-processing was carried out in a certified biosafety level-2 facility as necessary for working with human tissue and/or blood bourne pathogens.

Healthy brush biopsy samples were all collected from the buccal mucosa, while clinical samples were collected from the lesion site or surgically excised tissue using similar protocols. When possible, a "mirror image" brush specimen was collected from the contralateral oral cavity site relative to the lesion. In addition, when multi-focal regions of irregularity were present, multiple brush biopsies from the same lesions were taken sampling clinically distinct lesion areas.

4.2.3 LOC Cellular Assay and Data Extraction

Based upon the combined influences and results presented in chapter 3, the overall LOC sensor assay for EGFR biomarker detection and cytomorphometry in exfoliative brush cytology specimens was instituted as outlined in Figure 3-9. Here, approximately 2,500 – 5,000 fixed/processed cells suspended in 50% glycerol/PBSA were delivered and captured in the LOC sensor membrane at a flow rate of 2 mL/min for 30 seconds followed by a 2.5 minute PBS buffer wash at 1 mL/min flow rate. Next, immunolabeling was carried out through sequential delivery of immunoreagents, consisting of primary (10 μg/mL anti-EGFR in PBSAT) and secondary (20 μg/mL goat anti-mouse/AlexaFluor®-488, 33 μM phalloidin/AlexaFluor®-647, and 5 μM DAPI in PBSAT) staining cocktails, delivered to the membrane-captured cells at 250 μL/min for 2.5 minutes with intermittent buffer washes at 1 mL/min for 2.5 minutes. Following the final wash, an automated fluorescent imaging sequence was initiated for collection of three-color RGB micrographs from sixteen fields of view (4x, 4y membrane scan), at three 5 μm z-focal planes each, for a total of 54 images. Exported images were then analyzed in ImageJ and Cell Profiler as described using custom macros for identification and measurement of cellular and nuclear morphology and EGFR expression. A minimum of fifty cells were measured in each biopsy sample. All together, fifty-one parameters, nine morphological and forty-two intensity parameters, were extracted or calculated for each cell based upon the identified whole cell and nuclear ROIs. Particular attention was focused on the cellular area and diameter, nuclear area and diameter, N/C ratio and mean cellular EGFR intensity as these features have been previously reported to be early indicators of malignancy.[70, 139, 140]

4.2.4 Statistical Analysis of Data

A Student's t-test (Analyze-It® for MSExcel®) was utilized to assess statistically significant differences in the measured cellular parameters within each study group, including benign lesions, dysplasia, and invasive SCC, when compared to the healthy controls ($p < 0.05$). In order to identify which parameters, alone or in combination, were most predictive of disease, a logistic regression model was generated using MedCalc® (MedCalc Software, Mariakerke, Belgium) statistical software. This method requires the input of parameter values measured for each sample (i.e. EGFR intensity, nuclear and cellular area, etc.) according to a binary classification of disease status where non-diseased samples received a value of zero and diseased samples one ("Non-diseased" = 0; "Diseased" = 1). The logistic function, with general equation of $f(z) = 1/(1+exp(-z))$ serves to predict the probability of an outcome (disease occurrence) between 0 and 1 based upon one or more of these input parameters or factors. The variable (z), is a measure of the total contribution of all the factors used in the model, according to the logit equation $(z = a_0 + a_1xBM_1+a_2xBM_2+.....a_nxBM_n)$ where a_0 is the intercept and $(a_1....a_n)$ are the regression coefficients for each biomarker $(BM_1....BM_n)$. Predicted values using the linear regression model were utilized to build receiver operating characteristics (ROC) curves plotting the projected true positive and false positive rates (sensitivity vs. 1 – specificity) for disease classification based upon the model.

4.3 RESULTS

A total of 34 oral brush cytology samples from healthy and disease participants were examined using the LOC sensor method. Eleven specimens were obtained from healthy individuals while twenty-three were from clinically suspicious lesions identified in twenty patients. Histopathological diagnosis confirmed one case of benign hyperkeratosis and submucosal fibrosis, three lesions exhibited dysplasia, fifteen invasive

carcinomas, and one malignant lymphoma (Table 4-1). Two of the SCC samples were exhausted during the initial assay development stages, while another two specimens were found to be inadequate due to poor cell sampling (2 out of 32, 6.2%), including one SCC and one dysplasia specimen from the tongue. Table 4-2 summarizes the LOC sensor results obtained from the remaining 30 brush cytology specimens analyzed for cytomorphometry and EGFR expression.

Since this data was pooled from multiple patient sources and populations, statistical differences in sensor data and results according to facility were examined for validation purposes. No significant differences were identified between patient samples collected at UTHSC at San Antonio (n = 9) and Houston (n = 11) for any of the parameters listed is Table 4-2 ($p > 0.2$). However, healthy control specimens collected at UTHSC Houston (n = 2) and UT Austin (n = 9) did exhibit a significant difference in their respective nuclear area measurements ($p = 0.026$). This discrepancy may be linked to an elevation in nuclear size with advancing age as there was a significant difference between the average age of these groups.[163] This reflects a minor flaw in the study design where healthy participants were recruited from a younger student population than the typical OSCC patient, 50 years and older. This age difference evolved due to practical considerations associated with the collection of normal controls and the difficulty in the early stages of this program to secure age-matched samples from the clinical collaborators. Age matched healthy individuals would have been more appropriate and should be incorporated in futher studies. Given the promising results here obtained in the initial pilot study, it is clear that the additional effort to collect such age-matched patients is warranted. Nevertheless, overall the specimens from all institutions were quite similar and could reasonably be pooled for added value in determining the efficacy of the microchip sensor system.

4.3.1 Cytomorphometry

A significant reduction in cellular area was revealed in invasive SCC and a B-cell lymphoma malignancy (586 μm^2 and 524 μm^2, respectively) versus healthy control mucosa (1038 μm^2) ($p < 0.0001$). A slight decrease in cellular area was also seen in cases of dysplasia, although this difference was not significant. A similar pattern occurred with the cellular diameter in which there was a significant decrease found in both malignancies, but not in dysplasia. On the other hand, the nuclear area and diameter where shown to increase with malignancy and, in this instance, dysplastic cells exhibited significant nuclear enlargement over healthy controls as did SCC and lymphoma (Table 4-2). Interestingly, this rise in nuclear area appeared to be progressive from healthy mucosa through dysplasia and SCC (63.4 μm^2, 122 μm^2, and 143.5 μm^2, respectively), though the difference in nuclear area between dysplasia and SCC was not found to be significant. In line with the inverse relationship demonstrated between nuclear and cellular size, the nuclear-to-cytoplasm (N/C) ratio was also found to be significantly higher in dysplasia, SCC, and lymphoma over healthy controls, suggesting that all of these morphometric parameters measured may serve as indicators of malignancy.

Table 4-2. Results of LOC sensor assay and analysis of cytomorphometry and EGFR expression, reported as mean ± standard deviation, in study participants according to disease status.

	Healthy controls *n = 11*	***Benign*** † *n = 1*	***Dysplasia*** *n = 2*	***Invasive SCC*** *n = 14*	***Other Malignancy*** *n = 2*
Cellular Area (μm^2)	1040 ± 160	1670 ± 960	914 ± 200	586 ± 210* $p < 0.0001$	524 ± 120* $p < 0.0001$
Cellular Diameter (μm)	37.8 ± 3.2	46.9 ± 12	34.2 ± 2.0	27.7 ± 4.9* $p < 0.0001$	25.6 ± 3.9* $p < 0.0001$
Nuclear Area (μm^2)	63.4 ± 11	62.4 ± 59	122 ± 4.7* $p < 0.0001$	144 ± 47* $p < 0.0001$	116 ± 13* $p < 0.0001$
Nuclear Diameter (μm)	8.47 ± 0.5	8.49 ± 3.9	11.3 ± 1.0* $p < 0.0001$	12.3 ± 2.0* $p < 0.0001$	11.0 ± 0.8* $p < 0.0001$
N/C Ratio	0.063 ± 0.015	0.055 ± 0.062	0.138 ± 0.035* $p < 0.0002$	0.282 ± 0.14* $p < 0.001$	0.230 ± 0.079* $p < 0.0001$
Mean EGFR Intensity (au)	5.99 ± 1.4	5.23 ± 2.9	8.50 ± 1.3* $p < 0.04$	9.72 ± 6.1** $p < 0.035$	5.10 ± 0.75

* denotes statistical significance relative to healthy controls using paired t-test ($p < 0.05$)
† single case of benign submucosal fibrosis could not be statistically compared due to lack of replicates
** statistically significant with the removal of one outlier, sample UTSA-005
au – arbitrary units

Further examination of the nuclear area distribution within each sample population revealed additional features which could potentially be exploited for disease characterization. Box and whisker plots presented in Figure 4-1 depict the median, inter-quartile range and data outliers in the distribution of nuclear area measurements from each sample population analyzed using the LOC sensor. Here, the median nuclear area for healthy control samples ranged from 47 μm^2 to 63 μm^2, while the SCC samples exhibited median values from 66 μm^2 to 141 μm^2. Quite interestingly, it is the spread of outliers that appeared to be the most distinguishing characteristic in which to differentiate normal cytology specimens from dysplasia and SCC. As such, none of the healthy

controls specimens exhibited outliers over 500 μm^2 while all of the SCC specimens possessed numerous outliers over 500 μm^2. Indeed, the two cases of dysplasia also showed a shift toward increased nuclear area within the outlier subset of cells suggesting that the outlier population and/or the range in nuclear area distribution may be useful for early disease characterization.

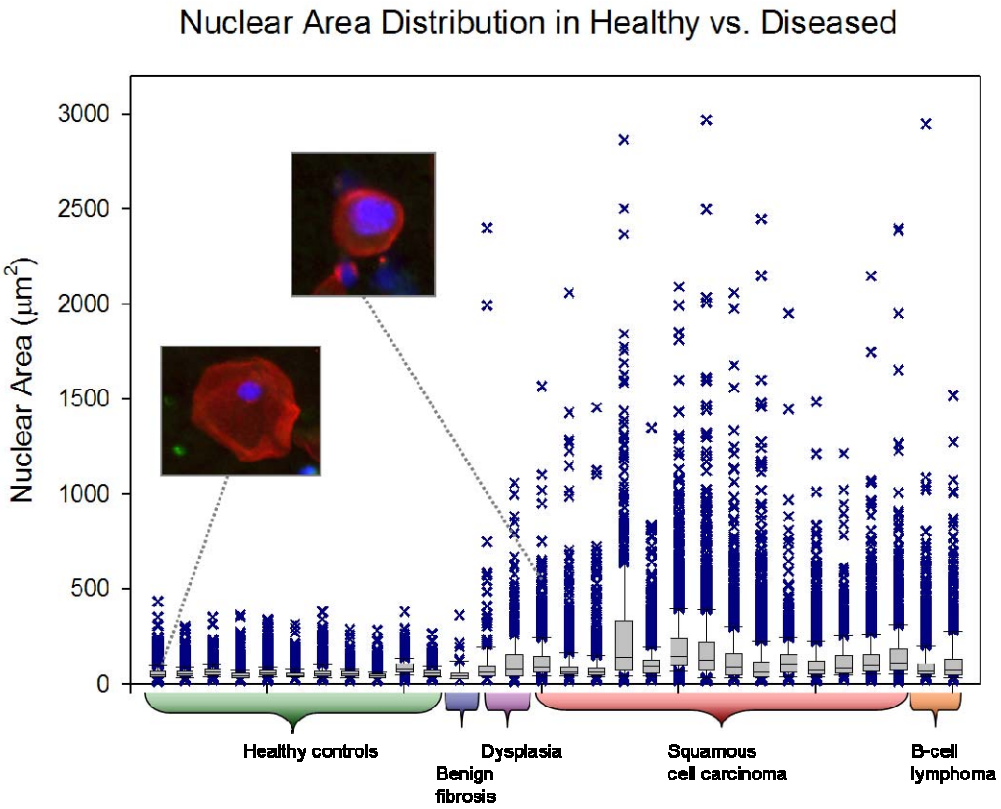

Figure 4-1. Box and whisker plot of the median, interquartile range, and the distribution of outliers in the nuclear area data for each cell population according to disease status. Two representative cells from a healthy participant and SCC patient are shown (inset).

4.3.2 EGFR Biomarker Expression

In addition to changes in cytomorphometry, the mean EGFR intensity was also demonstrated to be higher in lesions with diagnosed dysplasia and OSCC relative to

healthy epithelium (8.5 au, 9.7 au, and 6.0 au, respectively) (Table 4-2). While EGFR intensity increased with disease, the fraction of cells which express EGFR may also be indicative of malignancy. Therefore, an EGFR labeling index was calculated as the percentage of cells with positive staining above normal and isotype controls (6.0 au) as plotted in Figure 4-2. Among the healthy controls, a wide range of EGFR labeling indices was found; with two specimens in particular exhibiting indices nearly double that of their nearest neighbors. Within the clinical specimen group, over-expression of EGFR was identified using a rough threshold established from the mean EGFR labeling index for the healthy control subjects plus two standard deviations (0.028 ± 0.05). According to this criteria, nine out of fourteen SCC tumors (64%) and 50% of dysplastic lesions over-expressed EGFR. A representative image from one of these EGFR over-expressing carcinomas is shown in Figure 4-2 with strong EGFR staining apparent in the cell membranes of this adherent epithelial cluster. The one benign lesion displayed a low EGFR labeling index within the range for most healthy controls, while the non-epithelial malignancy, diagnosed as B-cell lymphoma, was similar to healty control tissue as well. Although this threshold serves only as a rough estimate to compare EGFR expression levels, it does not necessarily correspond to the optimal threshold with diagnostic decision making capacity which will be examined in further detail below.

Contralateral controls were available from six participants as shown in Figure 4-2 denoted with an (*) and lighter bar shade located adjacent to their matched lesion site. Over 80% of the contralateral controls demonstrated EGFR labeling indices that were lower than their respective lesions and well within the ranges of healthy mucosa. One contralateral control did exhibit elevated EGFR labeling index, although this occurred in a SCC which itself was not shown to over-express EGFR. With the limited dataset and

contralateral control specimens available, the presence or absence of field changes remains unclear. Further studies are required to explore this issue.

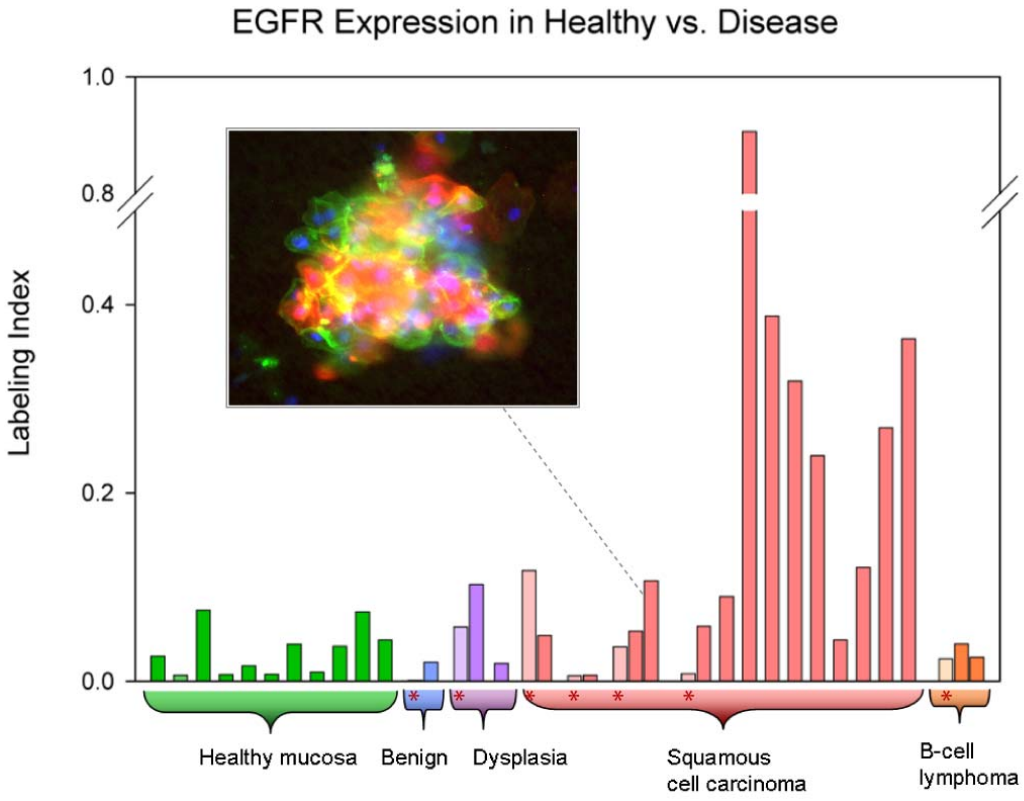

Figure 4-2. EGFR labeling index in all LOC specimens grouped according to disease status. A representative cluster of epithelial cells with strong EGFR staining is shown from a SCC specimen while available contralateral controls (*) taken from healthy appearing mucosa in clinical subjects serve to assess the extent of field changes in a subset of diseased patients.

4.3.3 Case Study: Comparison with Histopathology and Immunohistochemistry

While histopathology and EGFR immunohistochemistry was performed for all surgically biopsied oral tissue, two cases were selected to demonstrate the similarities and differences in the type or range of cellular features examined in traditional diagnostic methods versus the microchip sensor system using brush cytology (Figure 4-3). One case

was diagnosed as mild to moderate dysplasia in the soft palate (Figure 4-3(a)) and the other an invasive squamous cell carcinoma located on the ventral tongue (Figure 4-3(b)). In the hematoxylin and eosin (H&E) stained tissue shown in Figure 4-3(a), panel i, a thin keratin layer is seen at the surface of the epithelium with the various stratified layers beneath, relatively normal for mucosa at this oral cavity site. Upon higher magnification (Figure 4-3(a), panel iii), several dysplastic features are seen including enlarged, irregular and/or mitotic nuclei found above the basal cell layer, with possible loss of basal cell polarity. Corresponding EGFR immunohistochemistry (IHC) revealed EGFR staining in the lower layers of epithelium, including the basal cells, which dissipated in the more superficial layers and in the surface epithelium (Figure 4-3(a), panel v). Cytologic analysis using the LOC sensor assay from this patient displayed a combination of both positive and negative EGFR-labeled cells (Figure 4-3(a), panel vii) presumably derived from the differential EGFR-expressing epithelial layers apparent in IHC. This behavior suggests that the sensor method and cytology effectively reflected molecular changes in tumor tissue, even at these early pre-malignant stages.

Similar pathological features were also seen in the SCC case, albeit more pronounced, where hyperkeratinization and a number of irregular or mitotic nuclei were visible in H&E histopathology sections (Figure 4-3(b), panels ii and iv) and IHC demonstrated strong EGFR staining throughout the tumor (Figure 4-3(b), panel vi). In the LOC sensor cytology assay, extremely high EGFR labeling intensity was evident in the cell membranes of adherent epithelial cell clusters and in some individual cells (Figure 4-3(b), panel viii). In the particular cluster shown in Figure 4-3(b), panel viii, a number of the nuclei present also appear irregular and/or enlarged, suggesting that these cells exhibit “cancer-like” nuclear characteristics reflective of what is seen in tumor tissue.

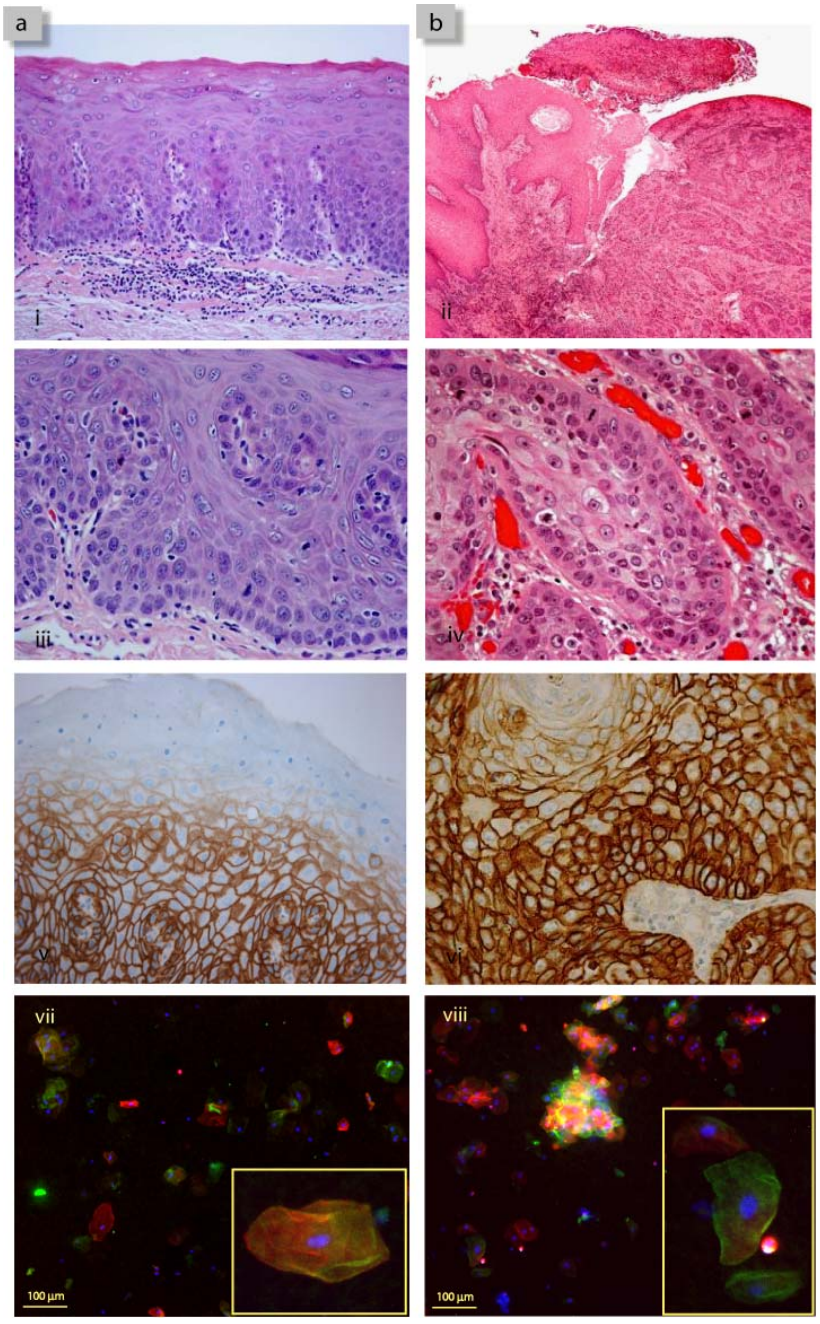

Figure 4-3. Comparison of histopathology, EGFR immunohistochemistry, and LOC sensor immunoassays in case studies of two patients, one with mild to moderate dysplasia (a) and one invasive SCC (b). Surgical biopsy tissue sections stained with hematoxylin and eosin are shown in panels i-ii and iii-iv at low and high magnification, respectively. Corresponding EGFR immunohistochemistry using peroxidase-DAB staining, panels v and vi. Representative images from LOC sensor assay using EGFR/phalloidin/DAPI staining, panels vii and viii, with inset of individual cells over-expressing EGFR.

4.3.4 Logistic Regression Model for Prediction of OSCC Disease

While these studies provide initial evidence supporting the value of cytomorphometry and EGFR expression in SCC detection, further exploration into which of these markers, and in what combinations, could be most effective toward diagnosis of oral cancer was necessary. Each individual biomarker was evaluated by a receiver operating characteristic (ROC) curve, as shown in Figure 4-4 for EGFR, N/C ratio, and nuclear area. The ROC curve is a plot of a diagnostic test's sensitivity, or true positive rate (TPR) versus 1-specificity, or the false positive rate (FPR) at various discrimination thresholds depicting the trade-offs between the true positives (benefits) and the false positives (costs) in diagnostic accuracy. All of the markers tested exhibited significant capacity for disease classification and discrimination between patients with OSCC or severe dysplasia, versus healthy controls or patients with mild-moderate dysplasia, as demonstrated by the area under the curve (AUC) values greater than 0.5. Of these markers, the N/C ratio exhibited the best performance characteristics with AUC of 0.99, followed by the nuclear area (0.97) and EGFR biomarker (0.67) (Figure 4-4). While the N/C ratio alone is an excellent diagnostic marker, the added value of these markers in a combined panel was further examined using logistic regression. Here, the ROC curve generated from the predicted values in the combined biomarker panel, exhibited AUC of 1.0 with a projected 100% sensitivity and 100% specificity for disease classification. Thus, the combined cytomorphometry and EGFR panel likely holds the greatest potential for cancer detection and diagnosis. Obviously, additional studies incorporating a larger patient sample size are needed to test and validate this model in order to define the true sensitivity and true specificity of the LOC sensor method in oral cancer diagnostics for

external blind studies. Nonetheless, these initial findings en route to devising a new method for cancer screening and diagnosis look promising.

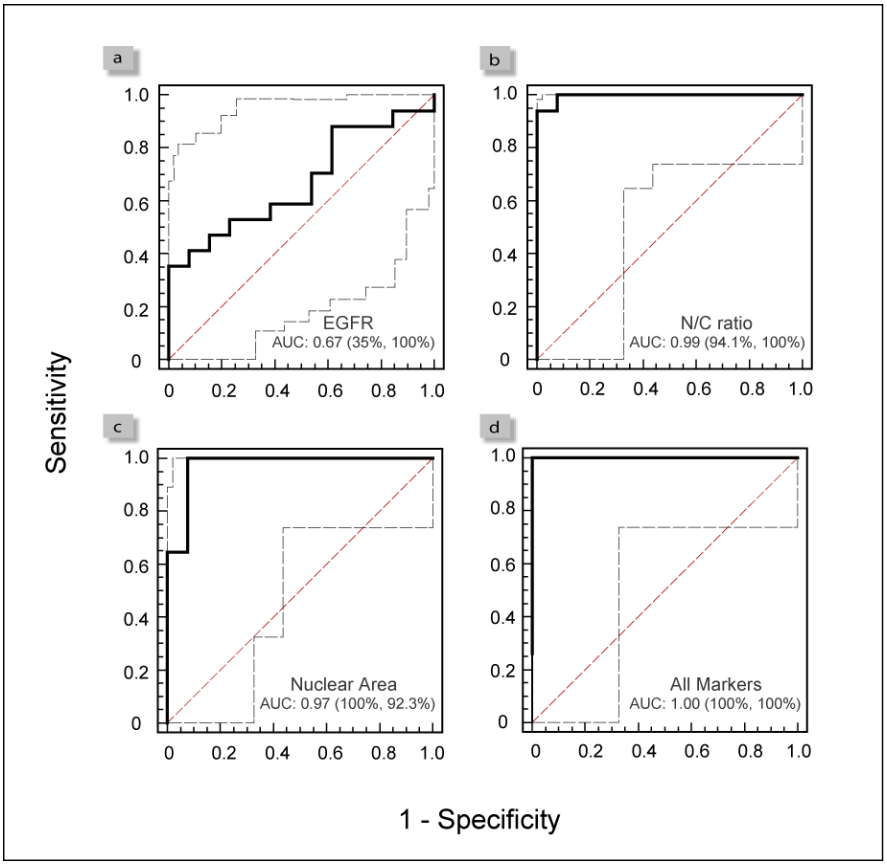

Figure 4-4. Receiver operating characteristic (ROC) curves were used to evaluate the performance characteristics of cytomorphometry and EGFR biomarker, alone and in a combined biomarker panel, for detection and diagnosis of oral cancer. Area under the curve (AUC) for single parameter measurements (a) EGFR biomarker is 0.67 and (c) nuclear area is 0.97; while two parameter ratiometric measurement of (c) the nuclear-to-cytoplasm ratio is 0.99. Using a logistic regression model the combined EGFR and cytomorphometry marker panel (c) is predicted to exhibit an AUC of 1.0 near diagnostic perfection.

4.4 DISCUSSION

In this small pilot study, the capacity of the LOC sensor assay and technique to detect oral cancer and pre-cancerous lesions was examined. Five morphological parameters were found to be significantly different in SCC versus healthy controls including: (1) cellular area, (2) cellular diameter, (3) nuclear area, (4) nuclear diameter, and (5) the nuclear-to-cytoplasm ratio (Table 4-2). The nuclear area, diameter, and N/C ratio were also found to be significantly different in cases exhibiting dysplasia, suggesting that these markers may serve as indicators of early pre-malignancy. The data presented here is very much in-line with earlier reports indicating significant morphological changes in cell and nuclear size, and N/C ratio associated with malignancy, while providing a new method for automated cytomorphometry that is rapid and highly amenable to point-of-care diagnostics.[137] In addition to cytomorphometry, the EGFR biomarker was also found to be significantly elevated in cases of epithelial dysplasia and SCC, supporting a role for EGFR in clinical diagnosis of malignant and pre-malignant lesions as well.

While examination of the mean values obtained for each cytology sample provides valuable information regarding the cell population as a whole, it is important to note that these samples represent a heterogeneous mixture of cell types. As such, healthy cytology specimens are expected to consist of combinations of basal, intermediate, and superficial cells with varying morphological characteristics and protein expression patterns. In the presence of disease, a mixture of normal and abnormal cells overlayed upon this inherent cellular diversity would be expected as well. Thus, examination of the population distribution, with particular attention toward the outliers in the data, may provide additional insight regarding the cellular phenotypes present and reveal any characteristic shifts within the population which may be related to the onset of disease.

These data outliers may represent the "rare events" important for disease detection which may be obscured or masked in mean measurements over the entire population. As shown in Figure 4-1, the spread of outliers in the nuclear area measurements can clearly distinguish healthy controls from dysplasia and SCC. A new parameter, such as a "polymorphic index", representing the range or spread in this distribution may provide an addition handle from which to classify disease with enhanced accuracy over mean values in future assays.

Along these same lines, the intensity of EGFR staining was shown to increase with disease, yet this may not represent the full extent of EGFR alterations associated with malignancy. For example, shifting patterns of EGFR expression, even at low levels, extending into the more superficial layers of epithelium may also be found in tumorigenesis.[116] How this translates from intact tissue to dissociated cytology specimens is likely to be related to the number of cells sampled which express EGFR. Thus, a labeling index calculated as the percentage of cells with EGFR intensity exceeding that of normal healthy controls was utilized for examination of the EGFR-positive cell subset (Figure 4-2). Here, most of the healthy controls exhibited relatively low labeling indices with a small fraction of EGFR-stained cells, possibly the basal cells known to express EGFR. Two healthy controls did show elevated EGFR labeling indices. The role of EGFR in non-malignant conditions, such as inflammation and wound healing, may account for the elevated EGFR expression found in these healthy individuals. Within the clinical group, EGFR over-expression was defined by a rough cut-off established from the mean labeling index of the healthy controls plus two standard deviations. Using this criterion, 64% of SCC tumors and 50% of lesions exhibiting dysplasia were identified to over-express the EGFR biomarker, congruent with previous literature reporting EGFR protein overexpression in 34-80% of OSCC tumors.[58, 70] These findings support EGFR as

an indicator of malignancy with diagnostic value, but allude to the need for a combined biomarker panel for cancer diagnostics, since EGFR alone is not likely to be sufficient for detection and characterization of malignancy due to its involvement in non-malignant conditions and the fact that not all OSCC or pre-malignant lesions express EGFR.

The EGFR expression was also used to explore potential field changes related to the field cancerization effect found in oral tumorigenesis. Here, 80% of the contralateral control sites exhibited EGFR labeling indices similar to normal healthy controls, and the one which did show elevated EGFR was in a patient whose SCC lesion itself did not over-express EGFR (Figure 4-2). While it appears that field changes were not evident in this study using the EGFR biomarker, the limited number of matched lesion and control samples restricts any firm conclusions. In this process though, the LOC sensor approach, with non-invasive cytology sampling, did demonstrate capacity for the ethical examination of normal appearing mucosa. As such, the sensor technique could be applied to probe the cancer field environment for molecular alterations beyond EGFR expression in the future.

Comparison of the LOC cellular analysis methods with standard histopathology and immunohistochemistry, as shown in Figure 4-3, offers insight into the types of cancerous features available with each method and their associated benefits and trade-offs. Based upon histopathology, panel (a) was diagnosed with mild to moderate dysplasia with several abnormal/enlarged nuclei and a loss of basal cell polarity seen in H&E histology stained tissue sections, but with the overall epithelial structure and stratification maintained (Figure 4-3(a), panels i and iii). IHC results revealed EGFR expression restricted to the lower layers of epithelium (Figure 4-3(a), panel v). These alterations in nuclear morphology and EGFR expression were successfully detected and quantitated in the LOC sensor assay using automated cell analysis techniques (Figure 4-

3(a), panel vii), suggesting that the sensor method adequately reflects cellular alterations in tumor tissue, even at early premalignant stages. A similar comparison could be seen in a patient with invasive SCC (Figure 4-3(b)). A trade-off does exist with the loss of information regarding cellular architecture and cell-cell or cell-matrix interactions while gaining the capacity to obtain statistical sampling of cells for automated cellular analysis successfully shown here for characterization of morphological and EGFR biomarkers in malignancy.

While these studies provide the initial evidence supporting the value of cytomorphometry and EGFR expression in SCC detection, identification of which markers, alone or in combination, could be most effective toward diagnosis of oral cancer was undertaken in a more quantitative manner using logistic regression and ROC curves analysis. Logistic regression serves as a model to predict the outcome of disease, based upon input of one or more variables, such as the N/C ratio, nuclear area, and EGFR biomarker measurements obtained in LOC sensor assays. The predicted values generated from logistic regression were used to build ROC curves. A ROC curve is a graphical representation of a diagnostic test's sensitivity, or true positive rate (TPR) versus 1-specificity, or the false positive rate (FPR) at various discrimination thresholds. An ideal diagnostic test would perfectly classify individuals with and without disease, yielding a point in the upper left corner or coordinate (0,1) of the ROC space, representing 100% sensitivity (all true positives are found) and 100% specificity (no false positives are found). Alternatively, a completely random guess would give a point along a diagonal line (the so-called line of no-discrimination) from the bottom left to the top right corners. Thus, the diagonal line determines the areas of good or poor classification with points above the diagonal line indicating good classification results, while points below the line indicate poor classification ability. Values of the area under the curve (AUC), or C

statistic are computed, as well as the standard error (SE), and applied using a two-tailed p-value at the 95% confidence level, providing a measure of a diagnostic test's performance to accurately discriminate diseased from non-diseased individuals. In Figure 4-4, the ROC curves for the EGFR biomarker, nuclear area, and N/C ratio are presented. According to the prediction model, the EGFR biomarker exhibited only moderate disease discrimination capability with an AUC value of 0.67 and a curve located somewhat close to the diagonal. The ROC curves for the nuclear area and N/C ratio, on the other hand, were located very close to the top left corner with AUC values 0.97 and 0.99, respectively, indicating excellent disease classification performance. Thus, the two morphological parameters out performed the EGFR biomarker and hold the greatest potential for detection of OSCC in the current LOC sensor assay with a projected sensitivity and specificity of 100% and 92%, respectively for nuclear area and 94% and 100% for N/C ratio (Figure 4-4). In a combined panel with all three markers, ROC curve and AUC of 1.0 reveal a predicted 100% sensitivity and 100% specificity for diagnosis of OSCC and dysplasia based upon the current model and dataset. Validation of this model requires testing of additional samples from a larger patient population, with particular emphasis on pre-malignancies, but holds strong promise as a new tool for oral cancer diagnostics.

Evolving issues regarding the best approach toward early detection of oral cancer must consider advantages and disadvantages of the three competing methodologies using cellular, mRNA, or protein-based analyses. Previous studies by Li *et. al.*, demonstrated the use of seven salivary mRNA transcripts for discrimination of OSCC from healthy controls with a calculated area under the ROC curve of 0.95, yielding 91% sensitivity and 91% specificity.[72] However, practical concerns exist regarding the stability of mRNA in this unproven diagnostic approach. In addition, mRNA is not currently implemented in

cancer diagnostics or as widely accepted by the medical community when compared to cellular approaches, such as cervical cytology, or protein-based methods using biomarkers such as prostate specific antigen (PSA) and CA-125. Using a single protein, interleukin-8 (IL-8), Tan *et. al.* recently demonstrated an optical procedure for oral cancer diagnosis with an AUC value of 0.83.[164] As in many biomarker studies, single biomarkers alone often fall short of the necessary performance characteristics indicating the need for multiple diagnostic markers in order to achieve high sensitivity and specificity. In the current study, the capacity of a new cell-based imaging sensor for dual molecular and morphological analysis was explored for the first time. Area under the curve values for single parameter measurement of nuclear area were 0.97, while two parameter ratiometric measurement of the N/C ratio was 0.99. Either of these morphometric markers provides enhanced diagnostic performance over emerging mRNA or protein-based biomarkers. In addition, a logistic regression model of the combined EGFR and cytomorphometry marker panel was predicted to exhibit an AUC of 1.0 near diagnostic perfection. Of course, further validation of these diagnostic approaches is necessary in order to evaluate which method and markers are optimal for early detection of oral cancer in clinical practice.

4.5 CONCLUSIONS AND FUTURE DIRECTIONS

This dissertation has demonstrated a successful automated cellular analysis procedure using a lab-on-a-chip approach which integrates cell capture, staining, and measurement of both molecular and morphological biomarkers. This new method has been applied in a small pilot study isolating the important assay and imaging variables in order to secure an initial understanding of the diagnostic accuracy of such biosensor systems in clinical settings. While the method described herein projected 100% sensitivity and 100% specificity based upon a linear regression model, it is important to

note that this has been done only with a limited internal data set and LOC assays in additional samples are needed to test this model. Nonetheless, the rapid approach for cytopathological diagnosis of oral cancer on a chip shows strong promise. The next steps toward the development of a clinical device are to complete larger clinical studies, with particular emphasis on early OSCC and dysplasia, in order to validate the microchip sensor approach. Plans are currently underway for such studies.

APPENDIX A: CAD DRAWING OF THE LAB-ON-A-CHIP SENSOR

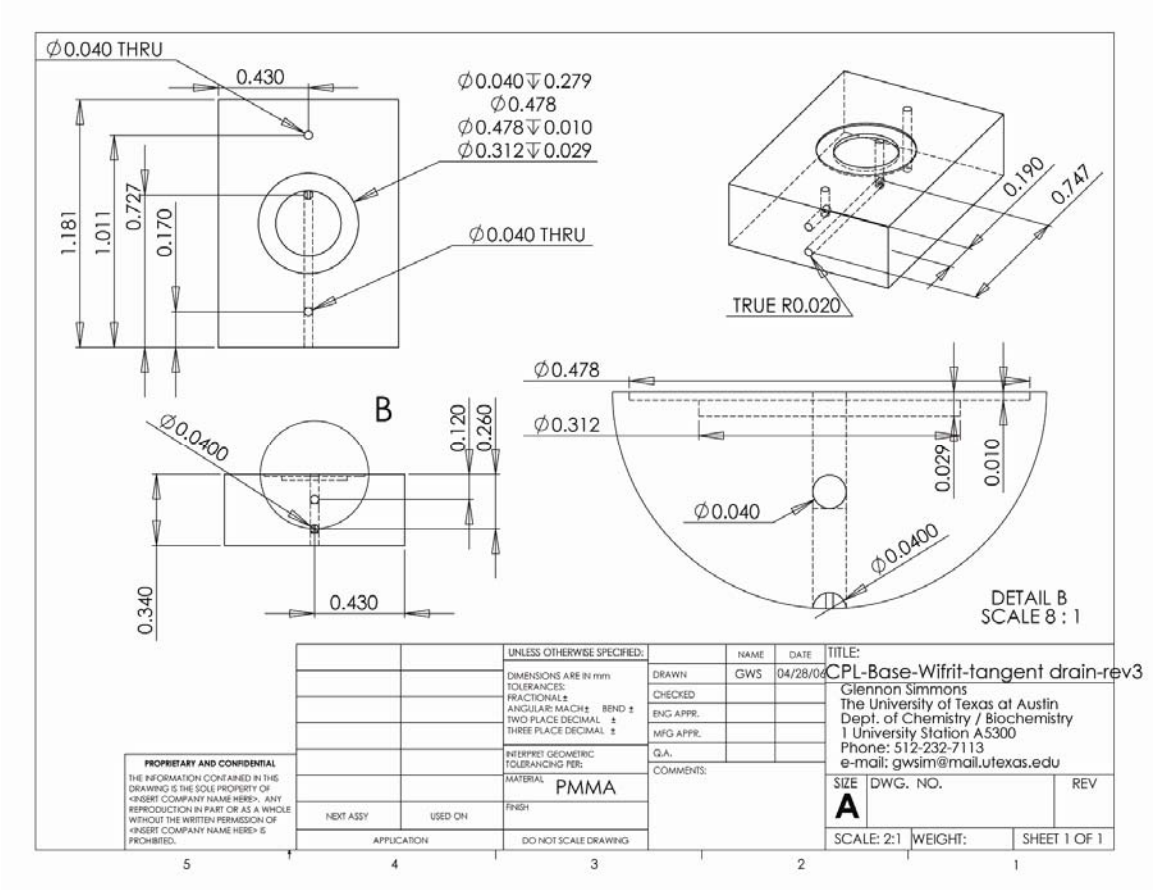

Figure A-1. Materials, design and machining specifications for the lab-on-a-chip sensor base utilized in the oral cancer studies.

Appendix B: Microscope Standardization and Monitoring

Since it was not feasible to complete all LOC assays within a single day, it was important to monitor and minimize the day to day fluctuations in microscope performance to enable reasonable comparison of all assays. The daily output of the mercury lamp and overall microscope functioning was monitored using a fluorescence reference slide (Fluor-Ref™ Green Intensity Slide Standard, Microscopy Sciences, Ltd.) prior to LOC sensor assays. Following Hg lamp warm-up period of at least 30 minutes, two images were collected of the Fluor-Ref™ slide, a brightfield and a darkfield image at 0.05 second exposure time with five-frame averaging for noise reduction. A neutral density filter (5.0) was utilized to attenuate the light source and bring exposure times into ranges relevant for immunoassays. Images were obtained at a z-position of -20 μm below the surface of the slide to minimize intensity variations due to surface imperfections. The darkfield image, which provided a measure of the dark current background, was subtracted from the brightfield image. Measurement of the mean intensity and standard deviation in the resulting image was plotted over time as shown in Figure B-1. Over an initial period of 2 months, the average intensity ±10% was utilized to establish the upper and lower boundaries for acceptable levels of microscope variation. Deviation from this intensity range signified need for microscope adjustment or maintenance, including replacement of the Hg bulb (Figure B-1, arrows). The Fluor-Ref™ slide also served as the homogeneous standard for measurement of field uniformity and field illumination correction as described above.

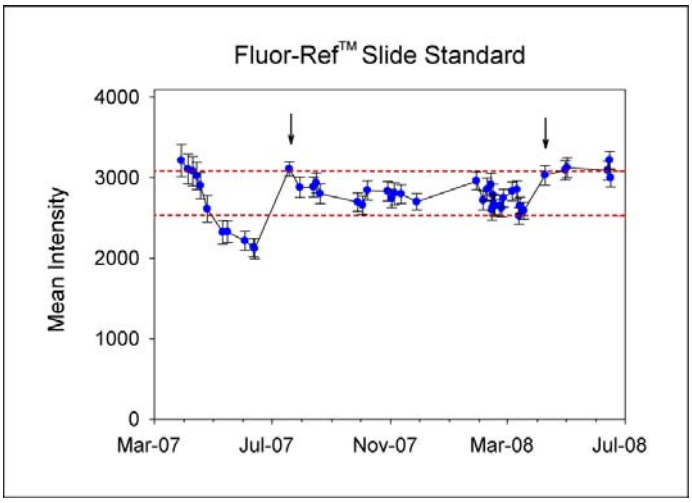

Figure B-1. The mean ± SD of a homogeneous fluorescent slide standard (Fluor-Ref™) was utilized to monitor microscope performance and Hg lamp output prior to each assay. Progressive decrease beyond the acceptable 10% deviation range typically signaled need for microscope adjustment and/or replacement of Hg bulb, shown at arrows.

Appendix C: EGFR Antibody Titration

The optimal antibody concentrations for LOC sensor assays were determined by titration of primary and secondary antibodies using a standard flow cytometry protocol and the A253 squamous cell carcinoma cell line. Here, cells were labeled with primary anti-EGFR antibody at concentrations ranging from 1 µg/mL– 20 µg/mL and a secondary goat anti-mouse IgG antibody conjugated to FITC fluorophore, packaged with the QIFI kit, which was reported to be at saturating concentrations. EGFR intensity was measured via flow cytometry with the resulting primary titration curve shown in Figure C-1, left. The optimal concentration of 10 µg/mL anti-EGFR was selected as the lowest concentration reaching saturation which was then applied in all subsequent EGFR assays. Secondary antibody titration was performed using 10 µg/mL primary antibody at increasing concentrations of goat anti-mouse IgG F(ab')$_2$ secondary antibody conjugated to AlexaFluor®-488 (Figure C-1, right). A concentration of 20 µg/mL was identified as the ideal secondary concentration with less than 10% increase in intensity when the antibody concentration was doubled, designated as saturation.

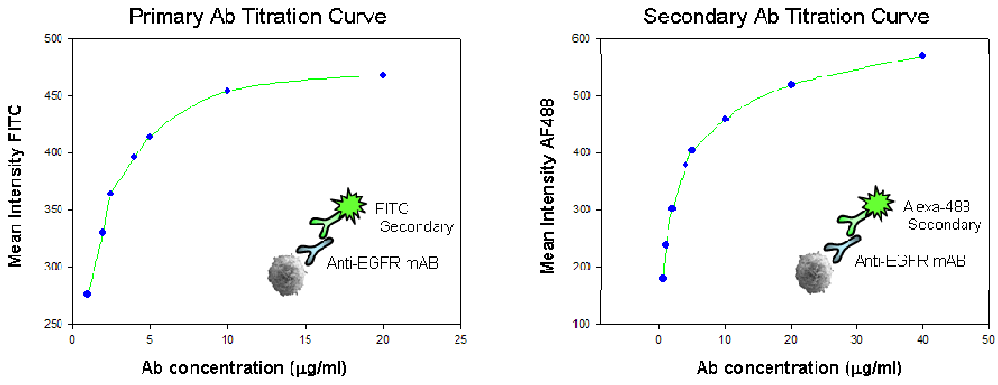

Figure C-1. Primary and secondary antibody titration curves to determine the optimal EGFR assay concentrations with 10 µg/mL primary and 20 µg/mL secondary antibody.

Appendix D: QIFIKIT® Quantitation in LOC Sensor

While the QIFIKIT® standards were designed for use in flow cytometry, their application in the LOC sensor for absolute quantification of EGFR biomarker expression was explored. Here, the set of five bead standards were labeled in the microchip sensor using the same protocol as for tumor derived cell lines with imaging performed in a 5 x 10 (x, y) membrane scan, 20X objective (0.4NA). Data extracted using established automated image analysis routines is presented as log transformed intensity histograms in Figure C-1. The QIFIKIT® standards (Figure C-1(a)) exhibited five visible intensity peaks from which the standard curve relating mean fluorescence intensity with the antibody binding capacity (ABC) of each bead was generated. Parallel EGFR assay and analysis performed on the tumor derived cell lines is shown in Figure D-1(b) with reported geometric mean and coefficient of variation for each population. Extrapolation from the standard curve identified the number of EGF receptors per cell (EGFR/cell) in each cell line as follows: 1.2 x 10^4 EGFR/cell in MDA-MB-435S cell line, 5.6 x10^5 EGFR/cell in MDA-MB-468, 1.1 x 10^5 in UMSCC-22A, 1.2 x 10^5 in SqCC/Y1, and 1.4 x 10^5 in A253 cells. When compared with EGFR/cell measured via flow cytometry, the two methods appeared to be well correlated with an r^2 value of 0.98 (Figure D-1(c)). However, upon closer examination the position of the cell lines relative to the bead standards was altered. For example, the OSCC cell lines in the sensor system were located between the third and fourth bead standards (Figure D-1(a), left panel), but in flow cytometry these same cells exhibited intensity ranges between the fourth and fifth bead standards (Figure 2-6) significantly affecting the extrapolated values. Calculation of the percent difference between the EGFR/cell for each cell line using flow cytometry and LOC sensor method revealed up to 52% difference (range 31% - 52%) between these two

methods, with the LOC sensor consistently exhibiting lower EGFR/cell values. This data indicated that while a nice correlation may exist, the agreement between the absolute EGFR values obtained using these two methods is poor and inappropriate for integration into the LOC sensor system.

There are a number of factors which may have contributed to this result. Foremost is the limited depth of field of the microscope optics (3.25 μm) which was below the average size of the QIFI beads (6.0 μm in diameter). Under these conditions, the full bead was not in focus within a single z-focal plane and therefore, light above and below may not be fully collected. This was even more pronounced in the measurement of cultured epithelial cells with a typical diameter of 20 μm or more. As such, measurable intensity from the beads/cells was only a fraction of the total intensity present and a disproportional fraction at that when intensity was compared from the beads to the cells due to the difference in size. Accounting for the consistently lower intensity measured in cells, where less than one-sixth of the cellular intensity was sampled, relative to the QIFI beads with over half of the bead found in one field depth. While in the current situation absolute quantitation using the QIFI standards in the microchip sensor was unsuccessful, use of a microscope objective with a lower numerical aperture, such as a 10X objective (0.3 NA) with calculated depth of field of 5.8 μm, and incorporation of z-scan imaging approach may help to overcome these limitations.

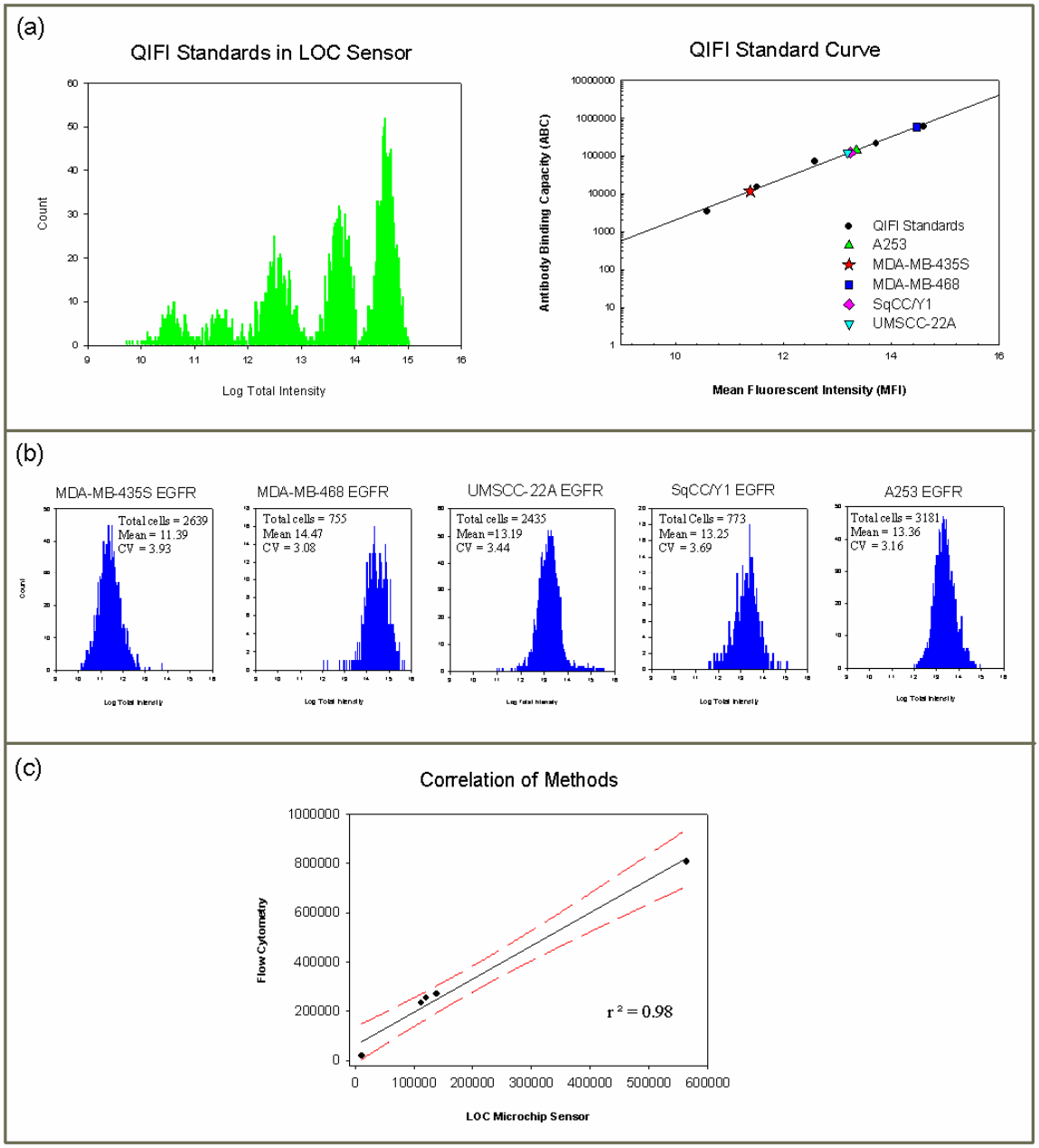

Figure D-1. Results of QIFIKIT® labeling and analysis as performed in the membrane-based LOC sensor system. (a) The LOC sensor successfully detected all five of the standard bead populations generating a standard curve relating the fluorescence intensity to antibody binding capacity (ABC) or EGF receptors per cell. (b) Parallel assays in five tumor-derived cell lines. (c) Correlation between the standard quantitative flow cytometry technique and LOC microchip system, with 95% confidence interval, yielded an r^2 value of 0.98 indicating good correlation between these methods.

Appendix E: Materials and Suppliers

Buffers and Reagents

- Phosphate buffered saline (PBS) (#28374 BupH™ Modified Dulbecco's Phosphate Buffered Saline, Pierce/Thermo Fisher Scientific, Rockford, IL) containing 0.008 M sodium phosphate, 0.002 M potassium phosphate, 0.14 M sodium chloride, 0.01 M potassium chloride, and 0.05% sodium azide was prepared in 500 mL deionized water (diH_2O) at final pH of 7.4.
- PBSA, consisting of PBS with 0.1% bovine serum albumin (BSA, #A3059, Sigma-Aldrich, St. Louis, MO), was used as a blocking agent and for storage of all cell suspensions at 4^0C.
- PBSAT, PBSA with 0.1% Tween-20 (#BP337, Thermo Fisher Scientific, Rockford, IL), was used for all antibody solutions unless otherwise stated.
- Formaldehyde fixative solutions, 0.5% - 4.0%, were prepared fresh for each assay by diluting 16% stock solution (#18814 Polysciences Inc., Warrington, PA) in PBS buffer.

Cell Culture Media and Supplements

- All cell culture media was obtained from American Type Culture Collection (ATCC Manassas, VA) including McCoy's 5A culture media (#30-2007) containing 1.5 mM L-glutamine and 2200 mg/L sodium bicarbonate; DMEM: F-12 medium (#30-2006) containing 2.5 mM L-glutamine, 0.5 mM sodium pyruvate, 15 mM HEPES, and 1200 mg/L sodium bicarbonate; Eagle's Minimum Essential Medium (EMEM, #30-2003) containing non-essential amino acids, 1 mM sodium pyruvate, 2 mM L-glutamine,

and 1500 mg/L sodium bicarbonate; and Liebovitz's L-15 medium (#30-2008) containing 2 mM L-glutamine with no added sodium bicarbonate.

- Fetal bovine serum (10% FBS, #10082 Gibco/Invitrogen, Carlsbad, CA) was supplemented to all media along with penicillin/streptomycin antibiotic solution (#30-2300 ATCC) at a final concentration of 50 IU and 50 µg/mL, respectively.
- Supplemental L-glutamine (GlutaMAX™, #35050-061 Gibco/Invitrogen, Carlsbad, CA) was added to media formulations as necessary to extend shelf-life of media.
- Trypsin/EDTA (0.25%) solution (#25200-56 Gibco/Invitrogen) dissociated *in vitro* cells from adherent culture flasks and/or brush cytology suspenstions.
- Trypan blue (0.4%) solution (#T8154 Sigma-Aldrich, St. Louis, MO) served to count and/or assess the cell viability at a 1:1 dilution with culture suspension in PBS or PBSA.

Antibodies and Fluorescent Dyes/Stains

Table E-1. Supplier and concentration information for all antibodies and fluorescent dyes/stains utilized in oral cancer studies.

	Supplier	Product #	Stock Concentration	Final Concentration in PBSAT
Primary Antibodies				
EGFR Ab-10 (clone 111.6)	Thermo Scientific-Lab Vision	#MS-378-P	200µg/ml in PBS with BSA and azide	10µg/ml in PBSAT
AE1	Abcam Inc.	#ab31117	0.2 mg/ml in PBS with BSA and azide	10µg/ml in PBSAT
Cytokeratin-14	Epitomics Inc.	#2001-1	undefined in Tris-glycine buffer with BSA and azide	1:30 dilution in PBSAT
Pan cytokeratin	US Biological	#C9097	0.68 mg/ml in PBS with BSA and azide	10µg/ml in PBSAT
β-Actin	Novus Biologicals	#NB110-55433	undefined in Tris-glycine buffer with	1:50 dilution in PBSAT

			BSA and azide	
Mouse IgG_1 (Isotype)	Sigma-Aldrich	#M-9035	1.1mg/ml	10μg/ml in PBSAT
Normal rabbit serum	Accurate Chemical and Scientific Corp.	#JNZ000001	60 mg/ml in PBS with azide	10 μg/ml in PBSAT
Secondary Antibodies				
Goat anti-mouse IgG $F(ab')_2$ AlexaFluor-488 conjugate	Invitrogen-Molecular Probes	#A11017	2mg/ml in buffer with azide	20μg/ml in PBSAT
Goat anti-rabbit IgG $F(ab')_2$ AlexaFluor-647 conjugate	Invitrogen-Molecular Probes	#A21246	2mg/ml in buffer with azide	20μg/ml in PBSAT
Goat anti-rabbit IgG $F(ab')_2$ AlexaFluor594 conjugate	Invitrogen-Molecular Probes	#A110037	2mg/ml in buffer with azide	20μg/ml in PBSAT
Fluorescent Dye/Stain				
DAPI	Invitrogen-Molecular Probes	#D3571	10.9 mM in diH_2O	5 μM in PBSAT
Phalloidin-AlexaFluor®647	Invitrogen-Molecular Probes	#A22287	6.6 μM in methanol	0.33 μM in PBSAT
Sulforhodamine 101	Invitrogen-Molecular Probes	#S359	1 mg/ml in PBS	20 μg/ml in PBSAT
FM®4-64	Invitrogen-Molecular Probes	#T13320	100 μg/ml in diH_2O	10 μg/ml in PBSAT

References

1. W. R. Rodriguez, N. Christodoulides, P. N. Floriano, S. Graham, S. Mohanty, M. Dixon, M. Hsiang, T. Peter, S. Zavahir, I. Thior, D. Romanovicz, B. Bernard, A. P. Goodey, B. D. Walker and J. T. McDevitt, A microchip CD4 counting method for HIV monitoring in resource-poor settings. *PLoS Med*, 2005, **2**, e182.

2. *Cancer Facts and Figures 2007* 500806, American Cancer Society, Atlanta, GA, 2007.

3. D. M. Parkin, F. Bray, J. Ferlay and P. Pisani, Global cancer statistics, 2002. *CA Cancer J Clin*, 2005, **55**, 74-108.

4. T. Y. Seiwert and E. E. Cohen, State-of-the-art management of locally advanced head and neck cancer. *Br J Cancer*, 2005, **92**, 1341-1348.

5. M. D. Ries LAG, Krapcho M, Mariotto A, Miller BA, Feuer EJ, Clegg L, Horner MJ, Howlader N, Eisner MP, Reichman M, Edwards BK (eds). SEER Cancer Statistics Review, 1975-2004, National Cancer Institute. Bethesda, MD, http://seer.cancer.gov/csr/1975_2004/, based on November 2006 SEER data submission, posted to the SEER web site, 2007.

6. J. B. Epstein, L. Zhang and M. Rosin, Advances in the diagnosis of oral premalignant and malignant lesions. *J Can Dent Assoc*, 2002, **68**, 617-621.

7. J. Kim and D. M. Shin, Biomarkers of squamous cell carcinoma of the head and neck. *Histol Histopathol*, 1997, **12**, 205-218.

8. J. K. Nagpal and B. R. Das, Oral cancer: reviewing the present understanding of its molecular mechanism and exploring the future directions for its effective management. *Oral Oncol*, 2003, **39**, 213-221.

9. K. Sokolov, J. Aaron, B. Hsu, D. Nida, A. Gillenwater, M. Follen, C. MacAulay, K. Adler-Storthz, B. Korgel, M. Descour, R. Pasqualini, W. Arap, W. Lam and R. Richards-Kortum, Optical systems for in vivo molecular imaging of cancer. *Technol Cancer Res Treat*, 2003, **2**, 491-504.

10. B. W. Neville and T. A. Day, Oral cancer and precancerous lesions. *CA Cancer J Clin*, 2002, **52**, 195-215.

11. C. A. Squier and M. J. Kremer, Biology of oral mucosa and esophagus. *J Natl Cancer Inst Monogr*, 2001, 7-15.

12. T. A. Winning and G. C. Townsend, Oral mucosal embryology and histology. *Clin Dermatol*, 2000, **18**, 499-511.

13. L. P. Gartner, Oral anatomy and tissue types. *Semin Dermatol*, 1994, **13**, 68-73.

14. K. D. Hunter, E. K. Parkinson and P. R. Harrison, Profiling early head and neck cancer. *Nat Rev Cancer*, 2005, **5**, 127-135.

15. J. Ferlay, F. Bray, P. Pisani and D. Parkin, *GLOBOCAN 2002: Cancer Incidence, Mortality and Prevalence Worldwide*, IARC*Press*, 2004.

16. E. M. Iype, M. Pandey, A. Mathew, G. Thomas and M. K. Nair, Squamous cell cancer of the buccal mucosa in young adults. *Br J Oral Maxillofac Surg*, 2004, **42**, 185-189.

17. R. J. Oliver, J. Dearing and I. Hindle, Oral cancer in young adults: report of three cases and review of the literature. *Br Dent J*, 2000, **188**, 362-365.

18. S. Warnakulasuriya, Smokeless tobacco and oral cancer. *Oral Dis*, 2004, **10**, 1-4.

19. P. C. Gupta, Mouth cancer in India: a new epidemic? *J Indian Med Assoc*, 1999, **97**, 370-373.

20. R. B. Capone, S. I. Pai, W. M. Koch, M. L. Gillison, H. N. Danish, W. H. Westra, R. Daniel, K. V. Shah and D. Sidransky, Detection and quantitation of human papillomavirus (HPV) DNA in the sera of patients with HPV-associated head and neck squamous cell carcinoma. *Clin Cancer Res*, 2000, **6**, 4171-4175.

21. M. L. Gillison, W. M. Koch, R. B. Capone, M. Spafford, W. H. Westra, L. Wu, M. L. Zahurak, R. W. Daniel, M. Viglione, D. E. Symer, K. V. Shah and D. Sidransky, Evidence for a causal association between human papillomavirus and a subset of head and neck cancers. *J Natl Cancer Inst*, 2000, **92**, 709-720.

22. C. H. Shiboski, B. L. Schmidt and R. C. Jordan, Tongue and tonsil carcinoma: increasing trends in the U.S. population ages 20-44 years. *Cancer*, 2005, **103**, 1843-1849.

23. B. R. Das and J. K. Nagpal, Understanding the biology of oral cancer. *Med Sci Monit*, 2002, **8**, RA258-267.

24. J. J. Sciubba, Oral cancer. The importance of early diagnosis and treatment. *Am J Clin Dermatol*, 2001, **2**, 239-251.

25. R. Jackler and M. Kaplan, in *Current Medical Diagnosis and Treatment*, Editon edn., 2004.

26. S. Silverman, Jr., M. Gorsky and F. Lozada, Oral leukoplakia and malignant transformation. A follow-up study of 257 patients. *Cancer*, 1984, **53**, 563-568.

27. J. J. Pindborg, D. K. Daftary and F. S. Mehta, A follow-up study of sixty-one oral dysplastic precancerous lesions in Indian villagers. *Oral Surg Oral Med Oral Pathol*, 1977, **43**, 383-390.

28. K. P. Schepman, E. H. van der Meij, L. E. Smeele and I. van der Waal, Malignant transformation of oral leukoplakia: a follow-up study of a hospital-based population of 166 patients with oral leukoplakia from The Netherlands. *Oral Oncol*, 1998, **34**, 270-275.

29. J. Reibel, Prognosis of oral pre-malignant lesions: significance of clinical, histopathological, and molecular biological characteristics. *Crit Rev Oral Biol Med*, 2003, **14**, 47-62.

30. J. J. Pindborg, P. A. Reichart, C. J. Smith and I. Van der Waal, eds., *Histological Typing of Cancer and Precancer of the Oral Mucosa*, 2 edn., Springer-Verlag, Berlin, 1997.

31. J. J. Pindborg, J. Reibel and P. Holmstrup, Subjectivity in evaluating oral epithelial dysplasia, carcinoma in situ and initial carcinoma. *J Oral Pathol*, 1985, **14**, 698-708.

32. A. Karabulut, J. Reibel, M. H. Therkildsen, F. Praetorius, H. W. Nielsen and E. Dabelsteen, Observer variability in the histologic assessment of oral premalignant lesions. *J Oral Pathol Med*, 1995, **24**, 198-200.

33. J. J. Lee, W. K. Hong, W. N. Hittelman, L. Mao, R. Lotan, D. M. Shin, S. E. Benner, X. C. Xu, J. S. Lee, V. M. Papadimitrakopoulou, C. Geyer, C. Perez, J. W. Martin, A. K. El-Naggar and S. M. Lippman, Predicting cancer development in oral leukoplakia: ten years of translational research. *Clin Cancer Res*, 2000, **6**, 1702-1710.

34. G. J. Kelloff and C. C. Sigman, Assessing intraepithelial neoplasia and drug safety in cancer-preventive drug development. *Nat Rev Cancer*, 2007, **7**, 508-518.

35. S. M. Lippman and W. K. Hong, Second malignant tumors in head and neck squamous cell carcinoma: the overshadowing threat for patients with early-stage disease. *Int J Radiat Oncol Biol Phys*, 1989, **17**, 691-694.

36. G. L. Day and W. J. Blot, Second primary tumors in patients with oral cancer. *Cancer*, 1992, **70**, 14-19.

37. D. P. Slaughter, H. W. Southwick and W. Smejkal, Field cancerization in oral stratified squamous epithelium; clinical implications of multicentric origin. *Cancer*, 1953, **6**, 963-968.

38. P. J. Thomson, Field change and oral cancer: new evidence for widespread carcinogenesis? *Int J Oral Maxillofac Surg*, 2002, **31**, 262-266.

39. W. M. Lydiatt, P. E. Anderson, T. Bazzana, M. Casale, C. J. Hughes, A. G. Huvos, D. D. Lydiatt and S. P. Schantz, Molecular support for field cancerization in the head and neck. *Cancer*, 1998, **82**, 1376-1380.

40. D. Hanahan and R. A. Weinberg, The hallmarks of cancer. *Cell*, 2000, **100**, 57-70.

41. J. Califano, P. van der Riet, W. Westra, H. Nawroz, G. Clayman, S. Piantadosi, R. Corio, D. Lee, B. Greenberg, W. Koch and D. Sidransky, Genetic progression model for head and neck cancer: implications for field cancerization. *Cancer Res*, 1996, **56**, 2488-2492.

42. A. Forastiere, W. Koch, A. Trotti and D. Sidransky, Head and neck cancer. *N Engl J Med*, 2001, **345**, 1890-1900.

43. M. P. Rosin, X. Cheng, C. Poh, W. L. Lam, Y. Huang, J. Lovas, K. Berean, J. B. Epstein, R. Priddy, N. D. Le and L. Zhang, Use of allelic loss to predict malignant risk for low-grade oral epithelial dysplasia. *Clin Cancer Res*, 2000, **6**, 357-362.

44. S. L. Rosas, W. Koch, M. G. da Costa Carvalho, L. Wu, J. Califano, W. Westra, J. Jen and D. Sidransky, Promoter hypermethylation patterns of p16, O6-methylguanine-DNA-methyltransferase, and death-associated protein kinase in tumors and saliva of head and neck cancer patients. *Cancer Res*, 2001, **61**, 939-942.

45. D. Sidransky, Emerging molecular markers of cancer. *Nat Rev Cancer*, 2002, **2**, 210-219.

46. A. M. Horowitz and M. C. Alfano, Performing a death-defying act. *J Am Dent Assoc*, 2001, **132 Suppl**, 5S-6S.

47. M. C. Downer, D. R. Moles, S. Palmer and P. M. Speight, A systematic review of test performance in screening for oral cancer and precancer. *Oral Oncol*, 2004, **40**, 264-273.

48. M. W. Lingen, Critical evaluation of diagnostic aids for the detection of oral cancer. *Oral Oncol*, 2007.

49. P. Allison, Effectiveness of screening for oral cancer not proven. *Evid Based Dent*, 2004, **5**, 40-41.

50. O. Kujan, A. M. Glenny, R. J. Oliver, N. Thakker and P. Sloan, Screening programmes for the early detection and prevention of oral cancer. *Cochrane Database Syst Rev*, 2006, **3**, CD004150.

51. J. B. Epstein, M. Gorsky, D. Fischer, A. Gupta, M. Epstein and S. Elad, A survey of the current approaches to diagnosis and management of oral premalignant lesions. *J Am Dent Assoc*, 2007, **138**, 1555-1562; quiz 1614.

52. I. van der Waal, K. P. Schepman, E. H. van der Meij and L. E. Smeele, Oral leukoplakia: a clinicopathological review. *Oral Oncol*, 1997, **33**, 291-301.

53. P. Holmstrup, P. Vedtofte, J. Reibel and K. Stoltze, Long-term treatment outcome of oral premalignant lesions. *Oral Oncol*, 2006, **42**, 461-474.

54. F. L. Green, D. L. Page, I. D. Fleming, A. G. Fritz, C. M. Balch, D. G. Haller and M. Morrow, eds., *AJCC Cancer Staging Handbook*, 6 edn., Springer, New York, 2002.

55. S. G. Patel and J. P. Shah, TNM staging of cancers of the head and neck: striving for uniformity among diversity. *CA Cancer J Clin*, 2005, **55**, 242-258; quiz 261-242, 264.

56. C. E. Palme, P. J. Gullane and R. W. Gilbert, Current treatment options in squamous cell carcinoma of the oral cavity. *Surg Oncol Clin N Am*, 2004, **13**, 47-70.

57. H. Quon, F. F. Liu and B. J. Cummings, Potential molecular prognostic markers in head and neck squamous cell carcinomas. *Head Neck*, 2001, **23**, 147-159.

58. G. R. Thomas, H. Nadiminti and J. Regalado, Molecular predictors of clinical outcome in patients with head and neck squamous cell carcinoma. *Int J Exp Pathol*, 2005, **86**, 347-363.

59. V. Tralongo, V. Rodolico, A. Luciani, G. Marra and E. Daniele, Prognostic factors in oral squamous cell carcinoma. A review of the literature. *Anticancer Res*, 1999, **19**, 3503-3510.

60. C. G. Gourin, Z. S. Xia, Y. Han, A. M. French, A. K. O'Rourke, D. J. Terris and B. L. Adam, Serum protein profile analysis in patients with head and neck squamous cell carcinoma. *Arch Otolaryngol Head Neck Surg*, 2006, **132**, 390-397.

61. C. Leethanakul, V. Patel, J. Gillespie, M. Pallente, J. F. Ensley, S. Koontongkaew, L. A. Liotta, M. Emmert-Buck and J. S. Gutkind, Distinct pattern of expression of differentiation and growth-related genes in squamous cell carcinomas of the head and neck revealed by the use of laser capture microdissection and cDNA arrays. *Oncogene*, 2000, **19**, 3220-3224.

62. C. Leethanakul, V. Patel, J. Gillespie, E. Shillitoe, R. M. Kellman, J. F. Ensley, V. Limwongse, M. R. Emmert-Buck, D. B. Krizman and J. S. Gutkind, Gene

expression profiles in squamous cell carcinomas of the oral cavity: use of laser capture microdissection for the construction and analysis of stage-specific cDNA libraries. *Oral Oncol*, 2000, **36**, 474-483.

63. C. E. Schmalbach, D. B. Chepeha, T. J. Giordano, M. A. Rubin, T. N. Teknos, C. R. Bradford, G. T. Wolf, R. Kuick, D. E. Misek, D. K. Trask and S. Hanash, Molecular profiling and the identification of genes associated with metastatic oral cavity/pharynx squamous cell carcinoma. *Arch Otolaryngol Head Neck Surg*, 2004, **130**, 295-302.

64. C. Sotiriou, P. Lothaire, D. Dequanter, F. Cardoso and A. Awada, Molecular profiling of head and neck tumors. *Curr Opin Oncol*, 2004, **16**, 211-214.

65. S. Kumar, A. Mohan and R. Guleria, Biomarkers in cancer screening, research and detection: present and future: a review. *Biomarkers*, 2006, **11**, 385-405.

66. J. A. Ludwig and J. N. Weinstein, Biomarkers in cancer staging, prognosis and treatment selection. *Nat Rev Cancer*, 2005, **5**, 845-856.

67. B. M. Brinkman and D. T. Wong, Disease mechanism and biomarkers of oral squamous cell carcinoma. *Curr Opin Oncol*, 2006, **18**, 228-233.

68. R. M. Nagler, Molecular aspects of oral cancer. *Anticancer Res*, 2002, **22**, 2977-2980.

69. R. G. Pomerantz and J. R. Grandis, The role of epidermal growth factor receptor in head and neck squamous cell carcinoma. *Curr Oncol Rep*, 2003, **5**, 140-146.

70. J. R. Grandis and D. J. Tweardy, Elevated levels of transforming growth factor alpha and epidermal growth factor receptor messenger RNA are early markers of carcinogenesis in head and neck cancer. *Cancer Res*, 1993, **53**, 3579-3584.

71. J. Rubin Grandis, M. F. Melhem, W. E. Gooding, R. Day, V. A. Holst, M. M. Wagener, S. D. Drenning and D. J. Tweardy, Levels of TGF-alpha and EGFR protein in head and neck squamous cell carcinoma and patient survival. *J Natl Cancer Inst*, 1998, **90**, 824-832.

72. Y. Li, M. A. St John, X. Zhou, Y. Kim, U. Sinha, R. C. Jordan, D. Eisele, E. Abemayor, D. Elashoff, N. H. Park and D. T. Wong, Salivary transcriptome diagnostics for oral cancer detection. *Clin Cancer Res*, 2004, **10**, 8442-8450.

73. M. F. Spafford, W. M. Koch, A. L. Reed, J. A. Califano, L. H. Xu, C. F. Eisenberger, L. Yip, P. L. Leong, L. Wu, S. X. Liu, C. Jeronimo, W. H. Westra and D. Sidransky, Detection of head and neck squamous cell carcinoma among exfoliated oral mucosal cells by microsatellite analysis. *Clin Cancer Res*, 2001, **7**, 607-612.

74. O. Driemel, R. Dahse, S. G. Hakim, T. Tsioutsias, H. Pistner, T. E. Reichert and H. Kosmehl, Laminin-5 immunocytochemistry: a new tool for identifying dysplastic cells in oral brush biopsies. *Cytopathology*, 2007, **18**, 348-355.

75. H. Xie, G. Onsongo, J. Popko, E. P. de Jong, J. Cao, J. V. Carlis, R. J. Griffin, N. L. Rhodus and T. J. Griffin, Proteomics analysis of cells in whole saliva from oral cancer patients via value-added three-dimensional peptide fractionation and tandem mass spectrometry. *Mol Cell Proteomics*, 2008, **7**, 486-498.

76. J. J. Sciubba, Improving detection of precancerous and cancerous oral lesions. Computer-assisted analysis of the oral brush biopsy. U.S. Collaborative OralCDx Study Group. *J Am Dent Assoc*, 1999, **130**, 1445-1457.

77. J. L. Schwartz, S. Panda, C. Beam, L. E. Bach and G. R. Adami, RNA from brush oral cytology to measure squamous cell carcinoma gene expression. *J Oral Pathol Med*, 2008, **37**, 70-77.

78. J. A. Veltman, A. H. Hopman, F. J. Bot, F. C. Ramaekers and J. J. Manni, Detection of chromosomal aberrations in cytologic brush specimens from head and neck squamous cell carcinoma. *Cancer*, 1997, **81**, 309-314.

79. R. C. Bast, Jr., H. Lilja, N. Urban, D. L. Rimm, H. Fritsche, J. Gray, R. Veltri, G. Klee, A. Allen, N. Kim, S. Gutman, M. A. Rubin and A. Hruszkewycz, Translational crossroads for biomarkers. *Clin Cancer Res*, 2005, **11**, 6103-6108.

80. D. C. Christian, Computer-assisted analysis of oral brush biopsies at an oral cancer screening program. *J Am Dent Assoc*, 2002, **133**, 357-362.

81. C. Scheifele, A. M. Schmidt-Westhausen, T. Dietrich and P. A. Reichart, The sensitivity and specificity of the OralCDx technique: evaluation of 103 cases. *Oral Oncol*, 2004, **40**, 824-828.

82. T. W. Poate, J. A. Buchanan, T. A. Hodgson, P. M. Speight, A. W. Barrett, D. R. Moles, C. Scully and S. R. Porter, An audit of the efficacy of the oral brush biopsy technique in a specialist Oral Medicine unit. *Oral Oncol*, 2004, **40**, 829-834.

83. T. J. Potter, D. J. Summerlin and J. H. Campbell, Oral malignancies associated with negative transepithelial brush biopsy. *J Oral Maxillofac Surg*, 2003, **61**, 674-677.

84. K. A. Warnakulasuriya and N. W. Johnson, Sensitivity and specificity of OraScan (R) toluidine blue mouthrinse in the detection of oral cancer and precancer. *J Oral Pathol Med*, 1996, **25**, 97-103.

85. J. B. Epstein, C. Scully and J. Spinelli, Toluidine blue and Lugol's iodine application in the assessment of oral malignant disease and lesions at risk of malignancy. *J Oral Pathol Med*, 1992, **21**, 160-163.

86. M. A. Onofre, M. R. Sposto and C. M. Navarro, Reliability of toluidine blue application in the detection of oral epithelial dysplasia and in situ and invasive squamous cell carcinomas. *Oral Surg Oral Med Oral Pathol Oral Radiol Endod*, 2001, **91**, 535-540.

87. I. C. Martin, C. J. Kerawala and M. Reed, The application of toluidine blue as a diagnostic adjunct in the detection of epithelial dysplasia. *Oral Surg Oral Med Oral Pathol Oral Radiol Endod*, 1998, **85**, 444-446.

88. M. A. Huber, S. A. Bsoul and G. T. Terezhalmy, Acetic acid wash and chemiluminescent illumination as an adjunct to conventional oral soft tissue examination for the detection of dysplasia: a pilot study. *Quintessence Int*, 2004, **35**, 378-384.

89. E. S. Oh and D. M. Laskin, Efficacy of the ViziLite system in the identification of oral lesions. *J Oral Maxillofac Surg*, 2007, **65**, 424-426.

90. S. Ram and C. H. Siar, Chemiluminescence as a diagnostic aid in the detection of oral cancer and potentially malignant epithelial lesions. *Int J Oral Maxillofac Surg*, 2005, **34**, 521-527.

91. A. R. Kerr, D. A. Sirois and J. B. Epstein, Clinical evaluation of chemiluminescent lighting: an adjunct for oral mucosal examinations. *J Clin Dent*, 2006, **17**, 59-63.

92. D. C. De Veld, M. J. Witjes, H. J. Sterenborg and J. L. Roodenburg, The status of in vivo autofluorescence spectroscopy and imaging for oral oncology. *Oral Oncol*, 2005, **41**, 117-131.

93. P. M. Lane, T. Gilhuly, P. Whitehead, H. Zeng, C. F. Poh, S. Ng, P. M. Williams, L. Zhang, M. P. Rosin and C. E. MacAulay, Simple device for the direct visualization of oral-cavity tissue fluorescence. *J Biomed Opt*, 2006, **11**, 024006.

94. E. Svistun, R. Alizadeh-Naderi, A. El-Naggar, R. Jacob, A. Gillenwater and R. Richards-Kortum, Vision enhancement system for detection of oral cavity neoplasia based on autofluorescence. *Head Neck*, 2004, **26**, 205-215.

95. J. M. Benavides, S. Chang, S. Y. Park, R. Richards-Kortum, N. Mackinnon, C. MacAulay, A. Milbourne, A. Malpica and M. Follen, Multispectral digital colposcopy for *in vitro* detection of cervical cancer. *OPTICS EXPRESS*, 2003, **11**, 1223-1236.

96. C. F. Poh, S. P. Ng, P. M. Williams, L. Zhang, D. M. Laronde, P. Lane, C. Macaulay and M. P. Rosin, Direct fluorescence visualization of clinically occult high-risk oral premalignant disease using a simple hand-held device. *Head Neck*, 2007, **29**, 71-76.

97. C. F. Poh, L. Zhang, D. W. Anderson, J. S. Durham, P. M. Williams, R. W. Priddy, K. W. Berean, S. Ng, O. L. Tseng, C. MacAulay and M. P. Rosin, Fluorescence visualization detection of field alterations in tumor margins of oral cancer patients. *Clin Cancer Res*, 2006, **12**, 6716-6722.

98. N. Christodoulides, M. Tran, P. N. Floriano, M. Rodriguez, A. Goodey, M. Ali, D. Neikirk and J. T. McDevitt, A microchip-based multianalyte assay system for the assessment of cardiac risk. *Anal Chem*, 2002, **74**, 3030-3036.

99. P. N. Floriano, N. Christodoulides, D. Romanovicz, B. Bernard, G. W. Simmons, M. Cavell and J. T. McDevitt, Membrane-based on-line optical analysis system for rapid detection of bacteria and spores. *Biosens Bioelectron*, 2005, **20**, 2079-2088.

100. N. Christodoulides, P. N. Floriano, S. A. Acosta, K. L. Ballard, S. E. Weigum, S. Mohanty, P. Dharshan, D. Romanovicz and J. T. McDevitt, Toward the development of a lab-on-a-chip dual-function leukocyte and C-reactive protein analysis method for the assessment of inflammation and cardiac risk. *Clin Chem*, 2005, **51**, 2391-2395.

101. P. N. Floriano, S. A. Acosta, N. J. Chrisotdoulides, S. E. Weigum and J. T. McDevitt, in *Methods in Molecular Biology - Microchip-Based Assay Systems: Methods And Applications* ed. P. N. Floriano, Humana Press, Clifton, NJ, Editon edn., 2007, vol. 385.

102. M. F. Ali, R. Kirby, A. P. Goodey, M. D. Rodriguez, A. D. Ellington, D. P. Neikirk and J. T. McDevitt, DNA hybridization and discrimination of single-nucleotide mismatches using chip-based microbead arrays. *Anal Chem*, 2003, **75**, 4732-4739.

103. A. Goodey, J. J. Lavigne, S. M. Savoy, M. D. Rodriguez, T. Curey, A. Tsao, G. Simmons, J. Wright, S. J. Yoo, Y. Sohn, E. V. Anslyn, J. B. Shear, D. P. Neikirk and J. T. McDevitt, Development of multianalyte sensor arrays composed of chemically derivatized polymeric microspheres localized in micromachined cavities. *J Am Chem Soc*, 2001, **123**, 2559-2570.

104. N. Christodoulides, S. Mohanty, C. S. Miller, M. C. Langub, P. N. Floriano, P. Dharshan, M. F. Ali, B. Bernard, D. Romanovicz, E. Anslyn, P. C. Fox and J. T. McDevitt, Application of microchip assay system for the measurement of C-reactive protein in human saliva. *Lab Chip*, 2005, **5**, 261-269.

105. N. Christodoulides, P. N. Floriano, C. S. Miller, J. L. Ebersole, S. Mohanty, P. Dharshan, M. Griffin, A. Lennart, K. L. Ballard, C. P. King, Jr., M. C. Langub, R. J. Kryscio, M. V. Thomas and J. T. McDevitt, Lab-on-a-chip methods for point-of-care measurements of salivary biomarkers of periodontitis. *Ann N Y Acad Sci*, 2007, **1098**, 411-428.

106. V. W. Lui and J. R. Grandis, EGFR-mediated cell cycle regulation. *Anticancer Res*, 2002, **22**, 1-11.

107. J. Mendelsohn, A. Baird, Z. Fan and S. D. Markowitz, in *The Molecular Basis of Cancer*, eds. J. Mendelsohn, P. M. Howley, M. A. Israel and L. A. Liotta, W.B. Saunders Company, Philidelphia, Editon edn., 2001, pp. 137-161.

108. S. Kalyankrishna and J. R. Grandis, Epidermal growth factor receptor biology in head and neck cancer. *J Clin Oncol*, 2006, **24**, 2666-2672.

109. K. Oda, Y. Matsuoka, A. Funahashi and H. Kitano, A comprehensive pathway map of epidermal growth factor receptor signaling. *Mol Syst Biol*, 2005, **1**, 2005 0010.

110. R. Todd and D. T. Wong, Epidermal growth factor receptor (EGFR) biology and human oral cancer. *Histol Histopathol*, 1999, **14**, 491-500.

111. J. R. Grandis and J. C. Sok, Signaling through the epidermal growth factor receptor during the development of malignancy. *Pharmacol Ther*, 2004, **102**, 37-46.

112. A. Wells, EGF receptor. *Int J Biochem Cell Biol*, 1999, **31**, 637-643.

113. M. Mrhalova, J. Plzak, J. Betka and R. Kodet, Epidermal growth factor receptor--its expression and copy numbers of EGFR gene in patients with head and neck squamous cell carcinomas. *Neoplasma*, 2005, **52**, 338-343.

114. D. M. Shin, J. Y. Ro, W. K. Hong and W. N. Hittelman, Dysregulation of epidermal growth factor receptor expression in premalignant lesions during head and neck tumorigenesis. *Cancer Res*, 1994, **54**, 3153-3159.

115. W. Xia, Y. K. Lau, H. Z. Zhang, F. Y. Xiao, D. A. Johnston, A. R. Liu, L. Li, R. L. Katz and M. C. Hung, Combination of EGFR, HER-2/neu, and HER-3 is a stronger predictor for the outcome of oral squamous cell carcinoma than any individual family members. *Clin Cancer Res*, 1999, **5**, 4164-4174.

116. J. Rubin Grandis, M. F. Melhem, E. L. Barnes and D. J. Tweardy, Quantitative immunohistochemical analysis of transforming growth factor-alpha and epidermal growth factor receptor in patients with squamous cell carcinoma of the head and neck. *Cancer*, 1996, **78**, 1284-1292.

117. M. Shiraki, T. Odajima, T. Ikeda, A. Sasaki, M. Satoh, A. Yamaguchi, M. Noguchi, I. Nagai and H. Hiratsuka, Combined expression of p53, cyclin D1 and epidermal growth factor receptor improves estimation of prognosis in curatively resected oral cancer. *Mod Pathol*, 2005, **18**, 1482-1489.

118. K. Laimer, G. Spizzo, G. Gastl, P. Obrist, T. Brunhuber, D. Fong, V. Barbieri, S. Jank, W. Doppler, M. Rasse and B. Norer, High EGFR expression predicts poor prognosis in patients with squamous cell carcinoma of the oral cavity and oropharynx: a TMA-based immunohistochemical analysis. *Oral Oncol*, 2007, **43**, 193-198.

119. E. J. Smid, T. R. Stoter, E. Bloemena, M. V. Lafleur, C. R. Leemans, I. van der Waal, B. J. Slotman and J. A. Langendijk, The importance of immunohistochemical expression of EGFr in squamous cell carcinoma of the oral cavity treated with surgery and postoperative radiotherapy. *Int J Radiat Oncol Biol Phys*, 2006, **65**, 1323-1329.

120. M. Diniz-Freitas, T. Garcia-Caballero, J. Antunez-Lopez, J. M. Gandara-Rey and A. Garcia-Garcia, Pharmacodiagnostic evaluation of EGFR expression in oral squamous cell carcinoma. *Oral Dis*, 2007, **13**, 285-290.

121. S. M. Bentzen, B. M. Atasoy, F. M. Daley, S. Dische, P. I. Richman, M. I. Saunders, K. R. Trott and G. D. Wilson, Epidermal growth factor receptor expression in pretreatment biopsies from head and neck squamous cell carcinoma as a predictive factor for a benefit from accelerated radiation therapy in a randomized controlled trial. *J Clin Oncol*, 2005, **23**, 5560-5567.

122. R. G. Pomerantz and J. R. Grandis, The epidermal growth factor receptor signaling network in head and neck carcinogenesis and implications for targeted therapy. *Semin Oncol*, 2004, **31**, 734-743.

123. R. F. Ozols, R. S. Herbst, Y. L. Colson, J. Gralow, J. Bonner, W. J. Curran, Jr., B. L. Eisenberg, P. A. Ganz, B. S. Kramer, M. G. Kris, M. Markman, R. J. Mayer, D. Raghavan, G. H. Reaman, R. Sawaya, R. L. Schilsky, L. M. Schuchter, J. W. Sweetenham, L. T. Vahdat and R. J. Winn, Clinical cancer advances 2006: major research advances in cancer treatment, prevention, and screening--a report from the American Society of Clinical Oncology. *J Clin Oncol*, 2007, **25**, 146-162.

124. R. L. Chai and J. R. Grandis, Advances in molecular diagnostics and therapeutics in head and neck cancer. *Curr Treat Options Oncol*, 2006, **7**, 3-11.

125. J. A. Bonner, P. M. Harari, J. Giralt, N. Azarnia, D. M. Shin, R. B. Cohen, C. U. Jones, R. Sur, D. Raben, J. Jassem, R. Ove, M. S. Kies, J. Baselga, H. Youssoufian, N. Amellal, E. K. Rowinsky and K. K. Ang, Radiotherapy plus cetuximab for squamous-cell carcinoma of the head and neck. *N Engl J Med*, 2006, **354**, 567-578.

126. M. R. Posner and L. J. Wirth, Cetuximab and radiotherapy for head and neck cancer. *N Engl J Med*, 2006, **354**, 634-636.

127. W. S. Rasband, *ImageJ*, (19997-2006) U.S. National Institutes of Health, Bethesda, MD,USA.

128. V. S. Varga, J. Bocsi, F. Sipos, G. Csendes, Z. Tulassay and B. Molnar, Scanning fluorescent microscopy is an alternative for quantitative fluorescent cell analysis. *Cytometry A*, 2004, **60**, 53-62.

129. E. R. Hsu, E. V. Anslyn, S. Dharmawardhane, R. Alizadeh-Naderi, J. S. Aaron, K. V. Sokolov, A. K. El-Naggar, A. M. Gillenwater and R. R. Richards-Kortum, A far-red fluorescent contrast agent to image epidermal growth factor receptor expression. *Photochem Photobiol*, 2004, **79**, 272-279.

130. J. Anido, P. Matar, J. Albanell, M. Guzman, F. Rojo, J. Arribas, S. Averbuch and J. Baselga, ZD1839, a specific epidermal growth factor receptor (EGFR) tyrosine kinase inhibitor, induces the formation of inactive EGFR/HER2 and EGFR/HER3 heterodimers and prevents heregulin signaling in HER2-overexpressing breast cancer cells. *Clin Cancer Res*, 2003, **9**, 1274-1283.

131. R. Kimmig, D. Pfeiffer, H. Landsmann and H. Hepp, Quantitative determination of the epidermal growth factor receptor in cervical cancer and normal cervical epithelium by 2-color flow cytometry: evidence for down-regulation in cervical cancer. *Int J Cancer*, 1997, **74**, 365-373.

132. G. P. Cowley, J. A. Smith and B. A. Gusterson, Increased EGF receptors on human squamous carcinoma cell lines. *Br J Cancer*, 1986, **53**, 223-229.

133. Z. M. Naib, *Exfoliative Cytopathology*, 3 edn., Little, Brown and Company Boston, 1985.

134. P. B. Sugerman and N. W. Savage, Exfoliative cytology in clinical oral pathology. *Aust Dent J*, 1996, **41**, 71-74.

135. G. R. Ogden, The future role for oral exfoliative cytology--bleak or bright? *Oral Oncol*, 1997, **33**, 2-4.

136. G. R. Ogden, J. G. Cowpe and M. Green, Cytobrush and wooden spatula for oral exfoliative cytology. A comparison. *Acta Cytol*, 1992, **36**, 706-710.

137. T. Ramaesh, B. R. Mendis, N. Ratnatunga and R. O. Thattil, Cytomorphometric analysis of squames obtained from normal oral mucosa and lesions of oral leukoplakia and squamous cell carcinoma. *J Oral Pathol Med*, 1998, **27**, 83-86.

138. Z. O. Pektas, A. Keskin, O. Gunhan and Y. Karslioglu, Evaluation of nuclear morphometry and DNA ploidy status for detection of malignant and premalignant oral lesions: quantitative cytologic assessment and review of methods for cytomorphometric measurements. *J Oral Maxillofac Surg*, 2006, **64**, 628-635.

139. T. Ramaesh, N. Ratnatunga, B. R. Mendis and S. Rajapaksa, Exfoliative cytology in screening for malignant and premalignant lesions in the buccal mucosa. *Ceylon Med J*, 1998, **43**, 206-209.

140. J. G. Cowpe, R. B. Longmore and M. W. Green, Quantitative exfoliative cytology of abnormal oral mucosal smears. *J R Soc Med*, 1988, **81**, 509-513.

141. S. Sen, Aneuploidy and cancer. *Curr Opin Oncol*, 2000, **12**, 82-88.

142. D. Maraki, J. Becker and A. Boecking, Cytologic and DNA-cytometric very early diagnosis of oral cancer. *J Oral Pathol Med*, 2004, **33**, 398-404.

143. T. W. Remmerbach, H. Weidenbach, N. Pomjanski, K. Knops, S. Mathes, A. Hemprich and A. Bocking, Cytologic and DNA-cytometric early diagnosis of oral cancer. *Anal Cell Pathol*, 2001, **22**, 211-221.

144. T. W. Remmerbach, H. Weidenbach, A. Hemprich and A. Bocking, Earliest detection of oral cancer using non-invasive brush biopsy including DNA-image-cytometry: report on four cases. *Anal Cell Pathol*, 2003, **25**, 159-166.

145. J. Sudbo, W. Kildal, B. Risberg, H. S. Koppang, H. E. Danielsen and A. Reith, DNA content as a prognostic marker in patients with oral leukoplakia. *N Engl J Med*, 2001, **344**, 1270-1278.

146. M. Diniz-Freitas, A. Garcia-Garcia, A. Crespo-Abelleira, J. L. Martins-Carneiro and J. M. Gandara-Rey, Applications of exfoliative cytology in the diagnosis of oral cancer. *Med Oral*, 2004, **9**, 355-361.

147. G. R. Ogden, S. McQueen, D. M. Chisholm and E. B. Lane, Keratin profiles of normal and malignant oral mucosa using exfoliative cytology. *J Clin Pathol*, 1993, **46**, 352-356.

148. G. R. Ogden, J. G. Cowpe, D. M. Chisholm and D. P. Lane, p53 immunostaining as a marker for oral cancer in diagnostic cytopathology--preliminary report. *Cytopathology*, 1994, **5**, 47-53.

149. O. Driemel, R. Dahse, A. Berndt, H. Pistner, S. G. Hakim, L. Zardi, T. E. Reichert and H. Kosmehl, High-molecular tenascin-C as an indicator of atypical cells in oral brush biopsies. *Clin Oral Investig*, 2007, **11**, 93-99.

150. I. S. Scott, E. Odell, P. Chatrath, L. S. Morris, R. J. Davies, S. L. Vowler, R. A. Laskey and N. Coleman, A minimally invasive immunocytochemical approach to early detection of oral squamous cell carcinoma and dysplasia. *Br J Cancer*, 2006, **94**, 1170-1175.

151. M. P. Rosin, J. B. Epstein, K. Berean, S. Durham, J. Hay, X. Cheng, T. Zeng, Y. Huang and L. Zhang, The use of exfoliative cell samples to map clonal genetic alterations in the oral epithelium of high-risk patients. *Cancer Res*, 1997, **57**, 5258-5260.

152. S. E. Weigum, P. N. Floriano, N. Christodoulides and J. T. McDevitt, Cell-based sensor for analysis of EGFR biomarker expression in oral cancer. *Lab Chip*, 2007, **7**, 995-1003.

153. H. H. Engelhard, Flow cytometric applications of Sulforhodamine 101 as a fluorescent stain for total cellular protein. *Biotech Histochem*, 1997, **72**, 1-9.

154. H. H. Engelhard, 3rd, J. L. Krupka and K. D. Bauer, Simultaneous quantification of c-myc oncoprotein, total cellular protein, and DNA content using multiparameter flow cytometry. *Cytometry*, 1991, **12**, 68-76.

155. M. Stohr, M. Vogt-Schaden, M. Knobloch, R. Vogel and G. Futterman, Evaluation of eight fluorochrome combinations for simultaneous DNA-protein flow analyses. *Stain Technol*, 1978, **53**, 205-215.

156. A. E. Carpenter, T. R. Jones, M. R. Lamprecht, C. Clarke, I. H. Kang, O. Friman, D. A. Guertin, J. H. Chang, R. A. Lindquist, J. Moffat, P. Golland and D. M. Sabatini, CellProfiler: image analysis software for identifying and quantifying cell phenotypes. *Genome Biol*, 2006, **7**, R100.

157. P. E. Purkis, J. B. Steel, I. C. Mackenzie, W. B. Nathrath, I. M. Leigh and E. B. Lane, Antibody markers of basal cells in complex epithelia. *J Cell Sci*, 1990, **97 (Pt 1)**, 39-50.

158. T. T. Sun, R. Eichner, W. G. Nelson, S. C. Tseng, R. A. Weiss, M. Jarvinen and J. Woodcock-Mitchell, Keratin classes: molecular markers for different types of epithelial differentiation. *J Invest Dermatol*, 1983, **81**, 109s-115s.

159. H. Puchtler and S. N. Meloan, On the chemistry of formaldehyde fixation and its effects on immunohistochemical reactions. *Histochemistry*, 1985, **82**, 201-204.

160. L. Eversole, *Clinical Outline of Oral Pathology: Diagnosis and Treatment*, 2 edn., Lea & Febiger, Philadelphia, 1984.

161. http://www.dow.com/glycerine/resources/table18.htm, Editon edn.

162. F. H. Hayama, A. C. Motta, P. Silva Ade and D. A. Migliari, Liquid-based preparations versus conventional cytology: specimen adequacy and diagnostic agreement in oral lesions. *Med Oral Patol Oral Cir Bucal*, 2005, **10**, 115-122.

163. J. G. Cowpe, R. B. Longmore and M. W. Green, Quantitative exfoliative cytology of normal oral squames: an age, site and sex-related survey. *J R Soc Med*, 1985, **78**, 995-1004.

164. W. Tan, L. Sabet, Y. Li, T. Yu, P. R. Klokkevold, D. T. Wong and C. M. Ho, Optical protein sensor for detecting cancer markers in saliva. *Biosens Bioelectron*, 2008, **24**, 266-271.

Vita

Shannon Elise Weigum was born in Bossier City, Lousiana on July 24, 1975, the daughter of Betty J. Walling and Curtis J. Kinder Jr. She was raised in the suburbs of San Antonio, TX where in May of 1993 she graduated from Theodore Roosevelt High School. In the Fall of 1993, she entered Texas A&M University at College Station and spent the following four years earning a Bachelor of Arts in Biology with Secondary Science Education Certification. For the next three years, she taught high school Biology, Chemistry and Physics before attending Texas State University where she earned her Master's Degree in Biology in 2002. She entered the graduate program at the University of Texas at Austin in 2002, where she began her doctoral work under the advisement of Dr. John T. McDevitt in Biochemistry.

Permanent address: 11948 Battle Bridge Dr., Austin, TX 78748

This dissertation was typed by the author.